Aptasensors using Tunable Resistive Pulse Sensing

by

Emily Rose Billinge

A Doctoral Thesis

Submitted in partial fulfilment of the requirements for the award of Doctor of Philosophy of Loughborough University

7th September 2015

Acknowledgements

I would like to take this opportunity to thank all of the people who have supported me throughout this PhD.

To my Dad, I thank you for always teaching me to have courage in my beliefs and not to ever follow the crowd. Thank you for always being there for advice, and for instilling in me a sense of the importance of grammar and an extensive vocabulary, which has always been a great help in any of my studies.

To my Mum, thanks for all of the phone calls which helped keep me sane. Somewhat. Thank you for always being able to see the good in every situation, even if I couldn't see it myself.

Lastly, and perhaps most of all, thanks go to my supervisor Dr Mark Platt. Thank you so much for allowing me to work with you for this past three years. You have been a constant support for me and have been the best supervisor I could have hoped for. You never made me feel stupid, or small, you always made me feel like this was where I was meant to be. I've learnt so much more from you than just the work in this thesis, and I hope that in some way I've done you proud.

Dedication

I dedicate this thesis to Lilian Sylvia Swain (nee Kent) whose unerring pride and love taught me to always try my best, to be kind, and to be generous. These lessons helped me through my PhD more than any scholastic learning.

Abstract

In recent years there has been an increased drive towards point of care testing (POCT), in which assays are performed at the site of the patient. This has many benefits, critically; the time for a result to be obtained will be significantly reduced, allowing for greater and more effective decision making. Many currently used bioassay methods are not affordable in resource poor areas where infectious disease is most prevalent, in order to combat this issue many research groups are attempting to miniaturise equipment for portability and make assays more affordable and therefore more accessible. With the aims of generating a new assay platform which is highly portable and affordable, the work in this thesis presents the development of several generic methods utilising nano- and micro-scale beads coated with aptamer which are then monitored interacting with target proteins with Tunable Resistive Pulse Sensing (TRPS).

Aptamers are short oligonucleotide sequences which are capable of binding to a wide range of targets with high selectivity and comparable affinity to antibodies while possessing greater stability and have begun to challenge the role of antibodies. When aptamers bind a target, they often undergo a conformational change. In the assays described herein, this conformational change is key to the observed signal changes. TRPS is a pore-based system in which beads moving through a pore cause a measurable increase in resistance which can be used to derive particle size, concentration, and mobility.

During the course of this thesis several template TRPS aptasensors have been developed. TRPS was successfully used to confirm the successful coating of nano- and micro-scale beads with DNA aptamers by monitoring an increase in electrophoretic mobility when the negatively charged DNA is added to the surface. Following on from this, TRPS was used to monitor the interaction of aptamer tagged beads with thrombin protein enabling thrombin detection down to 1.4 nM and the comparison of several thrombin-aptamers with results comparable to previously published SPR data. Thrombin was postulated to shield the negative DNA, resulting in a decrease in mobility, and the magnitude of this charge shielding was found to depend upon the binding mechanism of the aptamer used. This effect is not thought to be specific to our system nor to thrombin, the principles outlined here may be applied to other RPS technologies, or by interchanging of the aptamer, different proteins. In later chapters, this method is expanded to include multiplexed detection of growth factors and a significant improvement in signal.

Following on from this, the controlled aggregation of avidin coated beads in the presence of biotinylated-BSA was explored. Factors impacting upon this assay were discussed including magnetic separation, particle size and particle concentration, and different methods of data interpretation were presented. This aggregation study identified several key parameters in the use of TRPS in aggregation assays. Using the methods outlined by the study of aggregates, a dispersion assay was then designed in which the interaction of thrombin proteins with clusters of particles brought about the release of many small particles by the disruption of double stranded DNA linkages. This dispersion assay incorporated magnetic separation to simplify the read-out and relied on measuring particle concentration rather than mobility, enabling the use of additional pressure to increase speed and ease of use. Using this method, thrombin was able to be detected down to 100 fM, a significant advancement in TRPS aptasensors.

Table of contents

List of Figures

List of Tables

Chapter One

Introduction

1.1. Biomarkers and bioassays

A biomarker is defined as "a characteristic that is objectively measured and evaluated as an indicator of normal biological processes, pathogenic processes, or pharmacological responses to a therapeutic intervention" [1]. The measurement of biomarkers can therefore provide information for diagnoses, as well as for the improvement of treatment strategies hence, there is great demand for new assay techniques[2–4].

Bioassays are used to quantify the abundance or activity of a biomarker, for example proteins expressed in disease states[5]. In order to improve healthcare for all, including those in resource-poor areas, it is desirable for new bioassays to be developed which are affordable, easy to use, and highly portable[6]. In addition to considerations of cost and portability there is a drive to reduce bioassay time and move toward point-of-care testing[7].

Due to the complexity of biological processes one biomarker measured in isolation could be attributed to many diseases, therefore to provide greater confidence in diagnoses it is advantageous to be able to detect multiple biomarkers simultaneously. Monitoring biomarkers increases the ability to personalise medicine based on individual differences and disease subtype; off-target effects are then reduced and treatment is more effective. Being able to perform multiple measurements simultaneously would reduce total assay time and negate the need for repeated testing. Many current gold standard bioassays such as Enzyme Linked Immunosorbent Assays (ELISAs) and Polymerase Chain Reaction (PCR) often require large equipment and are labour intensive, requiring skilled technicians to perform. Many new technologies have emerged to address the demand for sensitive, rapid, portable, and inexpensive tests.

With the miniaturisation of equipment and greater precision in electronics it is possible to generate smaller devices, with instruments that would have at once occupied a whole lab now able to be carried[8]. Some of the most successful point-of-care tests can easily fit in a pocket and be used at home by the individual, these include lateral flow tests (e.g. home pregnancy testing)[9,10] and electrochemical sensors (e.g. hand-held glucometers for the monitoring of blood glucose)[11]. Several groups have adapted these popular and readily available tests to be the transducer for the detection of a wide range of analytes including food contaminants[12,13] and infectious agents[14,15].

1.2. Bead based bioassays

Several recently developed bioassays employ the use of nano and microscale synthetic beads, sometimes known as nano or microparticles[16]. The size of bead chosen largely depends on the desired detection method and the resolution of the technology used to read a signal. In order for these nanoparticles to be of use in bioassays they must be functionalised with a molecule to recognise the desired target. Nanoparticles can be conjugated to aptamers and antibodies to bind to the target, and/or to fluorophores to aid detection and are now routinely characterised by light scattering[20], fluorescence[9,12,23], colourimetry[17–19] and flow cytometry[24,25].

A problem in bioassays can be the low signal-to-noise ratio and significant non-specific adsorption due to the complexity of the media analysed (e.g. serum), to overcome some of these issues superparamagnetic (SPM) particles are being incorporated into assays. Suitably small ferro- and ferrimagnetic nanoparticles are capable of a phenomenon known as superparamagnetism [20,21], these particles hold no permanent dipole and in the presence of an external magnetic field their magnetic moments align leading to magnetisation, which is then abolished on the removal of the field. SPM particles have been proven to be useful in sample preparation to aid washing and remove unwanted entities without the need for complicated or expensive equipment[21,22]. SPM allows the particles to be separated, washed and pre-concentrated in electrolyte buffer without affecting the subsequent measurements with only a handheld magnet, unlike more aggressive methods such as centrifugation which may damage the sample. SPM particles have been incorporated into a variety of both diagnostic and therapeutic interventions[20,21]. SPM particles have been used as contrast agents in Magnetic Resonance Imaging (MRI)[23,24], for the measurement of disease biomarkers through Surface Plasmon Resonance (SPR)[25], and for the targeted delivery of drugs[24,26].

Magnetic bead based bioassays have also been developed around controlled aggregation of particles upon the introduction of the target. When the target contains multiple binding sites it is possible for one target molecule to interact with multiple beads simultaneously, leading to the formation of aggregates[27–31]. In these assays the concentration of the target is related to changes in the aggregate size or frequency[32]. The use of aggregates allows for a simple and label-free detection approach and has been used with gold particles[19,33], fluorescence, or fluorescence resonance energy transfer[34] often in conjunction with optical, cytometry[35], magneto resistive sensing[36], and dynamic light scattering detection platforms[28,37]. Alternative detection strategies for monitoring aggregation using superparamagnetic beads (SPBs) have

relied upon light scattering techniques to monitor the size of the aggregates using chain length[37] or turbidity[28,36] and changes in magnetic properties as particles are forced to be in close proximity to each other[31]. These technologies have been demonstrated with detection levels down to picomolar levels, with assay times as low as 5 minutes, however light scattering and optical techniques can have a limited dynamic range and could prove difficult to multiplex[38] as it would not be possible to separate the signals.

1.3. Aptamers

A key component of many biosensors is the analyte recognition. The ability to selectively capture one analyte amongst contaminants provides specificity in the sensor. Traditionally, this is done using antibodies. Antibodies are glycoproteins secreted by the immune system to detect and bind to foreign bodies by recognition of antigens on the target[39]. Each antibody binds to a specific epitope of the target antigen to disarm the potential hazard and signal other immunological cells to destroy it. Since their discovery, antibodies have been used extensively in both research and clinical settings commonly combined with fluorophores or enzymes to allow detection[40].

Raising antibodies to an analyte is a process both lengthy and expensive, requiring the use of animals and/or cell cultures and with no guarantee of success. Once antibodies have been generated their shelf-life is quite limited and they require careful handling to preserve activity. In addition, methods using antibodies are in themselves inherently difficult processes[41]. An alternative available capture probe with comparative properties are known as aptamers.

Aptamers are short single-stranded oligonucleotide sequences that recognise and bind to a wide range of specific targets of interest with high specificity due to their ability to form specific 3D shapes[42]. Aptamers have a longer shelf life than antibodies and unlike antibodies do not require the use of animals or cell culture. Aptamer generation is performed from a large pool of random oligonucleotide sequences (DNA, RNA or xenonucleic acid - XNA) which then undergoes a series of cycles of forced evolution in Systematic Evolution of Ligands by Exponential Enrichment (SELEX) which comprises around 6 – 20 rounds of binding, partition, elution, amplification and screening, conditioning and mutation as displayed in Figure 1.1A [43,44]. SELEX, while the method of choice for aptamer generation, carries several limitations. The number of rounds, PCR and synthesis increases the time and cost of the SELEX process; additionally sequencing and analysing the selected aptamers adds

time. SELEX which occurs in solution may also generate aptamers which will behave differently when anchored to a surface, such as a bead.

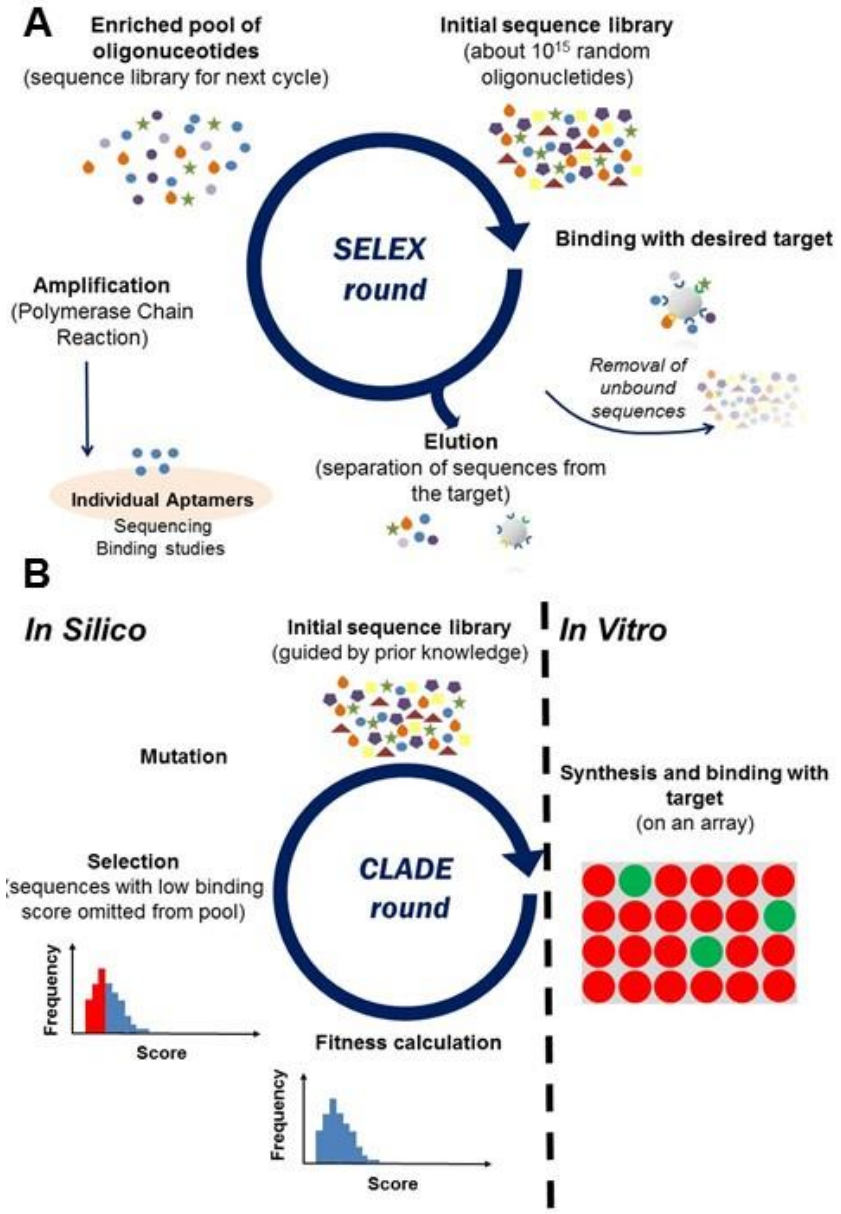

Figure 1. 1: Comparison of the aptamer generation methods SELEX (A) and CLADE (B).

Alternatively aptamers may be developed by a more recent adaptation known as Closed Loop Aptameric Directed Evolution (CLADE) [45–47] in which sequences are selected and mutated *in silico* prior to testing *in vitro* allowing for significant reduction in cost and time for each generated aptamer in addition sequences and their location are known throughout the process eliminating the need to perform polymerase chain reaction (PCR), as shown in Figure 1.1B.

Once aptamer sequences have been generated and are known they are able to be synthesised with relative ease and at low cost by any laboratory offering oligonucleotide synthesis however it is worth bearing in mind that although many sequences are available through primary research papers and online libraries, some sequences are protected by the creators and their use restricted.

New classes of aptamers are emerging with improved affinities and physical properties, for example Slow Off-rate Modified aptamers (SOMAmers)[48,49] to alter affinity, thiolated backbones[50] or speigelmers[51]. Speigelmers are built from artificial nucleotides that are a mirror-image of their naturally occurring counterparts, making them resistant to degradation by nucleases; due to their increased resistance to degradation and renal clearance speigelmers are being investigated as potential drug molecules.

1.3.1. Aptasensors

Since their discovery in 1990 aptamers have been increasingly integrated into both existing and emerging sensor platforms covered by the umbrella term "aptasensors" [52–54]. Aptamers can easily be modified and conjugated to other molecules with reliable immobilisation, making them ideal for incorporation into sensor devices. Many aptasensors rely on optical detection mechanisms such as fluorescence[52,55,56], and there have been many variations upon this method using fluorescent dyes[57–60] and by using nucleotides with fluorescent properties[61]. Adding a large molecule such as a dye to an aptamer can impact upon its primary purpose: binding[62]. Rather than using an additional dye, the incorporation of fluorescent nucleotides into the aptamer the interaction between the aptamer and target molecule has been shown not to be compromised and the effects of photobleaching are reduced[63]. These techniques have been used to generate assays using single reporters in which a fluorescent dye was affixed to the target via an aptamer or using multiple reporters such as combinations of fluorophores and quenchers to generate off/on signals specifically in the presence of an analyte[17,55,60]. An alternative to the use of fluorophores is a material known as quantum dots, which have far improved stability and narrower emission spectra compared to traditional fluorescent dyes allowing greater multiplexing power of optical techniques[64,65]. A draw back with fluorescing molecules is that detection and quantification require expensive equipment. A far simpler type of optical aptasensor utilises gold nanoparticles of which the aggregation or dispersion provides a clear colour change which is can be visualised with the naked eye[66,67], though this kind of measurement is not ideal as it is subjective.

Aptamers have also been integrated into existing techniques, such as Surface Plasmon Resonance (SPR)[68] and the Enzyme-Linked Immunosorbant Assay (ELISA)[69] which would usually incorporate two antibodies that sandwich a target with one to capture and one to detect. The Enzyme Linked Oligonucleotide Assay (ELONA) replaces one or both of these antibody elements with an aptamer sequence[54]. With the use of aptamers, pre-existing gold standard techniques are able to be improved considerably by decreasing cost, increasing stability, and also ease of use by the use of aptamers which are a more robust substrate to handle[69]. In addition, the ease of aptamer modification strategies enables the researcher to adapt the binding and signal generation with greater ease than in the same techniques employing antibodies.

Many aptasensors to date have been developed with the aim of being used in clinical measurements, as such comparison between these techniques is important so that the most reliable and valid aptasensor is chosen. Hence, commonly used targets include thrombin[45,70], Platelet Derived Growth Factor (PDGF)[19,71], IgE[72] and ATP[73,74] as these aptamer sequences are well established and characterised. By using these molecules as standards it is possible to compare emerging and existing techniques. Aside from proof-of-concept works aptasensors have been developed against high profile targets such as cancer biomarkers[75,76], HIV[77] and cocaine[55] as well as the detection of microbes[78].

1.4. Particle characterisation

For many years the gold standard of particle characterisation in terms of accuracy has been microscopy. Scanning and Transmission Electron Microscopy (SEM and TEM) direct an electron beam at a specimen and detect the electrons scattered or occluded by the sample[79,80]. Both SEM and TEM can detect a reported size range of 50 nm – 100 μm with a high level of accuracy[81] and can provide qualitative information regarding the visual characteristics of a sample. These methods have severely limited concentration determination and are further limited because only particles in the field of view can be measured requiring the sample to be very evenly dispersed. Furthermore, SEM and TEM cannot provide ζ-potential analysis or surface chemistry analysis.

In terms of a POCT device, SEM and TEM techniques are labour intensive and require very highly trained microscopy operatives to use. Additional factors preventing the use of SEM and TEM becoming widely used POCT devices are that the equipment is very large and expensive, there is low throughput and the particles cannot be analysed *in situ*[81].

One microscopy-based commercial platform available for particle characterisation is the NanoSight, a schematic for which is shown in figure 1.2, which attempts to use the precision of microscopy while reducing labour intensity. NanoSight combines microscopy and light scattering techniques to provide *in situ* analyses of nanoparticle movement in tandem with Nanoparticle Tracking Analysis Software (NTA). The NanoSight is able to provide both qualitative and quantitative information regarding the size, concentration, zeta-potential (ζ) and aggregation using Brownian motion[82]. The NanoSight is able to detect fluorescence and can utilise video for time-course experiments.

An advantage of the NanoSight over traditional light scattering techniques is the ability to observe polydisperse samples rather than providing an average reading for all the particles in the sample; however, light scattered by larger particles are sometimes able to occlude smaller particles behind them[38,83].

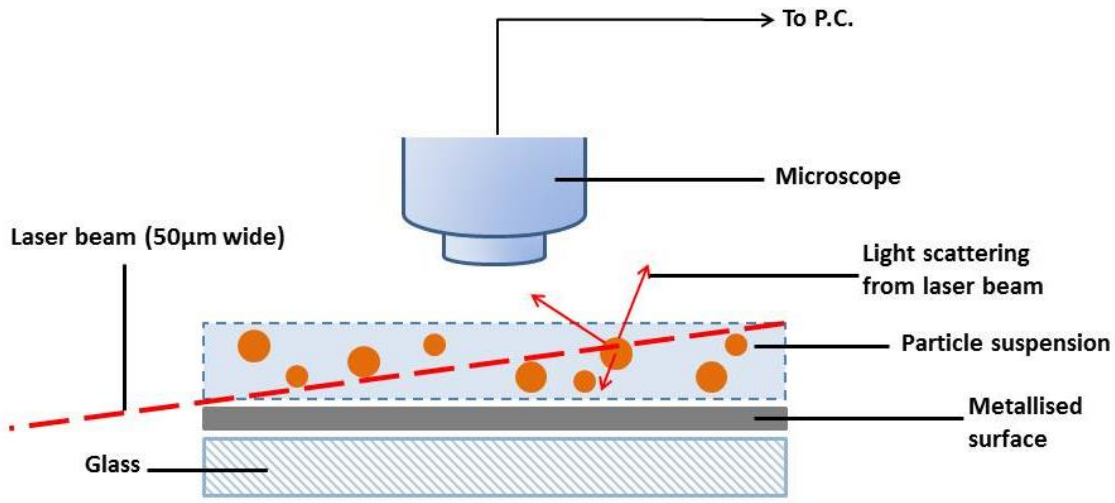

Figure 1. 1: Schematic displaying the NanoSight set up.

Dynamic light scattering (DLS) techniques focus light into a sample and detect photons scattered by particles in dispersion and uses Brownian motion to correlate information regarding average particle size and zeta-potential (ζ) in the colloidal dispersion[84], however concentration analysis is not possible[83]. One of the advantages of DLS is that it is quick, generating results in 5 - 10 minutes, and requires a relatively small amount of retrievable sample (~ 1 mL), furthermore the software and instrument are user-friendly; nevertheless there are several limitations which should be considered when using DLS.

DLS provides an average of all the particles which are measured simultaneously; smaller particles can be hidden behind the scattered light from larger particles and the end results can be significantly biased by the presence of small populations of large particles or aggregates, as such, DLS is not suitable for polydisperse samples. Another common problem encountered by DLS users is that larger particles (larger than 1 µm in diameter) can settle to the bottom of

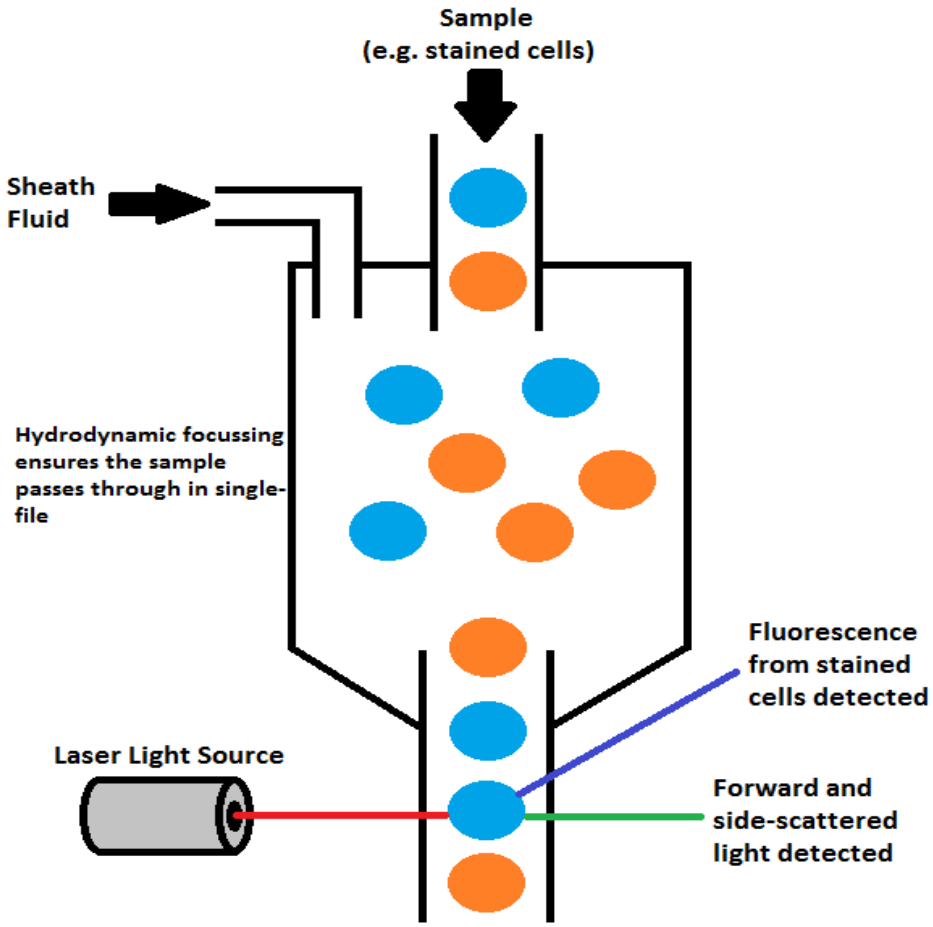

the cuvette[82].

Flow cytometry is a very high-throughput method of detecting scattered light/fluorescence of particles as they pass through the flow cell and are exposed to a laser light source, see figure 1.3 for schematic of a basic set up. Developed in the early 1970s for analysis of blood samples, flow cytometry is able to conduct particle-by-particle analysis on particles between 500 nm and 40 µm in diameter. Flow cytometry is able to provide relative concentration and size analysis using only 500 µL of sample. The detected optical signal is processed by specialised hardware and received by a computer containing software to receive and store data[85,86].

Figure 1. 2: Illustration of a general flow cytometry set-up.

By quantification of the structural features of each entity (cells, organelles, nanoparticles *et cetera*) which pass through the flow cell it is possible to distinguish and sort through many different cell types within one mixture, in addition fluorescence intensity is measured at several different wavelengths so that the quantities of specific components can be determined at once[86].

Flow cytometry has been used extensively since its development for many different biomedical applications including analysis of cell cycles, protein expression, and diagnostics. Some major diagnostic applications of flow cytometry are surface analysis of cancers, detection of HIV[87], and whole red blood cell analysis (malaria, sickle cell anaemia); however it has yet to really emerge as a POC device. One reason for this may be the large size and expense of the flow cytometer and servicing. Several laboratories have attempted to miniaturise flow cytometers and reduce their overall cost by using microfluidics[88], however this is made problematic as the components required for cell flow, excitation and detection are traditionally bulky and their alignment is critical. Additionally, the impressive throughput seen in conventional flow cytometers is somewhat compromised as the volume of interrogated sample is reduced, Di Carlo's research group at UCLA have attempted to rectify this by parallelisation[88].

Luminex is a Texas-based biotechnology company which has developed several multiplexed bead-based assays and instrumentation for the detection of target analytes building upon flow cytometry[64]. Colour-coded microbeads pass through a laser and their emitted wavelengths are measured; the microbeads are permeated with dye mixture and used as an individual label for different assays enabling vast multiplexing[89].

In order to overcome several limitations of optical sensors, pore-based devices based on the Coulter Principle are being developed.

1.5. Pore-based sensors

An emerging technology platform that is increasingly being used for biosensing is based on the Coulter Principle. The Coulter Principle allows analytes suspended in any conducting liquid to be characterised by detecting disturbances in an electric field as they pass through an opening in a non-conductive membrane. In brief, Coulter counters comprise two fluid filled chambers with an electrode in each which are separated by a single pore, as illustrated in Figure 1.4A, as objects move through the pore, the movement of ions is blocked resulting in a

transient decrease in current, known as the "resistive pulse"[90] illustrated in Figure 1.4B. Wallace Coulter identified several parameters for utilisation of this phenomenon including the requirement for conducting fluid and constraint of the electrical field so that noticeable, recordable changes in current occur with particle movement[91]. Originally developed for counting biological cells, the measurement of synthetic nanoparticles was first reported by DeBlois and Bean in the 1970s, outlining several factors which should be considered when conducting an experiment[92]. Recently there has been an increase in interest in the use of Coulter counters for characterisation of colloidal particles, DNA and proteins[93]. Technologies based on the Coulter principle are collectively known as Resistive Pulse Sensing (RPS) although they have also been known as stochastic sensing and Scanning Ion Occlusion Sensing (SIOS).

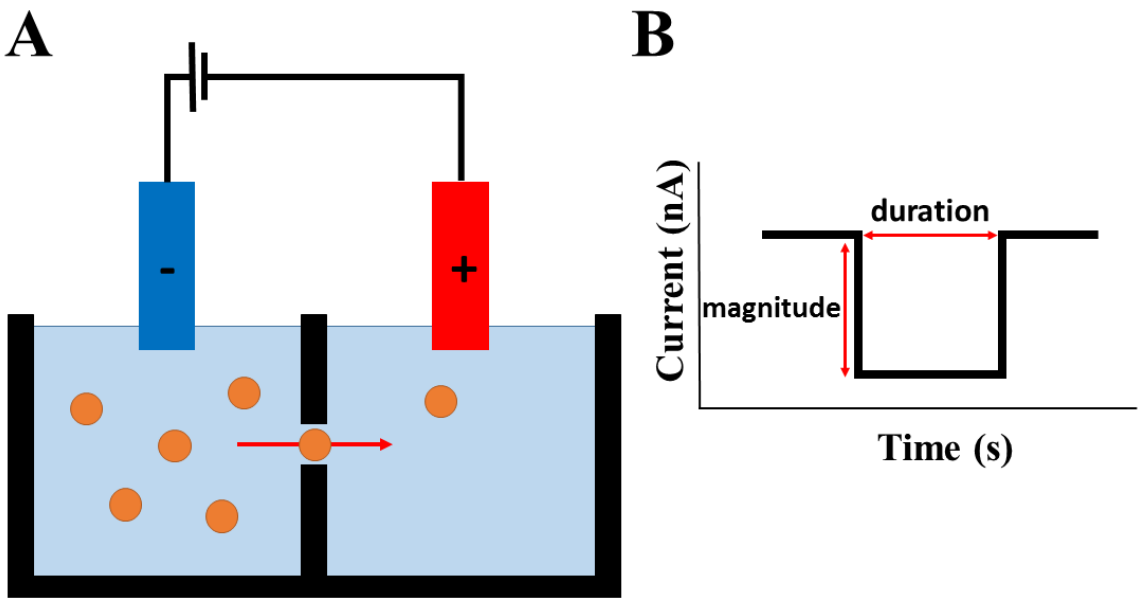

Figure 1. 4: A illustration of a generic RPS set up and B an example resistive pulse; a drop in current is observed whenever an object moves through the pore, the magnitude reflects the size of the object while the duration represents how long it takes the object to move through the pore.

The types of analyte able to be studied with RPS technology is limited by the availability of suitable pores with an appropriate size range for the analyte of interest. Since resurgence of the Coulter-counter in the mid-90s many different nanopores, in conjunction with RPS, have been explored. These include both biological and synthetic pores.

Perhaps one of the most utilised biological pores is α-haemolysin, first used in 1996 to detect single stranded DNA molecules[94]. α-haemolysin is secreted by staphylococcal bacteria to

create pores in phospholipid bilayers (cell membranes)[95,96], in normal physiology this disruption of the cell membrane causes lysis of red blood cells by allowing important molecules to uncontrollably flood out of the cell and the increased permeability to water to cause cell rupture. Improvements in synthetic biology allow researchers to purposefully create pores, using either wild-type or engineered α-haemolysin, in membranes and using a patch-clamp monitor changes in ionic current as objects move through the pore for a range of applications[97–100]. Since the detection of single-stranded DNA was demonstrated researchers have attempted to use RPS sensors to discriminate between different DNA nucleotides[90,91,101]. Towards the development of a DNA-sequencing RPS method, Vercoutere *et al.,* were able to discriminate different orientations of the terminal nucleotides of 9 base pair hair pins as they passed through an α-haemolysin pore[102], however, although current RPS technologies with biological pores are able to tell a difference between different known sequences of the same length[99], they lack the spatial and temporal resolution to read DNA base-by-base in a sequence[103]. Haemolysin pores have also been used to monitor the translocation of proteins under an applied voltage[104,105], obtain information regarding protein primary structure[98], the detection of metal ions[100] and other small molecules[106,107].

With advancements in fabrication and materials methodology myriad fixed-geometry nanopore synthesis techniques have emerged[108,109]. Synthetic nanopores are easier to manufacture at specific sizes and more stable than biological nanopores suspended in bilayers[101,108] making them highly desirable for the development of a more practical sensing device[110]. Nanopores are able to be synthesised with a range of techniques to give different features and many solid-state nanopores are now available including carbon nanotubes, nanopipettes[111,112], conical[109,110] or cylindrical pores[113], and even nanopore arrays for high-throughput sensing[108] or multiple pores in series to monitor time-dependent changes[114].

Both biological and synthetic "passive" nanopores are able to be modified to provide them with specific features to actively encourage specific ligands to enter the pore, for example aptamers to capture proteins[105], disaccharide ligands to explore multivalency[115] and the immobilisation of specific receptors within a nanopore[116].

One limitation of solid-state and biological pores is their fixed size which reduces the range of analytes able to pass through the pore and can result in irreversible blockages, requiring preparation of a new pore altogether. An alternative to solid-state nanopores, size-tunable pores have been developed which are able to be manipulated in real-time by stretching and

relaxing the pore[91]. Tunable pores are created by mechanically puncturing a thermoplastic polyurethane membrane[117] and their use in RPS technologies is currently termed Tunable Resistive Pulse Sensing (TRPS). TRPS is more versatile than solid-state RPS but there are limitations to how much each pore can be stretched or relaxed therefore pores are produced with differing optimal size ranges which determine the size of analyte able to be measured.

The iZON qNano is a Coulter-counter based device which can be used to derive information regarding particle size and the particle rate can be used to provide an estimate of particle concentration[118], recently, the qNano software has been updated to include facilities for measuring zeta-potential (ζ)[119,120]; these measurements can all be made simultaneously.

TRPS has been used for a wide range of applications including the measurement of whole cells such as bacteria[121] and viruses[122], vesicle characterisation[123,124], aptamer-based bioassays[29] and the investigation of colloidal dispersions including oil-in-water emulsions[125] and nano/micro-scale beads[119,126,127].

Yu *et al.*, applied TRPS to the measurement of bacterial growth of two strains of bacteria[121], due to the particle-by-particle analysis available with TRPS it is possible to directly count the number of cells in solution and the ability to perform real-time analysis allowed the direct measurement of bacterial growth. The concentrations found via TRPS were more similar to cell counts than OD measurements, suggesting a greater degree of accuracy[121]. This study demonstrated the use of TRPS to obtain bacterial cell counts within a matter of minutes, which represents an improvement on the plate counting method which is time-consuming and shows large variance between laboratories[128] and with greater accuracy than optical density (OD) measurements[121].

In addition to the measurement of large cells, such as bacteria, TRPS has also been applied to the quantification of much smaller viruses. While the ability to detect particles below a diameter of 100 nm is often problematic for many platforms, using TRPS Vogel *et al.*, measured and sized adenoviruses with a diameter of 95 nm with a high level of reproducibility[127] and in a more recent work was able to characterise a multidispersed bacillovirus-containing pesticide with a range of 200 nm – 2 μm[122].

TRPS has also been applied to the study of microvesicles (MVs). MV is an umbrella term for membrane particles created by budding from the phospholipid bilayer of cells under physiological and pathophysiological conditions. Originally these were seen as an artefact of

biology, however research is increasingly demonstrating that MVs may be an important part of cell signalling cascades and cellular exchange and could therefore provide new biomarkers[129–132]. MVs range in size from around 20 nm to 5 μm, currently there is no gold standard for their characterisation[133,134] and instrument-instrument variation is large due to the individual working ranges of each instrument[135]. While microscopy techniques such as SEM and TEM offer great accuracy in sizing MVs, they are limited in their use for concentration determination[81]. As MV concentration has been found to vary in several different physiological states such as hypercholesterolaemia[123], atherosclerosis[136] and even exposure to pollutants[137] determining concentration is important. Flow cytometry has been used for high-throughput analysis of MVs, however the lack of resolution below 200 nm means that many subtypes of MV may be unaccounted for, leading to an underestimate in true concentration and possibly overlooking key markers[123]. The ability to easily and quickly change pores and alter geometry using TRPS offers a significant advantage to the characterisation of MVs and the provision of particle-by-particle analysis makes TRPS ideal for counting MVs[123,138] in an unbiased manner despite their polydispersity. In reality it is likely that several techniques will need to be incorporated to generate a full picture of an MV profile due to the individual strengths and limitations of each technique for example for size and concentration determination TRPS has a good level of accuracy, but a separate technique would need to be employed to measure the molecular composition of those MVs, such as in measuring the concentration of low-density-lipoprotein (LDL) cholesterol which has been recently measured by Connolly et al (2014) to be linked to familial hypercholesterolaemia and to be a valid marker for apheresis monitoring using TRPS for MV size and concentration with flow cytometry to determine MV origin and gas chromatography with flame ionisation detection (GC-FID) used to monitor the fatty acid composition of the MVs[123]; this multifaceted approach is likely the best way to gain a full view of the vesicles being investigated, however the individual techniques used in tandem will need to be guided by the goals of research being undertaken and the individual strengths and weaknesses of each instrument.

As well as biological particles, TRPS has been demonstrated to be well suited to the size and concentration analysis of synthetic particles of a range of compositions[126,139–141] as well as the measurement of surface charge[120,125]. The interaction of nanoparticles with several analytes has also been monitored via TRPS and several bead-based bioassays have recently been developed for use in TRPS. Typically, these use beads coated with capture probes, either

antibodies or aptamers, which cause a measurable change in the configuration of the beads upon ligand binding. Several such assays use aggregation as a signal for ligand binding.

Ang and Yung developed an assay for rapid detection of single-nucleotide polymorphisms by using gold particles coated with a spliced complementary sequence to the desired DNA target which causes aggregate formation only in the presence of the correct DNA sequence, giving rise to a simple yes/no read out. The use of a size-tunable pore was particularly advantageous as the pore stretch could be increased such that only aggregates were visible above the level of baseline noise[142].

Another TRPS based aggregation assay pioneered the use of 'nanorods' to provide a signal in response to specific aptamer-analyte interactions. Nanorods are nanoparticles which are created by electrodeposition to be cylindrical rather than spherical. Unlike spherical particles, where their orientation is unknown as they pass through the pore, because rods can vary in two dimensions, both length and diameter, it is possible to elucidated nanorod orientation. In addition to this, Platt *et al.,* were able to demonstrate that aggregate formation could be controlled by differing the composition of the nanorods such that aggregates could form either end-on-end or side-on aggregates. Different aggregate orientations were discriminated via TRPS, and this could be tailored such that different ligands produced a different response allowing increased multiplexing potential[29]. This assay was found to have a femtomolar limit of detection for platelet derived growth factor (PDGF), comparable to the sensitivity of ELISAs but with significant gains in speed and simplicity[29].

1.6. Summary

Currently there is a high demand for new portable, rapid and sensitive bioassay techniques. The work outlined in this thesis attempts to create and explore new bioassays using a combination of aptamers, synthetic beads, and TRPS to create an “aptaTRPS” sensor. Aptamers are short oligonucleotide sequences which are capable of binding to a wide variety of analytes with high selectivity and specificity. When aptamers bind a target they often undergo a conformational change which has been previously monitored in emerging analytical sensors. RPS technologies are small and highly portables devices which do not require the use of gas lines and carrier fluids and have already been proven as useful for the measurement of a variety of biological and synthetic objects. It is hypothesised that by anchoring aptamers to nano or microscale beads TRPS can be used to monitor changes arising from aptamer-ligand interaction, forming the basis of this PhD Thesis.

1.6. References

(1) Atkinson, A. J.; Colburn, W. A.; DeGruttola, V. G.; DeMets, D. L.; Downing, G. J.; Hoth, D. F.; Oates, J. A.; Peck, C. C.; Schooley, R. T.; Spilker, B. A.; Woodcock, J.; Zeger, S. L. *Clin. Pharmacol. Ther.* **2001**, *69*, 89–95.

(2) Patton, J. C.; Coovadia, A. H.; Meyers, T. M.; Sherman, G. G. *Clin. vaccine Immunol.* **2008**, *15*, 388–391.

(3) De la Rica, R.; Stevens, M. M. *Nat. Nanotechnol.* **2012**, *7*, 821–824.

(4) Chan, C.; Mak, W.; Cheung, K.; Sin, K.; Yu, C.; Rainer, T.; Renneberg, R. *Annu. Rev. Anal. Chem.* **2013**, *6*, 191–211.

(5) Rang, H.; Dale, M.; Ritter, J.; Moore, P. *Pharmacology*; Hunter, L., Ed.; 5th Editio.; Churchill Livingstone: Philidelphia, 2003.

(6) Karsten, S. L.; Tarhan, M. C.; Kudo, L. C.; Collard, D.; Fujita, H. *Talanta* **2015**, 1–5.

(7) Pai, N. P.; Vadnais, C.; Denkinger, C.; Engel, N.; Pai, M. *PLoS Med.* **2012**, *9*, e1001306.

(8) Yamada, K.; Henares, T. G.; Suzuki, K.; Citterio, D. *Angew. Chemie Int. Ed.* **2015**, *54*, 5294–5310.

(9) Kaylor, R.; Yang, D.; Knotts, M. Reading device, method, and system for conducting lateral flow assays Patent Number US 8367013 B2, 2013.

(10) Leuvering, J.; Thal, J.; van der Waart, M.; Schuurs, A. *J. Immunoass. Immunochem.* **1980**, *1*, 77–91.

(11) Wang, J. *Electrochem. Sensors, Biosens. their Biomed. Appl.* **2008**, 57–69.

(12) Wang, S.; Quan, Y.; Lee, N.; Kennedy, I. R. *J. Agric. Food Chem.* **2006**, *54*, 2491–2495.

(13) Wang, X.; Li, K.; Shi, D.; Xiong, N.; Jin, X.; Yi, J.; Bi, D. *J. Agric. Food Chem.* **2007**, *55*, 2072–2078.

(14) Mens, P. F.; De Bes, H. M.; Sondo, P.; Laochan, N.; Keereecharoen, L.; Van Amerongen, a.; Flint, J.; Sak, J. R. S.; Proux, S.; Tinto, H.; Schallig, H. D. F. H. *J. Clin. Microbiol.* **2012**, *50*, 3520–3525.

(15) Corstjens, P. L. a M.; Van Lieshout, L.; Zuiderwijk, M.; Kornelis, D.; Tanke, H. J.; Deelder, A. M.; Van Dam, G. J. *J. Clin. Microbiol.* **2008**, *46*, 171–176.

(16) Rosi, N. L.; Mirkin, C. A. *Chem. Rev.* **2005**.

(17) Chiu, T.-C.; Huang, C.-C. *Aptamer-functionalized nano-biosensors.*; 2009; Vol. 9.

(18) Wei, H.; Li, B.; Li, J.; Wang, E.; Dong, S. *Chem. Commun. (Camb).* **2007**, 3735–3737.

(19) Huang, C.-C.; Huang, Y.-F.; Cao, Z.; Tan, W.; Chang, H.-T. *Anal. Chem.* **2005**, *77*, 5735–5741.

(20) Lu, A.-H.; Salabas, E. L.; Schuth, F. *Angew. Chemie* **2007**, *46*, 1222–1244.

(21) Pankhurst, Q. A.; Connolly, J.; Jones, S. K.; Dobson, J. *J. Phys. D. Appl. Phys.* **2003**, *36*, 167–181.

(22) Llandro, J.; Palfreyman, J.; Ionescu, A.; Barnes, C. *Med. Biol. Eng. Comput.* **2010**, *48*, 977–998.

(23) Wang, Y.-X. J. *Quant. Imaging Med. Surg.* **2011**, *1*, 35–40.

(24) Schleich, N.; Sibret, P.; Danhier, P.; Ucakar, B.; Laurent, S.; Muller, R. N.; Jérôme, C.; Gallez, B.; Préat, V.; Danhier, F. *Int. J. Pharm.* **2013**, *447*, 94–101.

(25) Krishnan, S.; Mani, V.; Wasalathanthri, D.; Kumar, C. V.; Rusling, J. F. *Angew. Chemie - Int. Ed.* **2011**, *50*, 1175–1178.

(26) Yigit, M. V.; Moore, A.; Medarova, Z. *Pharm. Res.* **2012**, *29*, 1180–1188.

(27) Chang, W.-S.; Shang, H.; Perera, R. M.; Lok, S.-M.; Sedlak, D.; Kuhn, R. J.; Lee, G. U. *Analyst* **2008**, *133*, 233–240.

(28) Baudry, J.; Rouzeau, C.; Goubault, C.; Robic, C.; Cohen-Tannoudji, L.; Koenig, a; Bertrand, E.; Bibette, J. *Proc. Natl. Acad. Sci. U. S. A.* **2006**, *103*, 16076–16078.

(29) Platt, M.; Willmott, G. R.; Lee, G. U. *Small* **2012**, *8*, 2436–2444.

(30) Park, S. Y.; Ko, P. J.; Handa, H.; Sandhu, A. *J. Appl. Phys.* **2010**, *107*, 09B324.

(31) Koh, I.; Hong, R.; Weissleder, R.; Josephson, L. **2009**, *81*, 3618–3622.

(32) Gubala, V.; Lynam, C. C. N.; Nooney, R.; Hearty, S.; McDonnell, B.; Heydon, K.; O'Kennedy, R.; MacCraith, B. D.; Williams, D. E. *Analyst* **2011**, *136*, 2533–2541.

(33) Chang, J.-Y.; Wu, H.; Chen, H.; Ling, Y.-C.; Tan, W. *Chem. Commun. (Camb).* **2005**, 1092–1094.

(34) Pollitt, S. K.; Pallos, J.; Shao, J.; Desai, U. a; Ma, A. A. K.; Thompson, L. M.; Marsh, J. L.; Diamond, M. I.; Francisco, S. S. *Neuron* **2003**, *40*, 685–694.

(35) Arndt, P. A.; Garratty, G. *Transfus. Med. Rev.* **2010**, *24*, 172–194.

(36) Ranzoni, A.; Schleipen, J. J. H. B.; Van Ijzendoorn, L. J.; Prins, M. W. J. *Nano Lett.* **2011**, *11*, 2017–2022.

(37) Park, S. Y.; Handa, H.; Sandhu, A. *Nano Lett.* **2010**, *10*, 446–451.

(38) Anderson, W.; Kozak, D.; Coleman, V. a; Jämting, S. K.; Trau, M. *J. Colloid Interface Sci.* **2013**, *405*, 322–330.

(39) Vander, A.; Sherman, J.; Luciano, D. *Human Physiology*; Eight Edit.; McGraw Hill: New York, 2001.

(40) Haugland, R. P. *Monoclonal antibody protocols*; Davis, W. C., Ed.; 1st Editio.; Humana Press: Totowa, New Jersey, 1995.

(41) Jayasena, S. D. *Clin. Chem.* **1999**, *45*, 1628–1650.

(42) Bunka, D. H.; Stockley, P. G. *Nat. Rev. Biotechnol.* **2006**, *4*, 588–596.

(43) Tuerk, C.; Gold, L. *Science (80-.).* **1990**, *249*, 505–510.

(44) Ellington, A. D.; Szostak, Jack, W. *Nature* **1992**, *355*, 850.

(45) Platt, M.; Rowe, W.; Knowles, J.; Day, P. J.; Kell, D. B. *Integr. Biol.* **2009**, *1*, 116–122.

(46) Platt, M.; Rowe, W.; Wedge, D. C.; Kell, D. B.; Knowles, J.; Day, P. J. *Anal. Biochem.* **2009**, *390*, 203.

(47) Knight, C. G.; Platt, M.; Rowe, W.; Wedge, D. C.; Khan, F.; Day, P. J.; McShea, A.; Knowles, J.; Kell, D. B. *Nucleic Acids Res.* **2009**, *37*.

(48) Kraemer, S.; Vaught, J. D.; Bock, C.; Gold, L.; Katilius, E.; Keeney, T. R.; Kim, N.; Saccomano, N. a; Wilcox, S. K.; Zichi, D.; Sanders, G. M. *PLoS One* **2011**, *6*, e26332.

(49) Gold, L.; Ayers, D.; Bertino, J.; Bock, C.; Bock, A.; Brody, E. N.; Carter, J.; Dalby, A. B.; Eaton, B. E.; Fitzwater, T.; Flather, D.; Forbes, A.; Foreman, T.; Fowler, C.; Gawande, B.; Goss, M.; Gunn, M.; Gupta, S.; Halladay, D.; Heil, J.; Heilig, J.; Hicke, B.; Husar, G.; Janjic, N.; Jarvis, T.; Jennings, S.; Katilius, E.; Keeney, T. R.; Kim, N.; Koch, T. H.; Kraemer, S.; Kroiss, L.; Le, N.; Levine, D.; Lindsey, W.; Lollo, B.; Mayfield, W.; Mehan, M.; Mehler, R.; Nelson, S. K.; Nelson, M.; Nieuwlandt, D.; Nikrad, M.; Ochsner, U.; Ostroff, R. M.; Otis, M.; Parker, T.; Pietrasiewicz, S.; Resnicow, D. I.; Rohloff, J.; Sanders, G.; Sattin, S.; Schneider, D.; Singer, B.; Stanton, M.; Sterkel, A.; Stewart, A.; Stratford, S.; Vaught, J. D.; Vrkljan, M.; Walker, J. J.; Watrobka, M.; Waugh, S.; Weiss, A.; Wilcox, S. K.; Wolfson, A.; Wolk, S. K.; Zhang, C.; Zichi, D. *PLoS One* **2010**, *5*, e15004.

(50) Jeong, S. H.; Kim, C. S.; Yang, J. *BioChip J.* **2010**, *4*, 141–147.

(51) Eulberg, D.; Klussmann, S. *Chembiochem* **2003**, *4*, 979–983.

(52) Cho, E. J.; Lee, J.-W.; Ellington, A. D. *Annu. Rev. Anal. Chem. (Palo Alto. Calif).* **2009**, *2*, 241–264.

(53) Chiu, T.-C.; Huang, C.-C. *Aptamer-functionalized nano-biosensors.*; 2009; Vol. 9.

(54) O'Sullivan, C. K. *Anal. Bioanal. Chem.* **2002**, *372*, 44–48.

(55) Stojanovic, M. N.; de Prada, P.; Landry, D. W. *J. Am. Chem. Soc.* **2001**, *123*, 4928–4931.

(56) Mayer, G. *Angew. Chem. Int. Ed. Engl.* **2009**, *48*, 2672–2689.

(57) Yamamoto, R.; Kumar, P. K. R. *Genes to Cells* **2000**, *5*, 389–396.

(58) Gopinath, S. C. B.; Misono, T. S.; Kumar, P. K. R. *Crit. Rev. Anal. Chem.* **2008**, *38*, 34–47.

(59) Nutiu, R.; Li, Y. *J. Am. Chem. Soc.* **2003**, *125*, 4771–4778.

(60) Stojanovic, M. N.; Prada, P. De; Landry, D. W. **2000**, *122*, 11547–11548.

(61) Jhaveri, S. D.; Kirby, R.; Conrad, R.; Maglott, E. J.; Bowser, M.; Kennedy, R. T.; Glick, G.; Ellington, A. D. *J. Am. Chem. Soc.* **2000**, *122*, 2469–2473.

(62) E. Wang, R.; Zhang, Y.; Cai, J.; Cai, W.; Gao, T. *Curr. Med. Chem.* **2011**, *18*, 4175–4184.

(63) Nutiu, R.; Li, Y. *Methods* **2005**, *37*, 16–25.

(64) Giri, S.; Sykes, E.; Jennings, T.; Chan, W. *ACS Nano* **2011**, *5*, 1580–1587.

(65) Walling, M. a; Novak, J. a; Shepard, J. R. E. *Int. J. Mol. Sci.* **2009**, *10*, 441–491.

(66) Liu, J.; Lu, Y. *Nat. Protoc.* **2006**, *1*, 246–252.

(67) Wu, Y.; Liu, L.; Zhan, S.; Wang, F.; Zhou, P. *Analyst* **2012**, *137*, 4171–4178.

(68) Tombelli, S.; Minunni, M.; Mascini, M. *Biosens. Bioelectron.* **2005**, *20*, 2424–2434.

(69) Toh, S. Y.; Citartan, M.; Gopinath, S. C. B.; Tang, T.-H. *Biosens. Bioelectron.* **2015**, *64*, 392–403.

(70) Hong, P.; Li, W.; Li, J. *Sensors (Basel).* **2012**, *12*, 1181–1193.

(71) Green, L. S.; Jellinek, D.; Jenison, R.; Östman, A.; Heldin, C. H.; Janjic, N. *Biochemistry* **1996**, *35*, 14413–14424.

(72) Gokulrangan, G.; Unruh, J. R.; Holub, D. F.; Ingram, B.; Johnson, C. K.; Wilson, G. S. *Anal. Chem.* **2005**, *77*, 1963–1970.

(73) Dieckmann, T.; Suzuki, E.; Nakamura, G.; Feigon, G. *RNA* **1996**, *2*, 628–640.

(74) Gold, L.; Polisky, B.; Uhlenbeck, O.; Yarus, M. *Annu. Rev. Biochem.* **1995**, *64*, 763–797.

(75) Farokhzad, O. C.; Cheng, J.; Teply, B. a; Sherifi, I.; Jon, S.; Kantoff, P. W.; Richie, J. P.; Langer, R. *Proc. Natl. Acad. Sci. U. S. A.* **2006**, *103*, 6315–6320.

(76) Nonaka, Y.; Abe, K.; Ikebukuro, K. *Electrochemistry* **2012**, *80*, 363–366.

(77) Song, S.; Wang, L.; Li, J.; Fan, C.; Zhao, J. *TrAC Trends Anal. Chem.* **2008**, *27*, 108–117.

(78) Yoo, S. M.; Kim, D.-K.; Lee, S. Y. *Talanta* **2015**, *132*, 112–117.

(79) Smith, K.; Oatley, C. *Br. J. Appl. Phys.* **1955**, *6*, 391–399.

(80) Pease, R.; Nixon, W. *J. Sci. Instrum.* **1965**, *42*, 81–85.

(81) Gaumet, M.; Vargas, A.; Gurny, R.; Delie, F. *Eur. J. Pharm. Biopharm.* **2008**, *69*, 1–9.

(82) Filipe, V.; Hawe, A.; Jiskoot, W. *Pharm. Res.* **2010**, *27*, 796–810.

(83) Du, S.; Kendall, K.; Morris, S.; Sweet, C. *J Chem Technol Biotechnol* **2010**, *85*, 1223–1228.

(84) Pecora, R. **2000**, 123–131.

(85) Weaver, J. *Methods* **2000**, *21*, 199–201.

(86) Nunez, R. *Flow cytometry for research scientists: principles and applications*; 2001.

(87) McSharry, J. J. *Clin. Microbiol. Rev.* **1994**, *7*, 576–604.

(88) Hur, S. C.; Tse, H. T. K.; Di Carlo, D. *Lab Chip* **2010**, *10*, 274–280.

(89) Luminex assays: overview http://www.panomics.com/products/luninex-assays/technical-overview/overview (accessed Jan 31, 2013).

(90) Wanunu, M. *Phys. Life Rev.* **2012**, *9*, 125–158.

(91) Kozak, D.; Anderson, W.; Vogel, R.; Trau, M. *Nano Today* **2011**, *6*, 531–545.

(92) DeBlois, R. W.; Bean, C. P. *J. Colloid Interface Sci.* **1977**, *61*, 323–335.

(93) Henriquez, R. R.; Ito, T.; Sun, L.; Crooks, R. M. *Analyst* **2004**, *129*, 478–482.

(94) Kasianowicz, J. J.; Brandin, E.; Branton, D.; Deamer, D. W. *Proc. Natl. Acad. Sci. U. S. A.* **1996**, *93*, 13770–13773.

(95) König, B.; Ludwig, a; Goebel, W.; König, W. *Infect. Immun.* **1994**, *62*, 4611–4617.

(96) Wiseman, G. M. *Bacteriol. Rev.* **1975**, *39*, 317–344.

(97) Braha, O.; Walker, B.; Cheley, S.; Kasianowicz, J. J.; Song, L.; Gouaux, J. E.; Bayley, H. *Chem. Biol.* **1997**, *4*, 497–505.

(98) Nivala, J.; Marks, D. B.; Akeson, M. *Nat. Biotechnol.* **2013**, 1–5.

(99) Meller, a; Nivon, L.; Brandin, E.; Golovchenko, J.; Branton, D. *Proc. Natl. Acad. Sci. U. S. A.* **2000**, *97*, 1079–1084.

(100) Braha, O.; Gu, L. Q.; Zhou, L.; Lu, X.; Cheley, S.; Bayley, H. *Nat. Biotechnol.* **2000**, *18*, 1005–1007.

(101) Branton, D.; Deamer, D. W.; Marziali, A.; Bayley, H.; Benner, S. a; Butler, T.; Di Ventra, M.; Garaj, S.; Hibbs, A.; Huang, X.; Jovanovich, S. B.; Krstic, P. S.; Lindsay, S.; Ling, X. S.; Mastrangelo, C. H.; Meller, A.; Oliver, J. S.; Pershin, Y. V; Ramsey, J. M.; Riehn, R.; Soni, G. V; Tabard-Cossa, V.; Wanunu, M.; Wiggin, M.; Schloss, J. a. *Nat. Biotechnol.* **2008**, *26*, 1146–1153.

(102) Vercoutere, W. a.; Winters-Hilt, S.; DeGuzman, V. S.; Deamer, D.; Ridino, S. E.; Rodgers, J. T.; Olsen, H. E.; Marziali, A.; Akeson, M. *Nucleic Acids Res.* **2003**, *31*, 1311–1318.

(103) Ivanov, A. P.; Instuli, E.; McGilvery, C. M.; Baldwin, G.; McComb, D. W.; Albrecht, T.; Edel, J. B. *Nano Lett.* **2011**, *11*, 279–285.

(104) Cheley, S.; Xie, H.; Bayley, H. *ChemBioChem* **2006**, *7*, 1923–1927.

(105) Rotem, D.; Jayasinghe, L.; Salichou, M.; Bayley, H. *J. Am. Chem. Soc.* **2012**, *134*, 2781–2787.

(106) Cheley, S.; Gu, L. Q.; Bayley, H. *Chem. Biol.* **2002**, *9*, 829–838.

(107) Fennouri, A.; Przybylski, C.; Pastoriza-gallego, M.; Bacri, L.; Auvray, L.; Daniel, R. *ACS* **2012**, 9672–9678.

(108) Dela Torre, R.; Larkin, J.; Singer, A.; Meller, A. *Nanotechnology* **2012**, *23*, 385308.

(109) Lan, W. J.; Holden, D. a.; Liu, J.; White, H. S. *J. Phys. Chem. C* **2011**, *115*, 18445–18452.

(110) Sexton, L. T.; Horne, L. P.; Martin, C. R. *Mol. Biosyst.* **2007**, *3*, 667–685.

(111) Wang, Y.; Kececi, K.; Mirkin, M.; Mani, V.; Sardesai, N.; Rusling, J. *Chem. Sci.* **2013**, *4*, 655–663.

(112) Gong, X.; Patil, A. V; Ivanov, A. P.; Kong, Q.; Gibb, T.; Dogan, F.; deMello, A. J.; Edel, J. B. *Anal. Chem.* **2014**, *86*, 835–841.

(113) Han, Y.; Wu, H.; Liu, F.; Cheng, G.; Zhe, J. *Anal. Chem.* **2014**, *86*, 9717–9722.

(114) Wu, Y.; Benson, J. D.; Critser, J. K.; Almasri, M. *J. Micromechanics Microengineering* **2010**, *20*, 085035.

(115) Howorka, S.; Nam, J.; Bayley, H.; Kahne, D. *Angew. Chemie - Int. Ed.* **2004**, *43*, 842–846.

(116) Wei, R.; Gatterdam, V.; Wieneke, R.; Tampé, R.; Rant, U. *Nat. Nanotechnol.* **2012**, *7*, 257–263.

(117) Sowerby, S. J.; Broom, M. F.; Petersen, G. B. *Sensors Actuators, B Chem.* **2007**, *123*, 325–330.

(118) Davenport, M.; Healy, K.; Pevarnik, M.; Teslich, N.; Cabrini, S.; Morrison, A. P.; Siwy, Z. S.; Létant, S. E. *ACS Nano* **2012**, *6*, 8366–8380.

(119) Kozak, D.; Anderson, W.; Vogel, R.; Chen, S.; Antaw, F.; Trau, M. *ACS Nano* **2012**, *6*, 6990–6997.

(120) Vogel, R.; Anderson, W.; Eldridge, J. J.; Glossop, B.; Willmott, G. R. *Anal. Chem.* **2012**, *84*, 3125–3131.

(121) Yu, A. C. S.; Loo, J. F. C.; Yu, S.; Kong, S. K.; Chan, T. F. *Appl. Microbiol. Biotechnol.* **2014**, *98*, 855–862.

(122) Roberts, G. S.; Yu, S.; Zeng, Q.; Chan, L. C. L.; Anderson, W.; Colby, A. H.; Grinstaff, M. W.; Reid, S.; Vogel, R. *Biosens. Bioelectron.* **2012**, *31*, 17–25.

(123) Connolly, K. D.; Willis, G. R.; Datta, D. B. N.; Ellins, E. A.; Price, D. A.; Guschina, I. A.; Rees, D. A.; James, P. E. *J. Lipid Res.* **2014**, *55*, 2064–2072.

(124) Szabó, G. T.; Tarr, B.; Pálóczi, K.; Éder, K.; Lajkó, E.; Kittel, Á.; Tóth, S.; György, B.; Pásztói, M.; Németh, A.; Osteikoetxea, X.; Pállinger, É.; Falus, A.; Szabó-Taylor, K.; Buzás, E. I. *Cell. Mol. Life Sci.* **2014**, *71*, 4055–4067.

(125) Somerville, J. a; Willmott, G. R.; Eldridge, J.; Griffiths, M.; McGrath, K. M. *J. Colloid Interface Sci.* **2013**, *394*, 243–251.

(126) Willmott, G. R.; Platt, M.; Lee, G. U. *Biomicrofluidics* **2012**, *6*, 14103–1410315.

(127) Vogel, R.; Willmott, G.; Kozak, D.; Roberts, G. S.; Anderson, W.; Groenewegen, L.; Glossop, B.; Barnett, A.; Turner, A.; Trau, M. *Anal. Chem.* **2011**, *83*, 3499–3506.

(128) Lumley, M.; Burgess, R.; Billingham, L.; McDonald, D.; Milligan, D. *Br. J. Haematol.* **1997**, *May*, 481–484.

(129) Skog, J.; Wurdinger, T.; Rijn, S. Van; Meijer, D.; Gainche, L.; Sena-esteves, M.; Jr, W. T. C.; Carter, R. S.; Krichevsky, A. M.; Breakefield, X. O. *Nat. Cell Biol.* **2012**, *10*, 1470–1476.

(130) Meng, Y.; Kang, S.; Fishman, D. a. *Cancer Immunol. Immunother.* **2005**, *54*, 807–814.

(131) Lima, L. G.; Chammas, R.; Monteiro, R. Q.; Moreira, M. E. C.; Barcinski, M. a. *Cancer Lett.* **2009**, *283*, 168–175.

(132) Grange, C.; Tapparo, M.; Collino, F.; Vitillo, L.; Damasco, C.; Deregibus, M. C.; Tetta, C.; Bussolati, B.; Camussi, G. *Cancer Res.* **2011**, *71*, 5346–5356.

(133) Momen-Heravi, F.; Balaj, L.; Alian, S.; Tigges, J.; Toxavidis, V.; Ericsson, M.; Distel, R. J.; Ivanov, A. R.; Skog, J.; Kuo, W. P. *Front. Physiol.* **2012**, *3*, 354.

(134) Momen-Heravi, F.; Balaj, L.; Alian, S.; Trachtenberg, A. J.; Hochberg, F. H.; Skog, J.; Kuo, W. P. *Front. Physiol.* **2012**, *3*, 162.

(135) Van der Pol, E.; Coumans, F. a W.; Grootemaat, a E.; Gardiner, C.; Sargent, I. L.; Harrison, P.; Sturk, a; van Leeuwen, T. G.; Nieuwland, R. *J. Thromb. Haemost.* **2014**, *12*, 1182–1192.

(136) Burton, J. O.; Hamali, H. a; Singh, R.; Abbasian, N.; Parsons, R.; Patel, A. K.; Goodall, A. H.; Brunskill, N. J. *PLoS One* **2013**, *8*, e72663.

(137) Emmerechts, J.; Jacobs, L.; Van Kerckhoven, S.; Loyen, S.; Mathieu, C.; Fierens, F.; Nemery, B.; Nawrot, T. S.; Hoylaerts, M. F. *J. Thromb. Haemost.* **2012**, *10*, 96–106.

(138) Van der Pol, E.; Coumans, F.; Varga, Z.; Krumrey, M.; Nieuwland, R. *J. Thromb. Haemost.* **2013**, *11 Suppl 1*, 36–45.

(139) Willmott, G. R.; Vogel, R.; Yu, S. S. C.; Groenewegen, L. G.; Roberts, G. S.; Kozak, D.; Anderson, W.; Trau, M. *J. Phys. Condens. Matter* **2010**, *22*, 454116.

(140) Willmott, G. R.; Moore, P. W. *Nanotechnology* **2008**, *19*, 475504.

(141) Willmott, G. R.; Parry, B. E. T. *J. Appl. Phys.* **2011**, *109*, 094307.

(142) Ang, Y. S.; Yung, L.-Y. L. *ACS Nano* **2012**, *6*, 8815–8823.

Chapter Two

Theory

2.1. Introduction

As discussed in Chapter One, the aims of the work detailed in this thesis are to generate and explore new bioassay techniques using a combination of aptamers, particles, and tunable resistive pulse sensing (TRPS). Chapter two provides an overview of general theory relevant to these aims and used across all chapters. Additional detailed theory is included in each chapter where relevant.

2.2. Aptamers

Aptamers are short lengths of single stranded deoxyribonucleic acid (DNA), ribonucleic acid (RNA) or a synthetic alternative known as xenonucleic acid (XNA) which contains the same bases but is resistant to polymerase due to a different backbone. The experiments discussed in this thesis all utilise DNA aptamers, hence, from this point only DNA aptamers shall be discussed in detail. DNA is composed of four nitrogenous bases known as nucleotides. These can be divided into the purines adenine (A) and guanine (G), and the pyrimidines thymine (T) and cytosine (C). In DNA these are bonded to deoxyribose sugar and phosphate to form a unit termed a nucleoside. The nucleoside bases are joined covalently by phosphodiester bonds to form long polymer chains[1].

In the presence of a specific target these sequences undergo 3D conformational changes to cause binding in a lock and key fashion – this is known as induced fit binding[2–5]. Binding between the aptamer and target is dependent on structural compatibility, stacking of aromatic rings, hydrogen bond formation, and electrostatic and Van der Waals interactions[6]. For many aptamers the highly anionic oligonucleotide backbone interacts with positive residues on target proteins and is a strong factor in bringing the aptamer into the proximity of the binding site[7]. Because the binding mechanisms of aptamers are specific to each target, only aptamers used in the research undertaken will be discussed in detail.

Since the generation of an anti-thrombin aptamer in 1992[8], thrombin has been widely utilised in aptasensors and its mechanism widely studied[9,10]. The first aptamer to thrombin was described by Bock *et al.*, and is 15 base pairs long (termed thrombin-15) with the sequence 5'-GGT TGG TGT GGT TGG-3'[8] which has been adapted several times and used in many proof-of-concept aptasensor studies[9,11]. In the presence of thrombin, aptamers containing the sequence motif "GGNNGGNGNGGNNGG" (where N represents T or A) undergo a conformational change to form a G-quadruplex structure[11–13], illustrated in Figure 2. 3, which

has been found by circular dichroism spectroscopy to occur only in the presence of thrombin, implying that there is involvement of the induced fit binding mechanism[14,15].

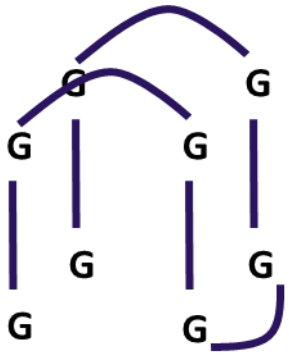

Figure 2. 3: Illustration of an example G-quadruplex structure.

Aptamers to growth factors have also been generated for both therapeutic and diagnostic interests[16]. Vascular endothelial growth factor (VEGF) is one such protein for which aptamers have been generated. Aptamer VEa5 (also denoted as aHt[7] or $VEap_{165}$[17] in the literature) with the sequence 5'-ATA CCA GTC TAT TCA ATT GGG CCC GTC CGT ATG GTG CTG GCC AC-3' binds to the heparin binding domain of $VEGF_{165}$ via the formation of stem-loop structures and electrostatic interactions[7,17,18]. In contrast, aptamer V7t1 with the sequence 5'-TGT GGG GGT GGA CGG GCC GGG TAG A-3' has been generated to the receptor binding domain of VEGF and is currently thought to bind by the formation of a G-quadruplex. However, the G-quadruplex formed here is specific to VEGF and does not interact with other quadruplex-binding targets, such as thrombin[19]. Platelet derived growth factor (PDGF) has also been detected using a high-affinity aptamer with the sequence: 5' CAG GCT ACG GCA CGT AGA GCA TCA CCA TGA TCC TG-3'[20–23] which forms a secondary structure characterised by three double-stranded DNA hairpins[20,21].

2.3. Particles

2.3.1. Superparamagnetic particles

Magnetic nanoparticles can be utilised to separate analytes from solution and perform washing or pre-concentration steps, as such it is important to consider their properties. In its most basic form, magnetism refers to forces of attraction and repulsion between objects produced by electric charge and fundamental magnetic moments of atoms. However, there are in fact several different types of magnetism, some of which will be addressed here.

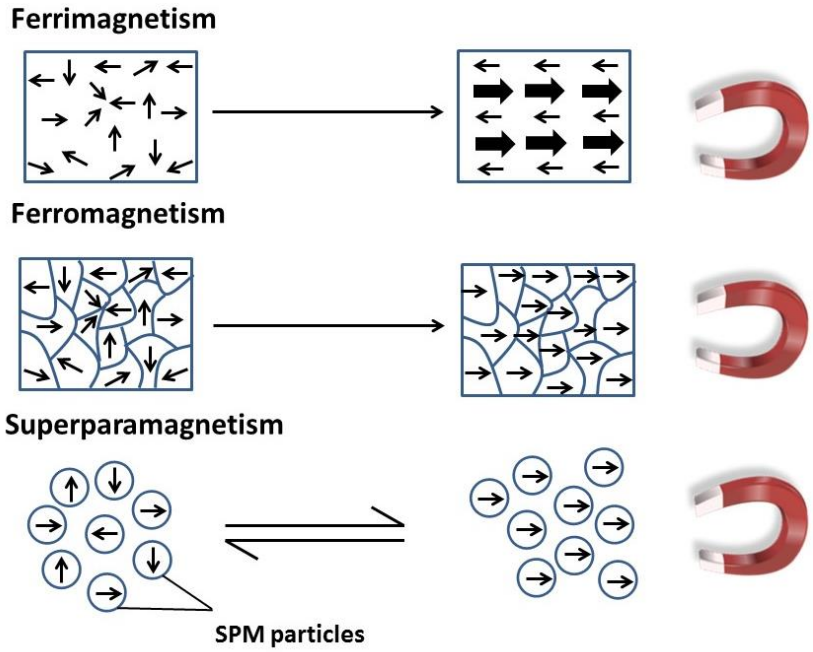

Figure 2. 4: Illustration of ferrimagnetic, ferromagnetic, and superparamagnetic materials and their response to an external magnetic field.

Both ferro- and ferri-magnetic materials are capable of becoming permanent magnets in the presence of an external magnetic force[24]. These materials contain several "domains", separated by thin domain walls[25]. When an external magnetic field is applied to a ferromagnetic material, the domains rotate to align in the direction of the magnetic field and the material is drawn to the magnet, as demonstrated in Figure 2. 4. In ferrimagnetic materials, the magnetic moments of the atoms are opposing; however these opposing moments are unequal, allowing for spontaneous magnetisation. According to the Néel theory of ferrimagnetism, ferrimagnetism is reported to be a consequence of non-identical magnetic substructures within the material and negative interactions between them[26], as illustrated in Figure 2. 4.

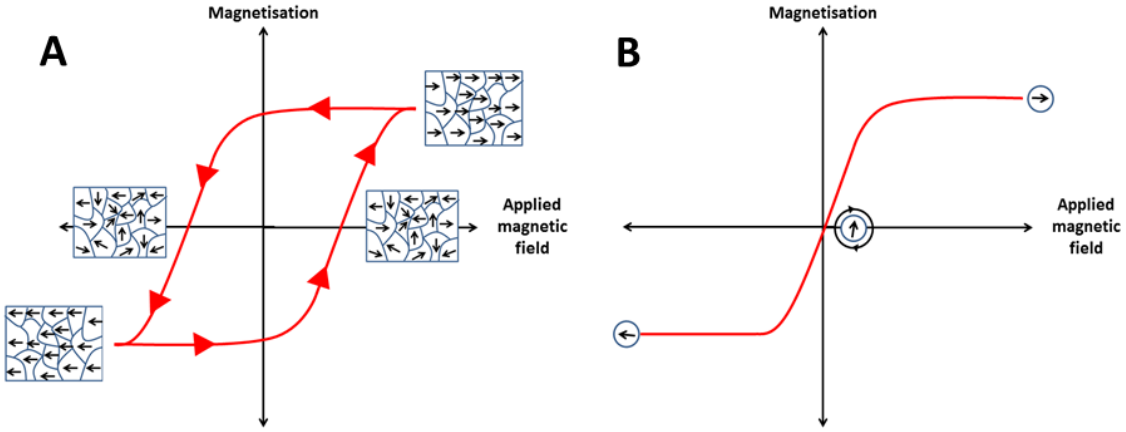

Figure 2. 5: Example hysteresis loops for a ferromagnetic material (A) and a paramagnetic particle (B) at room temperature.

While ferro- and ferrimagnetic materials would separate from solution by being attracted to a magnetic, they are subject to effects of hysteresis[24] whereby magnetisation is retained. Hysteresis is perhaps best described via the hysteresis loop in Figure 2. 5A which shows that a ferromagnetic material requires application of a reversed magnetic field, an increase in temperature, or a lengthy time period before the material returns to a non-magnetic state. Hysteresis is believed to be due to a "pinning" of the domains on defects in the crystal lattice structure within the material, preventing the domains from relaxing into a random orientation[27,28] as such they need more energy to overcome the barrier to moment reversal. If such materials were used in magnetic separation, this would lead to an inability to redisperse the particles unless subjected to an opposing magnetic field or increased temperature – which may disturb any target analytes. Hence, in order to use magnetic particles for washing and extraction it is important that they return to a non-magnetised, separated state in which they do not aggregate together and can be analysed.

Paramagnetic particles display no hysteresis at room temperature, making them useful materials for magnetic separation. By reducing the size of the particles of a ferri- or ferromagnetic material to that of a single domain, typically tens of nanometers[29,30], they become superparamagnetic (SPM) due to the fact that the domains are no longer pinned as described above, which can rotate freely to align with an external field and are not pinned on crystal lattice defects as there are no domain walls to move[24,30,31] while displaying both a higher magnetic saturation, and a steeper gradient of magnetic susceptibility. As presented in the hysteresis curve Figure 2. 5B, SPM particles do not display any hysteresis at room temperature[32]. In addition, the energy required for them to lose their magnetism is reduced,

allowing the SPM domains to separate at room temperature and rotate back to random orientations once the external magnetic field has been removed, as displayed in equations 2. 1 and 2. 2.

$$\tau = \tau_0 \exp\left(\frac{\Delta E}{K_B T}\right) \quad \textbf{2. 1}$$

$$\Delta E = KV \quad \textbf{2. 2}$$

Where τ is the relaxation time, ΔE is the energy barrier to moment reversal, K_B is Boltzmann's constant, T is temperature, K is the anisotropy energy density and V is the volume of the particle. Hence, reducing the volume of the particle reduces the energy barrier to moment reversal and for sufficiently small particles ΔE is comparable to K_B at room temperature and the particles can separate[24].

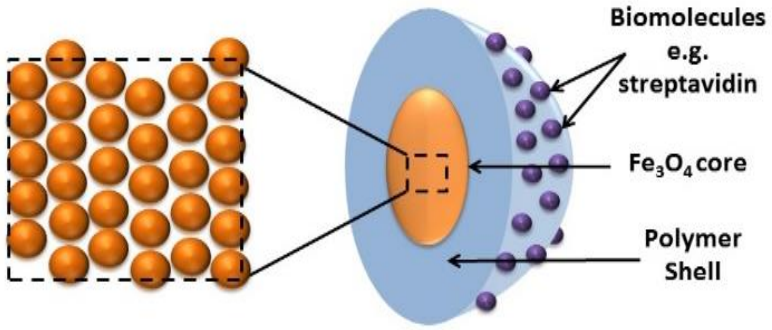

Figure 2. 6: Illustration of an example cross-section for a superparamagnetic bead coated with streptavidin. The inner Fe_3O_4 core is composed of many sub-100 nm individual superparamagnetic particles.

By using SPM particles, it is possible to separate them from solution and remove/replace buffer or pre-concentrate a sample and then remove the magnet and allow the particles to disperse by Brownian motion. These particles can be tagged with biomolecules that can selectively capture chosen targets in solution and confounding proteins can be removed via magnetic separation[33,34].

The SPM beads used in the experiments in this thesis are composed of a core containing many individual single-domain iron oxide particles, as displayed in Figure 2. 6. In the presence of an external magnetic field, all of the single SPM domains inside the bead align and they are drawn toward the magnet, allowing the SPM beads to precipitate on the side of an eppendorf and facilitating wash stages as illustrated in Figure 2. 7. Larger particles contain

a greater number of SPM cores therefore move toward the magnet more quickly due to the higher iron oxide content compared with smaller particles as expected from equation

2. 3 below:

$$F = \frac{V.\Delta\chi}{\mu_0}(B.\nabla)B \qquad \textbf{2. 3}$$

Where *F* is the force on a magnetic particle inside a magnetic field, *V* is the volume of the particle, Δχ is the difference in susceptibility between the particle and surrounding buffer solution, μ is the magnetic permeability and *B* is the magnetic field strength. As such, as volume of the magnetic material increases, so does the force acting upon it, leading to a faster separation.

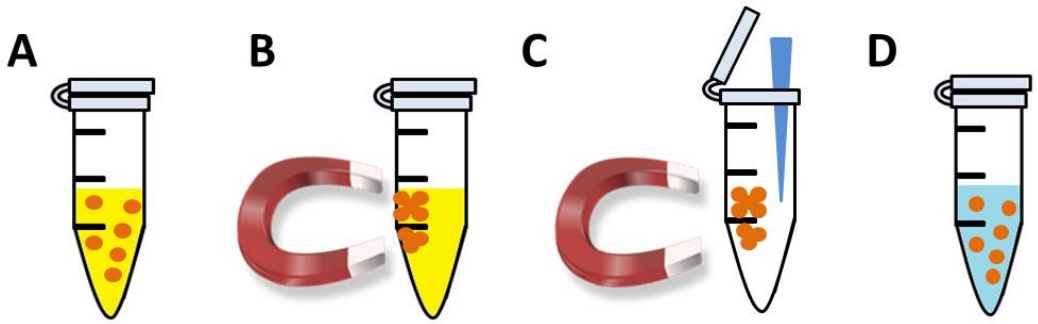

Figure 2. 7: Schematic displaying the operation of magnetic separation. A = SPM particles functionalised with capture probes are dispersed into the sample. B = a hand-held magnet is introduced and a pellet forms on the side of the container, bringing with it any captured target molecules. C = any fluid is carefully pipetted out and discarded (or saved for further analysis). D = particles are then suspended in clean buffer solution prior to analysis.

Once the magnet is removed, the atomic moments of the particles rotate into a random orientation and the magnetism is lost allowing the beads to disperse by Brownian motion. These particles can be modified with capture probes, such as aptamers and antibodies, and used to extract targets from solution, as displayed schematically.

2.3.2. Colloidal systems

The term “colloid” is used to refer to a dispersion of small particles of one material in another medium which does not settle under gravity[35]. These systems occur naturally in many biological products and can be created synthetically with wide variety in composition. A sol suspension is the term for solid particles dispersed in a liquid medium[36], for example, synthetic nano- or microparticles dispersed in an electrolyte buffer as used in the course of this thesis. For many applications the stability of colloids is key as either aggregation or complete dispersion might be required for differing tasks[36] and stability over time is often highly sought after[37]. A major factor in determining the stability of colloidal systems is the electric charge on the particle surfaces[35]; the level of stability is able to be measured via the ζ potential.

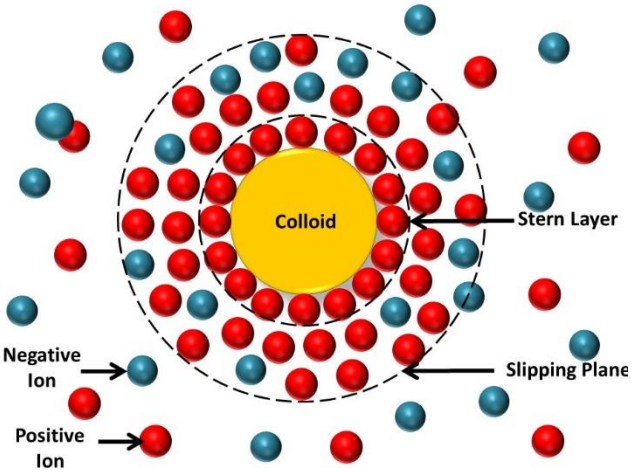

Figure 2. 8: Illustration describing the double layer of a negative particle

The net charge at the particle’s surface affects the distribution of ions in the surrounding medium. This results in an increased concentration of counter ions, forming an electrical double layer. The structure of the double layer comprises the Stern layer of stationary ions and a diffuse layer which is loosely bonded. Within the diffuse layer is a hydrodynamic layer known as the slipping plane or plane of shear[35,38].

ζ-potential is a function of the surface charge and is used as a measure of the electrokinetic potential in colloidal systems. ζ-potential (mV) refers to the potential difference between the stationary layer of ions surrounding the particle and the surrounding medium at the point of the slipping plane, see Figure 2. 8. If the ζ-potential is high, the repulsive forces between the

particles are greater and the colloid is described as highly stable, if the ζ-potential is low the particles are likely to form agglomerates (the forces of attraction overcome those of repulsion)[38].

It is important to consider the effect of the chosen buffer upon the stability and mobility of the dispersion. The movement of a solid colloidal particle in a stationary liquid under and applied electric field is known as electrophoresis. The electrophoretic mobility, μ, of a colloid is related to the ζ potential of the particle[36,37] as expressed in the following equations:

$$\mu = \frac{qD}{K_B T} \qquad \textbf{2. 4}$$

$$\zeta = \frac{\eta \mu}{\varepsilon} \qquad \textbf{2. 5}$$

Where q is the effective charge, D is the diffusion coefficient, K_B is Boltzmann's constant, T is temperature, η is the viscosity of the buffer solution and ε is the dielectric constant of the solution[39].

The charge of the particle is heavily dependent on the composition of the surrounding medium, and in buffers close to the isoelectric point (pI) of the particle the colloid loses stability and aggregates as the repulsive electrostatic forces between particles is diminished[37]. The isoelectric point of an object is the pH at which the particle has no net charge (i.e. it is overall neutral because the sum of positively charged species is equal to the sum of negatively charge species) due to the reduction or addition of protons. At pH above the pI of the particle the net charge is negative, while at pH below the pI have a net positive charge.

In addition to pH of the buffer it is important to consider ionic strength. Electrophoretic and electrostatic behaviour of colloids is largely controlled by the properties of the Stern and diffuse layers surrounding the particle[37,40]. The thickness of the diffuse layer is governed by the ionic strength of the chosen electrolyte and has a non-zero value that is estimated as the inverse value of the Debye parameter, κ, which is provided by the following equation:

$$\kappa = F \sqrt{\frac{2I}{\mathcal{E}RT}} \qquad \textbf{2. 6}$$

Where F is the Faraday constant, R is the gas constant, and I is the ionic strength[41]. As demonstrated by this equation, as ionic strength increases, the thickness of the diffuse layer

decreases, reducing drag and increasing mobility[42]. These are important considerations for systems where colloid behaviour under an applied electric field is observed and appropriate electrolytes must be somewhat carefully chosen.

2.4. Resistive Pulse Sensing

Modern Resistive Pulse Sensors (RPS) can be traced back to the Coulter Counter developed in the 1950s by Walter H Coulter. These devices are based on the "Coulter Principle" which describes the use of an electric field to count particles that are suspended in an electrolyte solution[43]. These devices were originally applied to the counting of the rapid and large-scale counting of blood cells, a practice which previously required laborious and time-consuming manual counting of immobilised cells with microscopy. Since then many different adaptations of Coulter counters have been developed with a wide range of targets including both synthetic and biological colloids.

A recent adaption to RPS based on these principles includes the incorporation of a conical elastomeric pore which is able to be mechanically stretched or relaxed in real time, this adaptation is known as Tunable Resistive Pulse Sensing (TRPS) developed by Izon Science, Oxford. The qNano is the commercially available instrument developed by Izon Sciences for TRPS and consists of an upper and lower fluid cell, separated by a non-conductive, flexible membrane with a singular central pore, and stretching apparatus[39,44,45]. The pores developed for use in TRPS are generated by puncturing 200 μm thick thermoplastic polyurethane (TPU) membranes with a tungsten needle, giving rise to an approximately conical pore[39,46].

The basic operation of RPS devices is as follows: two fluid filled chambers are separated by a single pore in a non-conductive membrane. Electrodes in each fluid chamber are used to establish a current across the pore. Resistance in a conical pore is determined by the conductivity of the electrolyte used and pore dimensions as described by equation 2. 7 below[39]:

$$R = \frac{4\rho L}{\pi AB} \qquad \textbf{2. 7}$$

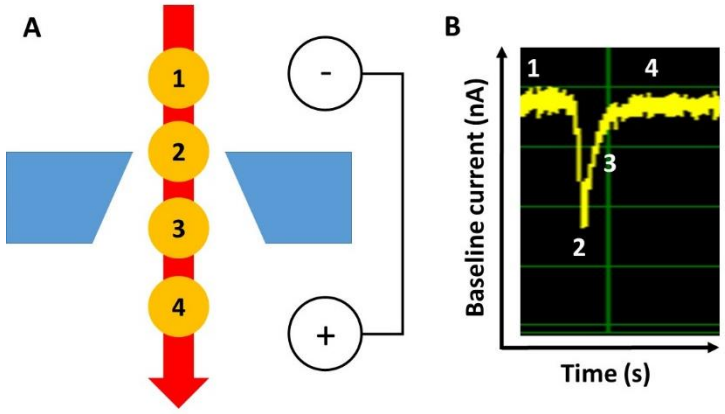

Figure 2. 9: (A) schematic representation of a particle traversing the pore opening. (B) Example resistive pulse observed with a conical pore annotated with reference to the particle position during the resistive pulse in (A).

Where ρ is the resistivity of the electrolyte, L is pore length, A is the small pore opening radius and B is the large pore opening radius. Ohm's law can then be applied to calculate the ionic current, i_p, at a given applied potential where V=iR, where R is resistance, providing a baseline current. When a particle moves through the pore this results in a local increase in resistance resulting in a so-called "resistive pulse" as the current transiently decreases until the object has passed through the pore as shown schematically in Figure 2. 9.

The conical shape of the pores used in TRPS give rise to an asymmetric resistive pulse shape, as resistance is highest at the narrowest part of the pore there is a sharp initial decrease in current which then tails back toward the initial baseline current as the object moves through the widening pore.

The magnitude of the resistive pulse, Δi_p, is dependent upon the volume of electrolyte displaced by the particle as it moves the pore and can be used to determine the dimensions of an object by its individual resistive pulse by the following equation 2. 8[22,47]:

$$\frac{\Delta i_p}{i_p} = \frac{S(d_p, d_s)(d_s^3)}{l_p(0.8d_p)(d_p^2)} \qquad \textbf{2. 8}$$

Where d_p is pore diameter, d_s is particle diameter, l_p is pore length and $S(d_p,d_s)$ is a correction factor that depends on the relative values of both the pore and particle diameters[22]. This estimation is applied to cylindrical pores but has been demonstrated to hold a good degree of accuracy for attaining particle size using conical pores[44]. As is apparent from equation 2. 8 the magnitude of the resistive pulse is dependent on the relationship between the dimensions of the particle and the pore orifice such that a smaller pore is able to analyse smaller particles.

This is especially important in the context of tunable pores as they are able to be tuned in real time to increase or decrease the pulse magnitude so that pulses are visible above the level of baseline noise and so that blockages do not occur.

In addition to finding particle size, TRPS can be used to find particle concentration. Particle concentration is related to the frequency of resistive pulses as particles move through the pore. Particle velocity (V_S) through the pore is determined by the sum of the forces of pressure driven flow (V_P), electrophoretic mobility of the particle (V_{EP}), electroosmosis (V_{EO}), and diffusion effects (V_D) as described in equation 2. 9 below[47]:

$$V_s = V_P + V_{EP} + V_{EO} + V_D$$
$$= \frac{d_p^2}{32\eta l_{p'}}\Delta P + \frac{\mu}{l_{p'}}E + \frac{\varepsilon\zeta pore}{4\pi\eta l_{p'}}E + \frac{D_S}{l_{p'}C}C \qquad \textbf{2. 9}$$

Where η is the solution viscosity, $l_{p'}$ is the length of the pore after a correction factor for end effects = $l_p + 0.8d_p$, ΔP is the pressure across the pore, μ is the electrophoretic mobility of the particle, E is the applied electric field, ε is the solution dielectric constant, ζ_{pore} is the zeta potential of the pore surface, D_S is the diffusion coefficient of the particle, and C is the particle concentration[47].

If particle concentration is already known using TRPS under fixed conditions it is possible to use resistive pulse frequency, *J*, to elucidate the surface charge of a colloid using the Nernst-Planck approach in the following equation[48,49]:

$$\frac{J}{C} = \varepsilon\frac{(\zeta_{particle} - \zeta_{pore})}{\eta}E + \frac{Q_p}{A} \qquad \textbf{2. 10}$$

Where Q_p is pressure driven flow, and A is the diameter of the narrowest pore constriction. As is apparent from equation 2. 10 the ζ-potential (or surface charge) of the particle is a factor in determining rate as alterations to zeta potential will subsequently alter the electrophoretic mobility of the particles as described earlier in equation 2. 5.

2.4.1. Theory of Operation

The instrument most associated with TRPS is the qNano, manufactured by Izon Sciences, Oxford. Similar to standard RPS, two fluid reservoirs are separated by a single pore which are filled with a conducting electrolyte buffer. In the qNano, the pore is mounted horizontally with reservoirs above and below the pore membrane, as displayed in Figure 2. 10. As stated previously, the qNano uses an elastic size-tunable pore which is fabricated in a thermoplastic polyurethane (TPU) membrane. The membranes are penetrated with a needle to create a single pore which is conically shaped[46]. The size and geometry of the fabricated aperture can be modified by modifying the puncturing needle thus allowing the detection of particles

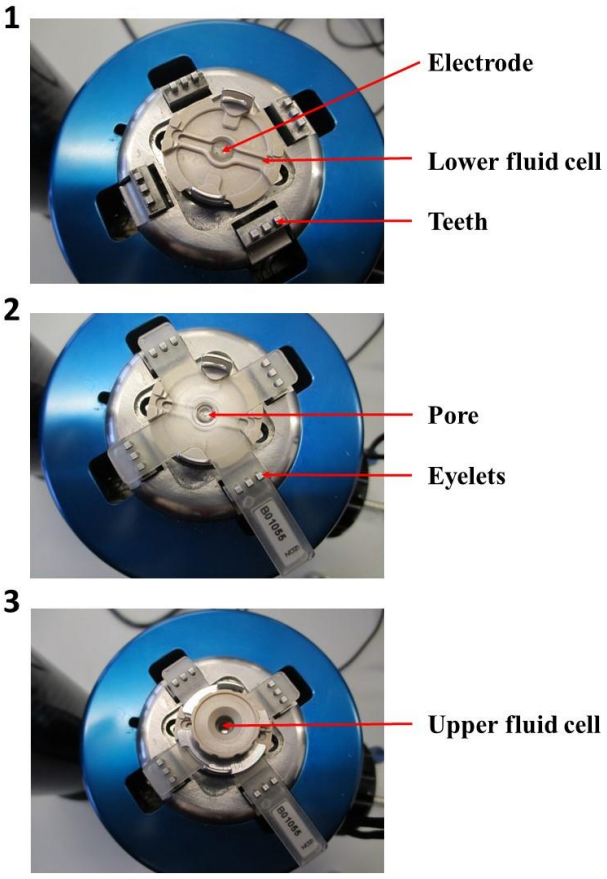

ranging from 50 nm to 10 µm over the full range of manufactured pores[50]. The cruciform pore is mounted by eyelets to teeth on the instrument, above the lower fluid cell, the system can be seen in figure 2.8. The arms can be altered to increase the stretch on the pore, where it

Figure 2. 10: Schematic showing the setup of the TRPS device. **1** birds-eye view of the lower fluid cell, this channel holds 75 – 80 µL of electrolyte buffer and contains an electrode. **2** the pore is mounted laterally to the device by eyelets on the pore being hooked to teeth on the instrument – these teeth are able to be moved apart or closer together, stretching or relaxing the pore respectively. **3** the upper fluid cell is fitted to the instrument securely, and a 40 µL sample is pipetted into it. **4** side-view of a particle traversing the conical pore and an illustration of the resultant asymmetric current trace.

has been shown that applying a stretch of 10 mm to the membrane increases the pore opening by 54%[45].

The setup of TRPS is relatively simple. Firstly, the pore is attached to the instrument as shown in figure 2.8 and the desired pore stretch is applied by separation of the teeth on the instrument (>41 mm, 41 being the smallest distance between the teeth applying no stretch to the membrane), the electrolyte is then carefully pipetted into the lower fluid cell under the pore (75 µl). Care needs to be taken to ensure no bubbles are introduced into the electrolyte, if bubbles do occur the electrolyte needs to be replaced. If no bubbles are present, the upper fluid cell can be placed on top and twisted into place. The electrolyte solution can then be placed into the upper fluid cell (40 µl). A faraday cage is placed over the fluid cell to reduce background noise and the system is switched on using the Izon Control Suite software. Upon the application of a voltage a stable baseline should be observed. Once a stable baseline is apparent, the electrolyte can be removed from the upper fluid cell and a sample introduced. Once the sample has been introduced the stretch applied to the pore can be fine-tuned so that the blockades produced by the sample are visible above the level of baseline noise. When stretch is increased, resistance through the pore decreases, represented by a current increase likewise, if the current were to decrease suddenly that may be indicative of a blockage in the pore as the pore orifice is occluded.

Unlike solid state pores where the size of the pore is always known, the tunable pore must first be characterised before the size of the analyte can be accurately measured using TRPS. This is done using calibration beads of a known size and must be done prior to sample analysis and under the same conditions. As stated above in equation 2.8, Δi_p is proportional to the volume of the object moving through the pore, by using a reference sample of known diameter beads with narrow size distribution, the Δi_p of an unknown sample can be calibrated with the reference sample to obtain the measured diameter. The same principal can be applied to particle concentration whereby a reference sample of known concentration can be measured to provide a baseline rate and because rate is proportional to concentration, stated in equation 2.9, it is possible to elucidate concentration from the rate of an unknown sample. Due to the fact that a number of factors, such as surface charge, can alter particle rate through the pore, to attain an accurate calibration it is necessary for a pressure to be applied to overcome the forces of electroosmosis and electrophoretic mobility[39,44,45,51].

The amount of pressure applied is based on the variable pressure module (VPM) used in conjunction with the Izon qNano. The VPM has a mobile 'arm' with a scale of 0-20 pressure units. The amount of pressure applied is relative to the length of the arm impacting on the system. For example, if the arm is inserted 5 cm into the system, a pressure of '5 cmH_2O' is applied. For a negative pressure, or vacuum, the length the arm is pulled out is equivalent to the magnitude of pressure applied and is denoted as '-5 cmH_2O', for example. Each cm of pressure is equivalent to approximately 1000 Pa. For greater precision the VPM is also able to operate from 0 – 20 mmH_2O.

2.5. References

1 B. Hames and N. Hooper, in *Biochemistry 2nd edition*, ed. B. Hames, BIOS Scientific Publishers Ltd, Oxford, Second., 2000, pp. 147–151.

2 Y. Yang, M. Kochoyan, P. Burgstaller, E. Westhof and M. Famulok, *Science*, 1996, **272**, 1343–1347.

3 P. Burgstaller, M. Kochoyan and M. Famulok, *Nucleic Acids Res.*, 1995, **23**, 4769–4776.

4 T. Dieckmann, E. Suzuki, G. Nakamura and G. Feigon, *RNA*, 1996, **2**, 628 – 640.

5 F. Jiang, R. A. Kumar, R. A. Jones and D. J. Patel, *Nature*, 1996, **382**, 183–186.

6 R. Stoltenburg, C. Reinemann and B. Strehlitz, *Biomol. Eng.*, 2007, **24**, 381–403.

7 I. Kanakaraj, W.-H. Chen, M. Poongavanam, S. Dhamane, L. J. Stagg, J. E. Ladbury, K. Kourentzi, U. Strych and R. C. Willson, *Int. J. Biol. Macromol.*, 2013, **57**, 69–75.

8 L. C. Bock, L. C. Griffin, J. A. Latham, E. H. Vermaas and J. J. Toole, *Nature*, 1992, **355**, 564–566.

9 E. J. Cho, J.-W. Lee and A. D. Ellington, *Annu. Rev. Anal. Chem. (Palo Alto. Calif).*, 2009, **2**, 241–64.

10 H. Ma, J. Liu, M. M. Ali, M. A. I. Mahmood, L. Labanieh, M. Lu, S. M. Iqbal, Q. Zhang, W. Zhao and Y. Wan, *Chem. Soc. Rev.*, 2015, **44**, 1240–1256.

11 B. Deng, Y. Lin, C. Wang, F. Li, Z. Wang, H. Zhang, X. Li and X. C. Le, *Anal. Chim. Acta*, 2014, **837**, 1–15.

12 M. Platt, W. Rowe, D. C. Wedge, D. B. Kell, J. Knowles and P. J. Day, *Anal. Biochem.*, 2009, **390**, 203.

13 R. F. Macaya, P. Schultze, F. W. Smith, J. A. Roet and J. Feigon, 1993, **90**, 3745–3749.

14 P.-H. Lin, R.-H. Chen, C.-H. Lee, Y. Chang, C.-S. Chen and W.-Y. Chen, *Colloids Surfaces B Biointerfaces*, 2011, **88**, 552–558.

15 P. H. Lin, S. L. Yen, M. S. Lin, Y. Chang, S. R. Louis, A. Higuchi and W. Y. Chen, *J. Phys. Chem. B*, 2008, **112**, 6665–6673.

16 D. H. Bunka and P. G. Stockley, *Nat. Rev. Biotechnol.*, 2006, **4**, 588 – 596.

17 Y. Nonaka, K. Abe and K. Ikebukuro, *Electrochemistry*, 2012, **80**, 363–366.

18 H. Hasegawa, K. Sode and K. Ikebukuro, *Biotechnol. Lett.*, 2008, **30**, 829 – 834.

19 Y. Nonaka, K. Sode and K. Ikebukuro, *Molecules*, 2010, **15**, 215–25.

20 L. S. Green, D. Jellinek, R. Jenison, A. Östman, C. H. Heldin and N. Janjic, *Biochemistry*, 1996, **35**, 14413–14424.

21 X. Fang, Z. Cao, T. Beck and W. Tan, *Anal. Chem.*, 2001, **73**, 5752–5757.

22 M. Platt, G. R. Willmott and G. U. Lee, *Small*, 2012, **8**, 2436–44.

23 K. Deng, Y. Xiang, L. Zhang, Q. Chen and W. Fu, *Anal. Chim. Acta*, 2013, **759**, 61 – 65.

24 Q. A. Pankhurst, J. Connolly, S. K. Jones and J. Dobson, *J. Phys. D. Appl. Phys.*, 2003, **36**, 167–181.

25 R. M. Bozorth, *Rev. Mod. Phys.*, 1947, **19**, 29 – 86.

26 J. S. Smart, *Am. J. Phys.*, 1955, **23**, 356.

27 D. C. Jiles and D. L. Atherton, *IEEE Trans. Magn.*, 1983, **19**, 2183–2185.

28 D. C. Jiles and D. L. Atherton, *J. Magn. Magn. Mater.*, 1986, **61**, 48–60.

29 Y. Todaka, M. Nakamura, S. Hattori, K. Tsuchiya and M. Umemoto, *Bull. Inst. Chem. Res.*, 2003, **44**, 34–39.

30 A.-H. Lu, E. L. Salabas and F. Schuth, *Angew. Chemie*, 2007, **46**, 1222–1244.

31 W. F. Brown, *Phys. Rev.*, 1963, **130**, 1677–1686.

32 N. a. Usov and Y. B. Grebenshchikov, *J. Appl. Phys.*, 2009, **106**, 023917.

33 J. Muzard, M. Platt and G. U. Lee, *Small*, 2012, **8**, 2289.

34 J. J. O'Mahony, M. Platt, D. Kilinc and G. U. Lee, *Langmuir*, 2013, **29**, 2546–2553.

35 P. Atkins and J. De Paula, *Atkins' Physical Chemistry*, Oxford University Press, Oxford, 9th Editio., 2010.

36 W. Norde, *Colloids and Interfaces in Life Sciences*, CRC press an inprint of Taylor and Francis Group, Boca Raton, 2nd editio., 2011.

37 C. Felix, a. Yaroshchuk, S. Pasupathi, B. G. Pollet, M. P. Bondarenko, V. I. Kovalchuk and E. K. Zholkovskiy, *Adv. Colloid Interface Sci.*, 2014, **211**, 77–92.

38 J. Olivier and P. Sennet, *Ind. Eng. Chem.*, 1965, **57**, 34–50.

39 G. R. Willmott, R. Vogel, S. S. C. Yu, L. G. Groenewegen, G. S. Roberts, D. Kozak, W. Anderson and M. Trau, *J. Phys. Condens. Matter*, 2010, **22**, 454116.

40 A. J. Bard and L. R. Faulkner, *Electrochemical methods: fundamental and applications*, John Wiley & Sons Inc., 2nd editio., 2001.

41 P. Debye and E. Huckel, *Phys. Zeitschrift*, 1924, **24**, 185 – 206.

42 R. W. O'Brien and L. R. White, *J. Chem. Soc. Faraday Trans. 2*, 1978, **74**, 1607.

43 T. Ito, L. Sun and R. M. Crooks, *Anal. Chem.*, 2003, **75**, 2399–406.

44 R. Vogel, G. Willmott, D. Kozak, G. S. Roberts, W. Anderson, L. Groenewegen, B. Glossop, A. Barnett, A. Turner and M. Trau, *Anal. Chem.*, 2011, **83**, 3499–506.

45 D. Kozak, W. Anderson, R. Vogel and M. Trau, *Nano Today*, 2011, **6**, 531–545.

46 S. J. Sowerby, M. F. Broom and G. B. Petersen, *Sensors Actuators, B Chem.*, 2007, **123**, 325–330.

47 R. R. Henriquez, T. Ito, L. Sun and R. M. Crooks, *Analyst*, 2004, **129**, 478–482.

48 R. Vogel, W. Anderson, J. J. Eldridge, B. Glossop and G. R. Willmott, *Anal. Chem.*, 2012, **84**, 3125–3131.

49 R. B. Schoch, J. Han and P. Renaud, *Rev. Mod. Phys.*, 2008, **80**, 839–883.

50 G. S. Roberts, S. Yu, Q. Zeng, L. C. L. Chan, W. Anderson, A. H. Colby, M. W. Grinstaff, S. Reid and R. Vogel, *Biosens. Bioelectron.*, 2012, **31**, 17–25.

51 G. S. Roberts, D. Kozak, W. Anderson, M. Broom, R. Vogel and M. Trau, *Small*, 2010, **6**, 2653 – 2658.

Chapter Three

Attachment of DNA to nanoscale beads and detection via TRPS

3.1. Abstract:

In order to create a TRPS-based biosensor, it is first necessary to have reliable methods of aptamer immobilisation and a means of detecting when the aptamers have been successfully immobilised. As such, the work discussed in this chapter sought to establish a method for the confirmation of successful DNA conjugation to the surface of nano- and micro-scale synthetic beads using TRPS following either conjugation via biotin-avidin linkage or EDC coupling chemistry. When DNA is added to the surface of beads by either method, the mobility of the beads increase as their negative surface charge is increased, this is visible as a signal in TRPS in both an increase in rate and decrease in Full Width Half Maximum (FWHM) representing an increase in mobility. Following confirmation that a detectable change in signal is observable when DNA is successfully bound to the beads using TRPS, the impact of factors including bead diameter and mass, in addition to DNA length and hybridisation of DNA complements on TRPS measurements were explored.

3.2. Introduction:

To develop an aptamer-based biosensor using TRPS it will be necessary to confirm the presence of aptamer on the surface of beads. Ideally, this measurement should also be able to be performed using TRPS to reduce the need for additional instrumentation, reagents, and time. DNA is composed of a negatively charged sugar-phosphate back bone and a combination of purine and pyramidine bases. When the negatively charged DNA is attached to the surface of the beads, this should lead to an increase in overall surface charge and an increase in electrophoretic mobility, visible as an increase in rate as discussed in chapter two and described in equation 2.9.

Two methods for immobilising DNA onto a beads surface have been chosen for investigation. First, the use of commercially available streptavidin coated superparamagnetic beads (SPBs) was explored. Oligonucleotide sequences are able to be synthesised with functional groups at either end; modification with biotin is now routinely offered from many custom oligonucleotide services; by fuctionalising one end of the DNA or RNA sequence the direction of immobilisation is consistent, in the case of an aptamer this is important to allow the binding motif to interact with the target. The streptavidin-biotin complex is the strongest known non-covalent interaction with a high affinity (K_d, = 10^{-15} M)[1] between a protein and a ligand. The bond between biotin and avidin is formed rapidly and is robust against pH, temperature and solvent exposure. Biotin is a relatively small molecule (244.3 daltons), as such it can be conjugated with many molecules without significantly altering biological activity. Streptavidin, in particular, is isolated from *streptomyces avidinii*[2]; this is more expensive to produce than avidin itself, but displays a lower degree of non-specific binding which is an important consideration in the development of a bioassay. The use of streptavidin coated beads and biotin tags, while reliable, does hold several limitations. Beads coated with streptavidin are more expensive and are available from fewer suppliers than carboxyl-latex beads. In addition, because the attachment of beads to biotinylated DNA is protein based there is a reduced shelf life and reduced stability in comparison to the use of carboxyl groups and amine modified DNA.

Secondly, an additional method of conjugating DNA sequences to beads explored was to use beads with carboxyl functional groups and amine functionalised aptamer sequences. As such, it was necessary to determine the presence of DNA on carboxyl beads which are already negatively charged.

3.3. Method:

3.3.1. Chemicals and reagents

The following chemicals were purchased from Sigma Aldrich, UK, without any further purification unless otherwise stated: Phosphate Buffered Saline (PBS – P4417), Tween 20 (P1379) and MES (2-[N-morpholino]ethane sulphonic acid) hydrate (M2933). EDC (1-ethyl-3-[3-dimethylaminopropyl]carbodiimide hydrochloride) was purchased from Thermo Scientific (22981). Water purified to a resistivity of 18.2 MΩ was used to make all solutions unless otherwise specified.

DNA sequences were purchased as lyophilised powders with HPLC purification, the following were sourced from Entelchon, Germany: 5'GGT TGG TGT GGT TGG TTT TTT TTT T-Biotin-3' (Thrombin-15 with 10 T spacer)[3] and 5'TGG GAG TAG GTT GGT GTG GTT GGG GCT CCC CTT TTT-Biotin-3' (Thrombin-MArray)[4]. The sequences 5' GGT TGG TGT GTT TGG TTT TTT TTT T-Amine-3' (Amine Thrombin 15), 5'GTT TGG TTT ATT TTA CTA GTG GCC AGG-Biotin-3' (ThrombinEvol)[5], a random biotin-tagged decamer, and 3'CCA ACC ACA CCA ACC 5' (target) a complementary sequence to Thrombin-15 were purchased from Sigma Aldrich's custom oligonucleotide service. These were made up to a stock concentration of 100 pmol/μL.

Streptavidin modified superparamagnetic beads of 120 nm (Bioadembeads streptavidin plus, 03211) and 300 nm (Bioadembeads streptavidin, 0.3130) in diameter were purchased from Ademtech (France). The following carboxyl beads of known diameter and concentration were purchased from Izon Sciences, UK: CPC100B (mode diameter 115 nm, 1×10^{13} beads/mL); SKP200B (mode diameter 203 nm, 1×10^{11} beads/mL); SKP400D (mode diameter 335 nm, 7×10^{10} beads/mL); CPC800C (mode diameter 750 nm, 9.5×10^{10} beads/mL). Dynabeads® MyOne™ carboxylic acid (650.12) were sourced from Invitrogen Dynal. All beads were diluted in 1 × PBST (0.05% tween 20).

3.3.2. Immobilisation of DNA

3.3.2.1. Streptavidin coated beads and biotinylated DNA

The supplied beads were first vortexed and sonicated to ensure monodispersity. 120 nm streptavidin coated beads were diluted to a concentration of approximately 3×10^9 beads/mL for use as a stock. To 40μL of beads a further 10μL of varied ratios of PBST and aptamer

dilutions was added to provide a range of final concentrations from 0.1nM up to 10 000nM of DNA. These were vortexed and placed on a rotary wheel for 30 minutes at room temperature prior to analysis.

3.3.2.2. Investigation of DNA hybridisation on the surface of beads

120nm beads were diluted in PBST to a concentration of 3×10^9 beads/mL to a volume of 2 mL. From this initial stock 8×200 µL samples were removed to separate clean vials. To each a varying amount of biotinylated Thrombin-15 was added to give a concentration range of 10 nM up to 210 nM, a range guided by the results of the first experiment. These samples were vortexed then placed on a rotary wheel for 30 minutes at room temperature after which time they were centrifuged for 2 minutes at 10 000 rpm and placed on a MagRack (Life Sciences). After 5 minutes a visible dark brown pellet had formed on the side of the vial adjacent to the magnet. The solution was carefully pipetted out and the beads resuspended in 200 µL of fresh PBST. This wash stage was carried out twice to remove any excess DNA. The samples were then analysed using the Izon qNano.

To each 200 µL sample 10 µL of the complementary DNA target was added at a concentration of 10 µM to provide a total concentration of 500 nM. The samples were vortexed and placed on a rotary wheel for 30 minutes. The samples were washed twice as described above and then analysed with the Izon qNano.

3.3.2.3. Attachment of DNA to carboxylated beads

45 µL of the bead stocks were diluted in MES hydrate buffer adjusted to pH 6 to a total volume of 450 µL. EDC was made up to 10 mg/mL concentration in MES hydrate buffer. 50 µL of 10 mg/mL EDC was then added to the 450 µL of beads. 4.5 nmol of the Amine-terminated DNA sequence was then added and the beads were left on a rotary wheel at room temperature for 2 hours. Following the incubation, the bead solution was removed from the rotary wheel and centrifuged for 5 minutes at 13 400 rpm at which point a white pellet had formed at the bottom of the vial. Any liquid was carefully pipetted out and the beads were resuspended in 450 µL of PBST, vortexed for 1 minute and sonicated for 1 minute. This procedure was repeated 3 times.

3.3.3. Tunable Resistive Pulse Sensing (TRPS) measurement

All measurements were performed with the Izon qNano system, purchased from Izon Sciences, UK, which incorporates the fluid cell, stretching apparatus, data recording and analysis software (Izon Control Suite). Pores are supplied by the manufacturer each with an optimal size range for analysis. For the measurement of CPC100 beads an np100 (size range 70 – 200 nm) was selected at 47 mm stretch; for 120 nm SPM beads an np200 (size range 100 – 400 nm) was used at a stretch of 44.50 mm and fixed applied voltage of 0.4 V, SKP400 beads were measured with an np400 (size range 200 – 400 nm) pore with 47 mm applied stretch and both CPC800s and Dynabeads MyOne were analysed with an np1000 (size range 500 – 2000 nm) pore and 45.25 and 47 mm applied stretch, respectively. 80 µL of PBS was pipetted into the lower fluid cell ensuring that no bubbles were present and 40 µL of PBST into the upper fluid cell. Initially a stretch of 47 mm was applied across the pore and a voltage applied which gave a baseline current of between 80 and 120 nA. Once a stable baseline was established the sample could be introduced and the applied stretch and voltage adjusted so that peaks were visible above the level of baseline noise (≤ 10 pA), once the appropriate stretch and voltage were established these conditions were maintained across all measurements. Typically, a bandwidth filter of 1 kHz was applied during measurements.

To analyse carboxylated beads they were first calibrated under a pressure of 2 cmH_20 to attain the sample concentration following EDC conjugation chemistry. A sample of carboxyl beads which had not undergone EDC chemistry was then diluted to the same concentration. Sample concentrations were then matched in line with the manufacturer's specifications for each pore used and both samples were then analysed under several voltages to give a baseline range of 30 to 130 nA for the pore being used. This range represents the working range of the instrument.

3.4. Results and Discussion:

3.4.1. Detection of DNA on particles: monitoring rate against DNA concentration

The first experiment modified the streptavidin coated beads with the biotinylated DNA of different lengths. Initially a 10-fold excess of biotinylated Thrombin-15 above the reported binding capacity of the beads was added to ensure that all the free binding sites were occupied. The beads were incubated at room temperature for 30 minutes before placing the sample in the TRPS instrument for measurement. During each experiment the pore stretch, ionic strength of the buffer, and applied voltage was constant. The applied voltage always had a positive bias applied to the electrode in the lower fluid cell underneath the pore, this orientation makes it easier to observe negatively charged beads[6]. Two distinct changes in signal were apparent upon the binding of the thrombin-15 aptamer to the beads. The first was an increase in rate from around 50 to 400 beads per minute, and the second was a decrease in FWHM values from 1.2 ms to 0.3 ms. These changes were expected from equation 2.7 which states that the surface charge and electrophoretic mobility contributes to the rate at which beads move through the pore. To demonstrate that these effects were dependent on the quantity of DNA immobilised on the bead surface, a series of experiments was performed where the concentration of DNA added was increased, the results for which are displayed in

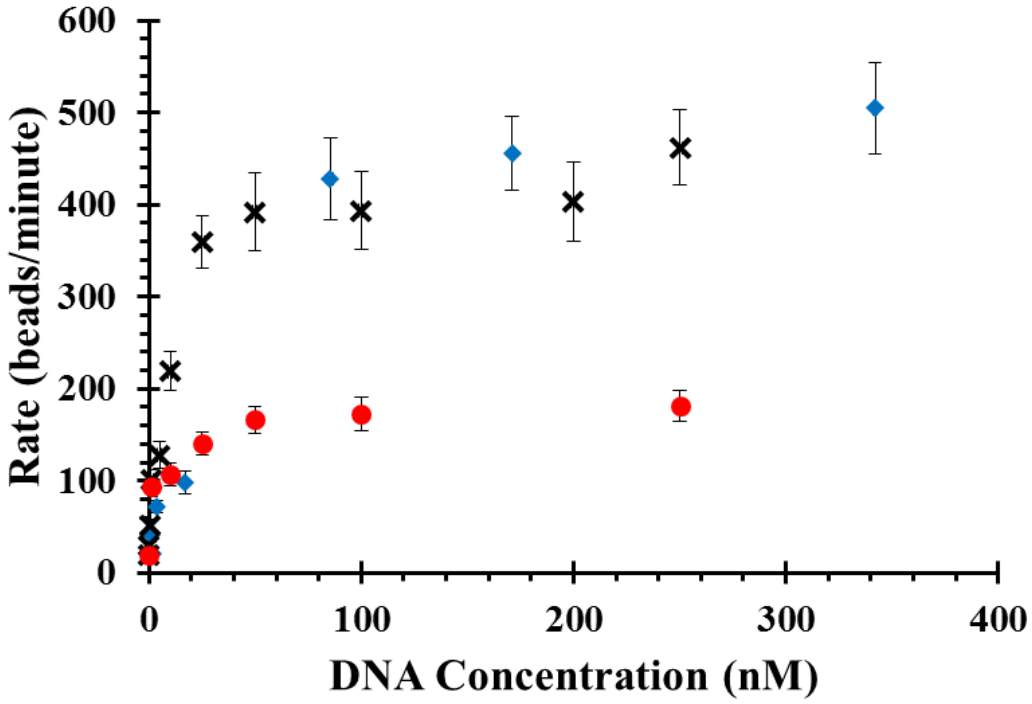

Figure 3. 1: Scatter plot displaying average rate against increasing concentrations of Thrombin-15 (black crosses), Thrombin-MArray (blue diamonds), or a random decamer (red circles), for each data set n = 3.

Figure 3. 1 and Figure 3. 2**.**

As the concentration of DNA increases, and thus the coverage on the bead surfaces, the FWHM and rate decrease and increase respectively until a steady value is obtained. This experiment was then repeated with a longer thrombin aptamer, termed Thrombin-MArray, and a short 10-nucleotide long random sequence.

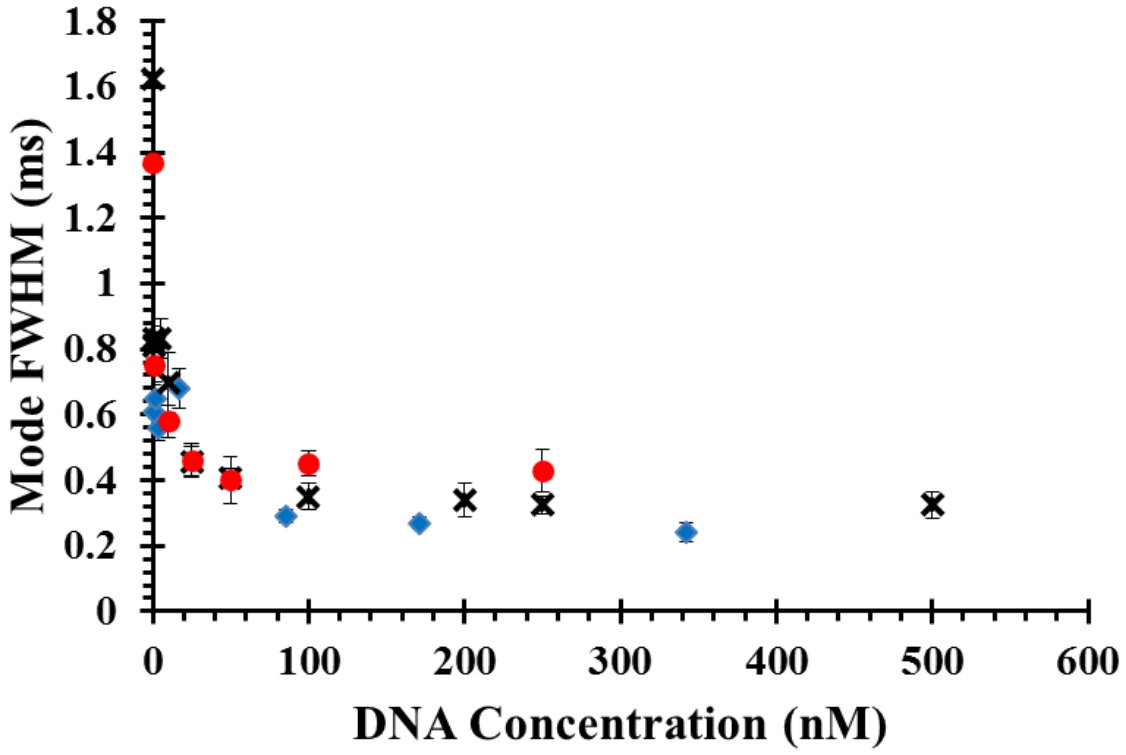

Figure 3. 2: Scatter plot displaying mode FWHM against increasing concentrations of Thrombin-15 (black crosses), Thrombin-MArray (blue diamonds), or a random decamer (red circles), for each data set n = 3.

Whilst similar trends were observed for all sequences and the FWHM data displays little difference, the magnitude of the change in rate is greatly reduced for the random decamer, increasing to only 180 beads per minute. It is not unexpected that a shorter sequence would produce a reduced response as the shorter sequence would yield a smaller charge density on the beads surface, therefore having a reduced effect on the translocation events. The increase in rate is less distinct from the Thrombin-15 for Thrombin-MArray aptamer, despite being 11 nucleotides longer. It is possible that a difference in rate or FWHM was not apparent because the beads are already maximally loaded and that the resolution of the current set up is not sufficient to discriminate small differences once the oligonucleotides have reached a certain length.

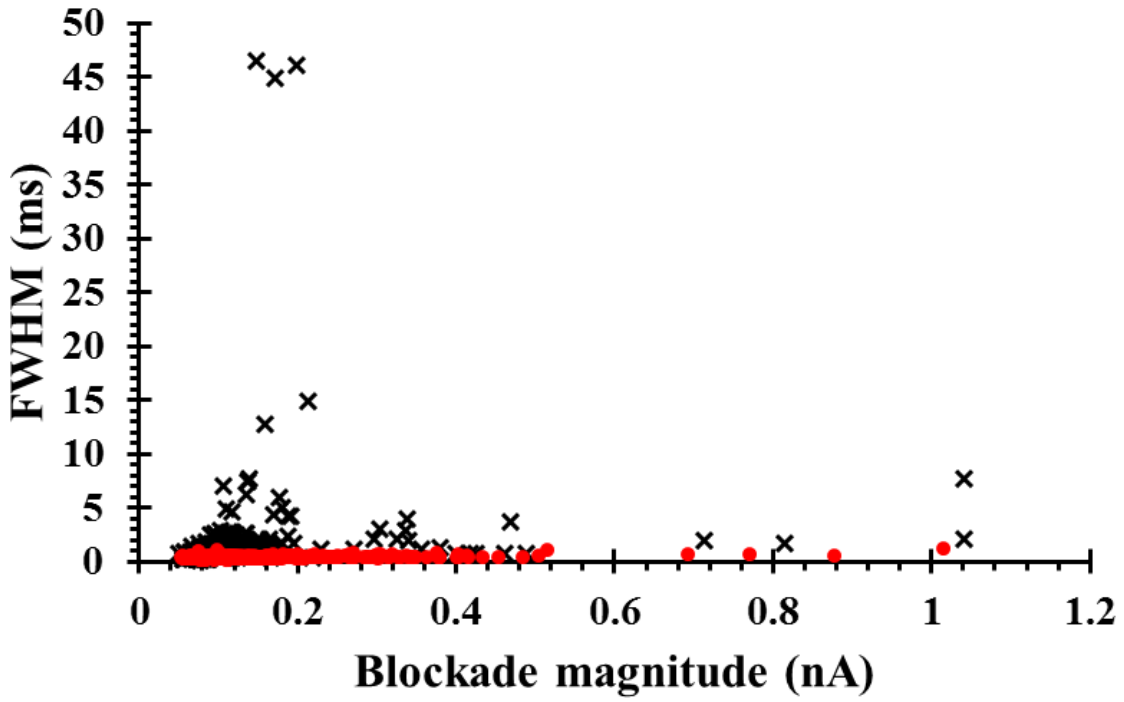

Figure 3. 3: Scatter plot displaying FWHM (ms) vs blockade magnitude (nA) for a sample incubated with either 0.1 nM (black crosses) or 50 nM (red circles) of Thrombin-15.

In addition to looking at averaged data, using TRPS it is possible to examine the data for individual particles. With this it is possible to observe that with increasing DNA concentration not only does FWHM decrease, but the distribution of FWHMs also narrows when the DNA concentration is increased as illustrated in Figure 3. 3. As can be observed when DNA concentration is low (0.1 nM) there is a vast range from 0.14 to 46.93 ms, whereas after incubation in 50 nM Thrombin-15 the range is from 0.18 to 1.2 ms. The range in FWHM at lower concentrations is likely due to non-uniform coating with DNA, whereas at high concentrations all available binding sites are likely occupied leading to greater uniformity with FWHM decreasing as more strands of DNA coat the beads.

In these experiments we failed to observe any increase in blockade magnitude (Δi_p) upon the binding of DNA meaning that a change in bead size was not detected as displayed in Figure 3. 4. A change in size was likely not detectable due to a lack of resolution for the current pore and set up used to resolve such small changes to overall bead diameter.

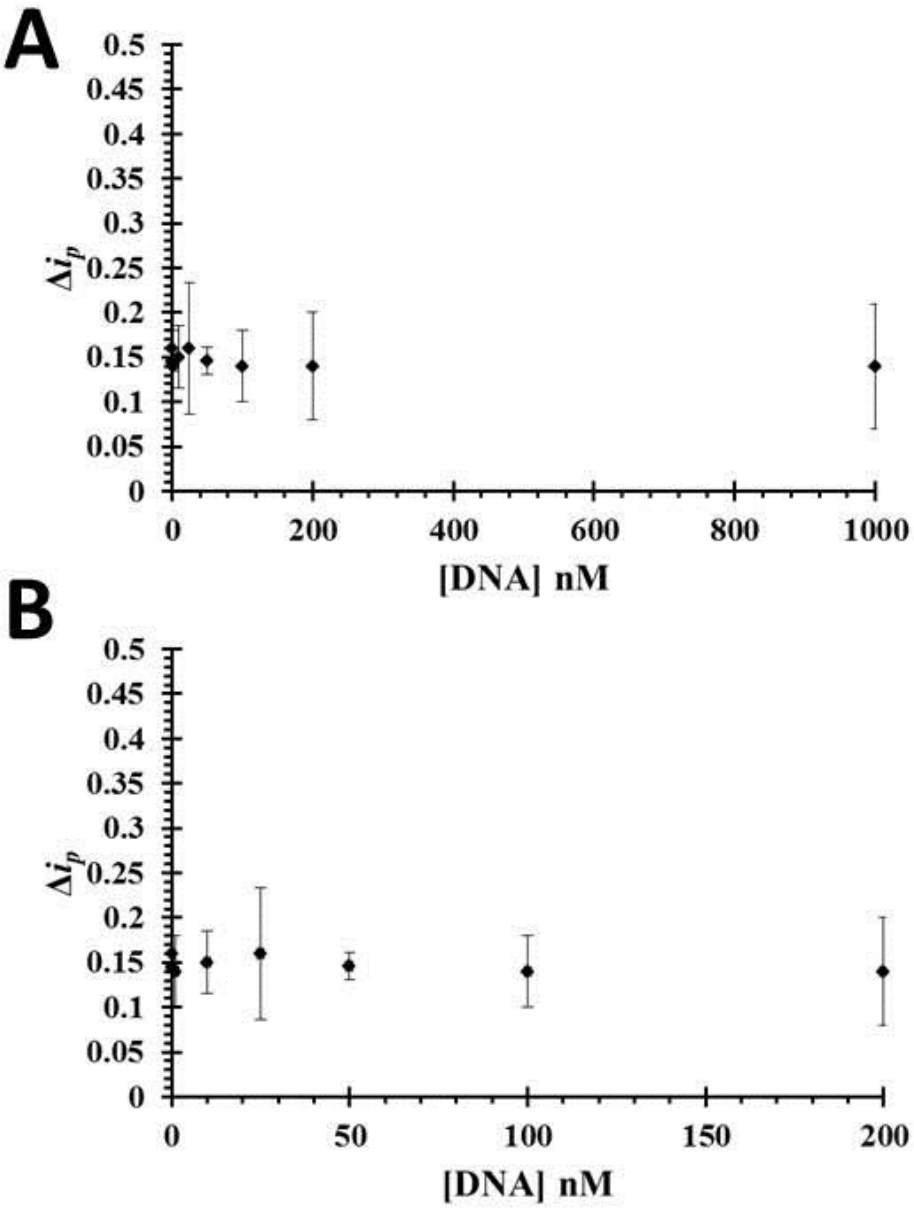

Figure 3. 4: A = Scatter plots displaying mean blockade magnitude (Δi_p) against DNA concentration. B = expanded view of A, error bars represent 1 standard deviation.

3.4.2. Detection of DNA on particles: rate against applied voltage

From the previous experiments detailing the effect of added aptamer on particle rate it is clear that biotinylated aptamers are able to bind streptavidin coated beads and provide a measurable signal of an increase in rate and decrease in FWHM. As such, the next experiment was to validate a different method for detecting DNA on the surface of beads. To negate the need to create a concentration curve to confirm DNA binding each time, a second experiment for confirming the presence of DNA on beads was conducted. As discussed previously adding DNA to the surface of beads increases the negative surface charge density and increases the electrophoretic mobility; making the bead more susceptible to changes in voltage therefore measuring the rate of beads under different applied voltages should provide confirmation that beads are coated with DNA. To provide an expected trend the response of streptavidin coated beads under several applied voltages was measured to provide a reference. The results of this experiment are displayed in Figure 3. 5.

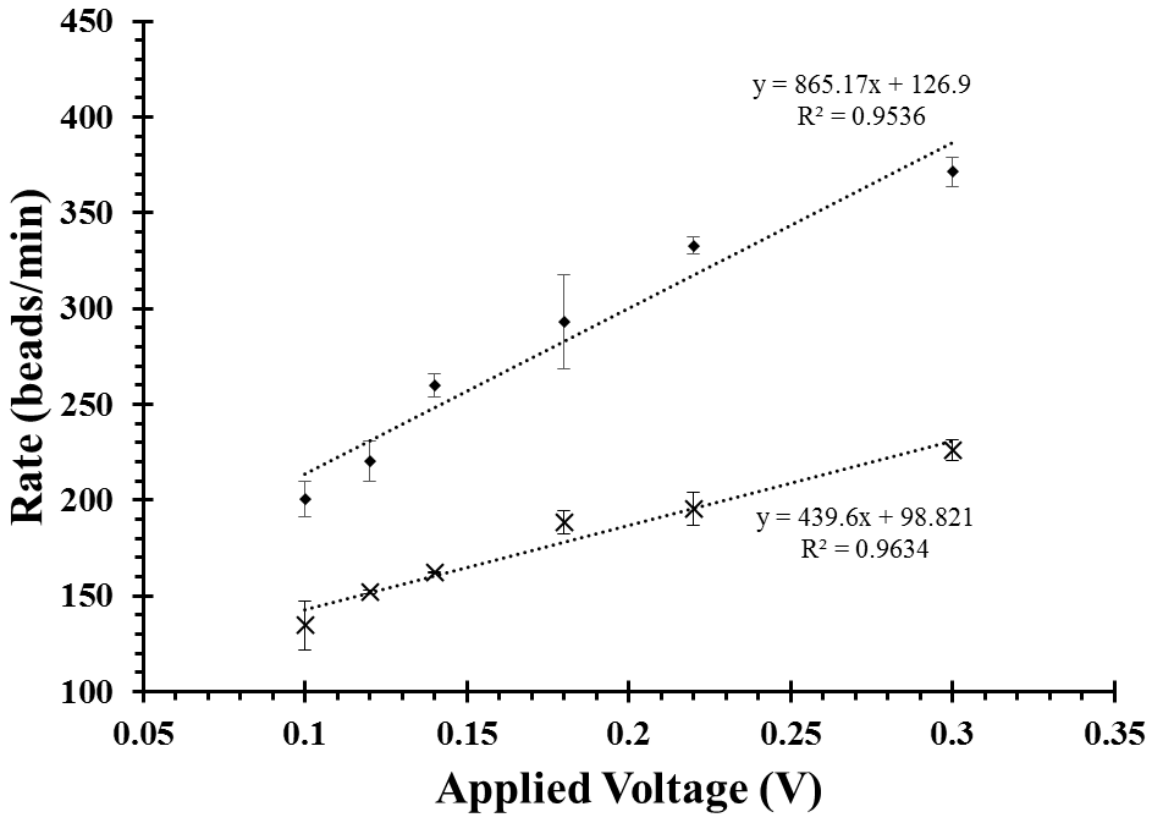

Figure 3. 5: Scatter plot displaying the relationship between average rate and voltage for blank 300 nm streptavidin beads (crosses) or those functionalised with biotinylated aptamer (diamonds); n = 3 and error bars represent the range of recorded rates.

Concentration of the particles is also a factor in determining blockade rate so the particle concentrations of both samples were first matched to remove this variable. Two key differences are apparent between the blank beads and those functionalised with the aptamer. Firstly, the rate, as expected, is higher for beads with DNA across the full range of voltages. Secondly, the gradient is steeper for beads with DNA than those without suggesting that they are under greater influence of the applied voltage. The difference in rate between beads with or without DNA increases with increasing voltage, suggesting that in order to see a clear difference between beads with or without DNA, a high voltage should be chosen.

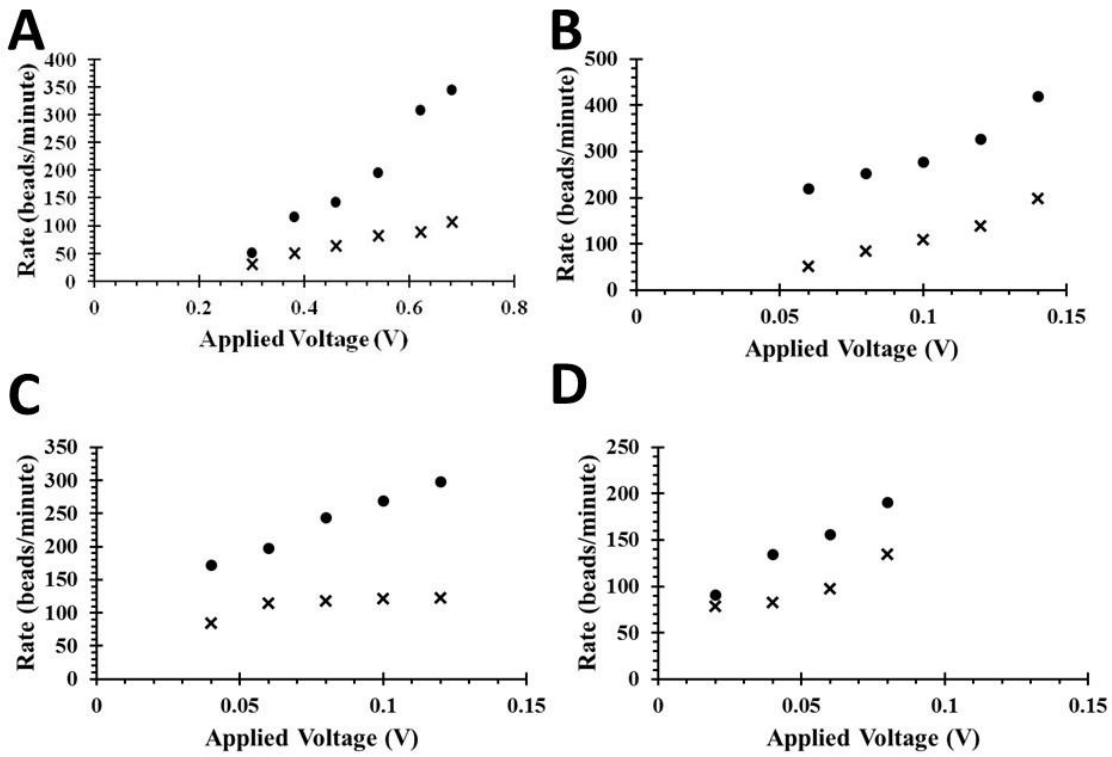

Figure 3. 6: Scatterplots displaying the relationship between rate and voltage for 100 nm carboxyl beads (A), 350 nm carboxyl beads (B), 750 nm carboxyl beads (C) and 1 µm Dynabeads MyOne (D) with (circles) or without (crosses) DNA.

Following on from this carboxylated beads of different diameter were investigated. Figure 3. 6 displays the results of altering voltage upon the rate of beads which underwent EDC conjugation chemistry. The translocation of beads through the pore orifice is dictated by a number of factors including surface charge, pressure, pore size, and the applied electric field, as discussed in chapter two. At low voltages the dominant force is likely to be from the inherent pressure head of gravity resulting in a small observable difference between the beads. As the voltage is increased, the surface charge of the bead becomes more dominant which makes it more susceptible to the applied field and results in an increased number of translocations.

As displayed in Figure 3. 6 for all of the bead types investigated there is an increase in both rate and gradient with increasing voltage for beads which had undergone conjugation chemistry. It is worth noting that for carboxyl DynaBeads MyOne (Figure 3. 6D) the difference between those which had undergone conjugation to DNA and those which had not is far smaller than the carboxyl beads. This is possibly due to the additional mass of the superparamagnetic core, which then lessens the impact of electrophoretic mobility as the effect of gravity increases.

3.4.3. Detection of DNA hybridisation on the surface of beads

After the detection of single-stranded DNA of different lengths an experiment was conducted to establish whether or not hybridisation of DNA strands would be able to be detected with TRPS. This is potentially of use in the detection of specific DNA fragments by the detection of double-stranded DNA formation.

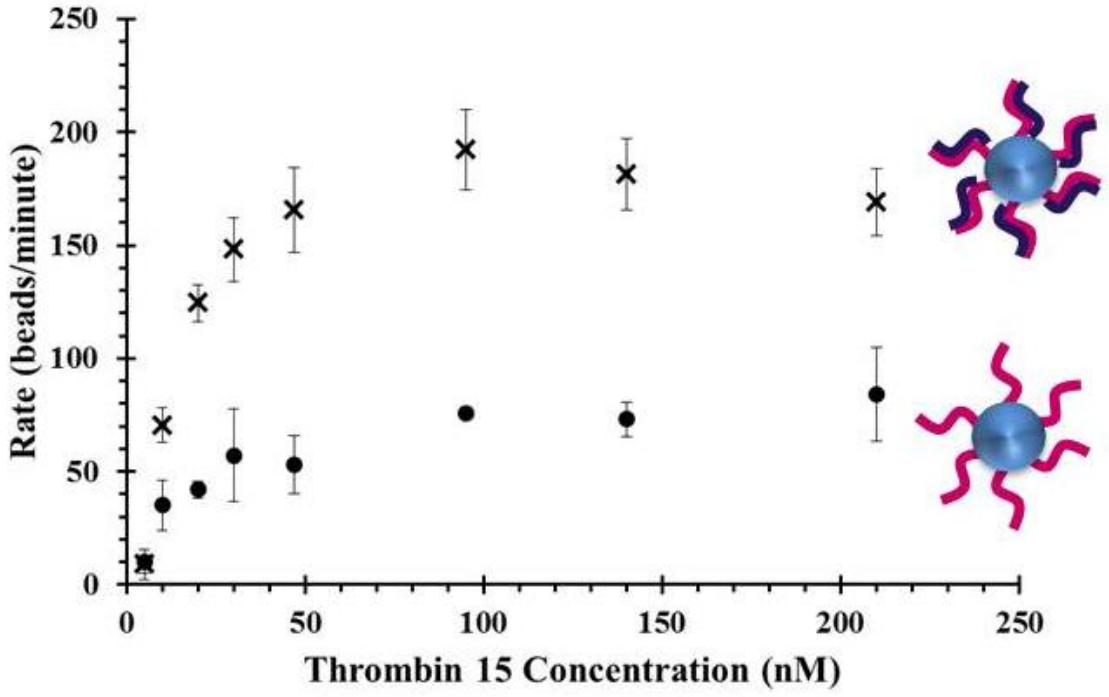

Figure 3. 7: Scatter plot displaying average rate against increasing concentrations of Thrombin-15 with (black crosses) or without (black circles) incubation with 500 nM of a complementary sequence. N = 3; error bars represent 1 standard deviation.

To do this a 15 nucleotide complementary sequence to Thrombin-15, with no further modification, was purchased for use as the target sequence. Firstly, a concentration curve for thrombin 15 against blockade rate was created with 8 concentrations of Thrombin-15. Samples were thoroughly washed so that any excess unbound DNA in solution is removed which would cause off-target binding and reduce sensitivity. After the measurement of these 8 samples they were each then incubated with 500 nM of target DNA for 30 minutes then again washed and resuspended to the same volume. It was found that when target DNA was added the rate increased significantly as displayed in Figure 3. 7. The target DNA does not have any impact upon rate unless the complementary Thrombin-15 is present in sufficient concentration, suggesting that DNA does not non-specifically attach to the bead surface or streptavidin coating.

3.5. Conclusions

In the experiments conducted in the chapter TRPS has been successfully utilised to monitor the changes in surface functionality on beads. Changes in rate and FWHM are sensitive enough to monitor the immobilisation of DNA aptamers on the bead surface which is affected by DNA concentration, DNA length and whether it is single or double stranded. In addition, by measuring the rate of beads under different applied voltages it is possible to gain qualitative information to confirm whether or not carboxylated beads are successfully functionalised with lengths of DNA following one-pot conjugation chemistry. This study also highlighted the need for optimisation of a chosen voltage as the difference in rate between blank and DNA coated beads is greater at higher voltages and at low voltages there is not a significant difference between the bead rates.

3.6. References

1 P. C. Weber, D. H. Ohlendorf, J. J. Wendoloski and F. R. Salemme, *Science*, 1989, **243**, 85–8.

2 L. Chaiet and F. Wolf, *Arch. Biochem. Biophys.*, 1964, **106**, 1–5.

3 L. C. Bock, L. C. Griffin, J. A. Latham, E. H. Vermaas and J. J. Toole, *Nature*, 1992, **355**, 564–566.

4 M. Platt, W. Rowe, J. Knowles, P. J. Day and D. B. Kell, *Integr. Biol.*, 2009, **1**, 116–122.

5 M. Platt, W. Rowe, D. C. Wedge, D. B. Kell, J. Knowles and P. J. Day, *Anal. Biochem.*, 2009, **390**, 203.

6 Y. Wang, K. Kececi, M. Mirkin, V. Mani, N. Sardesai and J. Rusling, *Chem. Sci.*, 2013, **4**, 655–663.

Chapter Four

Monitoring of aptamer-ligand interactions on the surface of beads

4.1. Abstract:

Having confirmed the aptamer conjugation onto the surface of beads in Chapter 3, a proof of concept protein assay was designed to detect aptamer-ligand interaction on the surface of beads. Here, a tunable resistive pulse sensing (TRPS) technology is used to monitor the interaction between several DNA aptamers and their target – thrombin. Aptamers were immobilised onto the surface of superparamagnetic beads, prior to their incubation with the thrombin protein. The protein binding to the aptamer caused a conformational change resulting in the shielding of the polyanion backbone; this was monitored by a change in the translocation time and pulse frequency of the particles traversing the pore. This signal was sensitive enough to allow the detection of thrombin down to nanomolar levels without the need for optical labelling. The power of TRPS was further demonstrated by performing real time detection as thrombin associates with its aptamer in the fluid cell. Real Time Detaction allowed characterisation of the aptamer-target interaction and measuring the association rates of the thrombin protein to the aptamer sequences.

4.2. Introduction:

TRPS technology has herein been used to observe the interaction between aptamer modified superparamagnetic particles with their target protein, thrombin. Thrombin is a protein involved in feedback mechanisms for haemostasis and in the clotting cascade where it catalyses the formation of fibrin[1]. The concentration of thrombin must therefore be tightly regulated by biological systems and monitored as any deviations from normal physiological concentrations could pose a risk of blood clot formation leading to heart attack or stroke[2–4].

Aptamers to thrombin have also been widely used to validate emerging aptasensors[5]. It's well characterised binding mechanism and high affinity makes thrombin an ideal protein target[6,7]. Attaching aptamers to nanoparticles combines the selectivity of the aptamer capture probe with established detection methods of nanoparticles[8]. Assay formats include colorimetry[9], lateral flow assays[10], fluorescence[11], light-scattering[12] and electrochemistry[13].

In the presence of thrombin, aptamer sequences containing a "GGNNGGNGNGGNNGG" (where N represents T or A) motif undergo a conformational change to form a G-quadruplex structure[14], see figure 2.1. As it possesses such a well-studied structure, it also allows the use of modified thrombin aptamer sequences. Here, the structure is deliberately controlled to study the effects upon the signal in the TRPS[7,15] using three previously generated aptamers specific to thrombin, represented in figure 4.1 below.

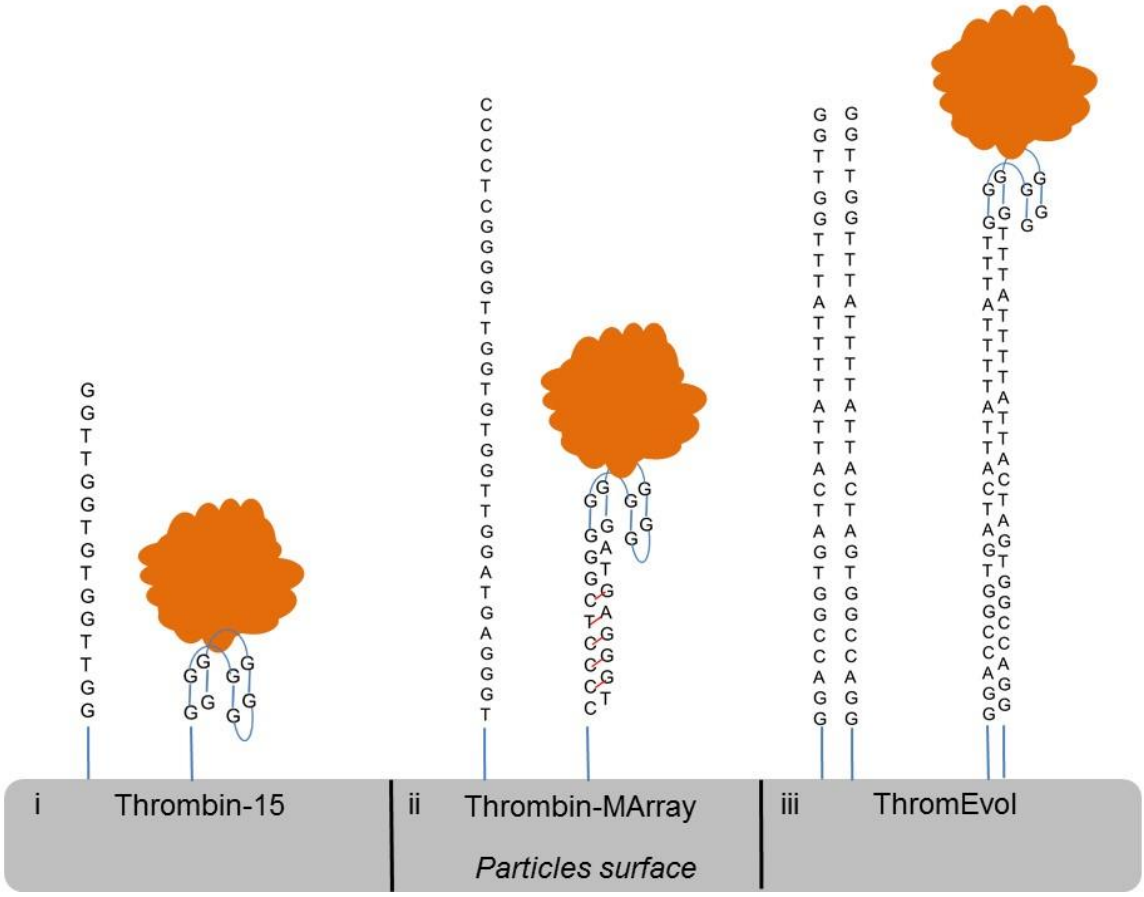

Figure 4. 1: Schematic of the thrombin protein binding to three different aptamer sequences.

As shown in Chapter 3, the immobilisation of DNA onto the particle surface can be confirmed by changes in the particle rate as well as a decrease in translocation times. In the case of streptavidin, these results confirmed the change in surface charge from a relatively neutral to negatively charged surface. In this chapter, we then go on to show that the incubation of the thrombin target with the aptamer modified beads then causes a shielding effect, where the thrombin protein masks the negative charge of the DNA aptamer causing the particle count rate and translocation times to change. This interaction was measured following incubation of the beads with the protein for 30 minutes and then also monitored in real time with detection of nanomolar quantities of thrombin. The ability of TRPS to measure each individual object passing through the pore in real time allowed the monitoring and comparison of binding kinetics for three different aptamers to thrombin each with a change in binding mechanism.

4.3. Method:

4.3.1. Chemicals and reagents

The following chemicals were sourced from Sigma Aldrich, United Kingdom, without any further purification unless otherwise stated: PBS (P4417), Tween 20 (P1379), BSA (A2153), and thrombin (T7513).

DNA sequences were purchased as lyophilised powders with HPLC purification from Entelchon (Germany) : 5'GGT TGG TGT GGT TGG TTT TTT TTT T-Biotin-3' (Thrombin-15)[16] and 5'TGG GAG TAG GTT GGT GTG GTT GGG GCT CCC CTT TTT-Biotin-3' (Thrombin-MArray)[15]. The sequences 5'GGT TGG TTT ATT TTA CTA GTG GCC AGG-Biotin-3' (ThrombinEvol)[7] and a random biotin-tagged 10mer were purchased as lyophilised powders with HPLC purification from Sigma-Aldrich (UK). These were made up to a stock concentration of 100pmol/μL with deionised water purified to a resistivity of 18.2 MΩ.

Streptavidin modified superparamagnetic beads of 120 nm (Bioadembeads streptavidin plus, 03211) were purchased from Ademtech (France). Carboxyl beads of known diameter and concentration were purchased from Izon Sciences, UK: SKP200B (mode diameter 203 nm, 1×10^{11} beads/mL). All beads were diluted in 1 × PBST (0.05% tween 20) electrolyte buffer.

4.3.2. Thrombin binding assay

4.3.2.1. Attachment of aptamer onto the beads

The supplied beads were first vortexed and sonicated to ensure monodispersity. 120 nm streptavidin coated beads were diluted to a concentration of approximately 3×10^9 beads/mL for use as a stock. A ten-fold excess (according to the binding capacity stated on the manufacturer specifications) of biotinylated thrombin binding aptamer was then added to the bead (to 100 μL of beads 17.1 pmol DNA is added). Each sample was then vortexed for 1 minute and then placed on a rotary wheel for 30 minutes at room temperature prior to analysis with TRPS.

4.3.2.2. Removal of excess DNA

The sample was centrifuged for 2 minutes at 10 000 rpm and immediately placed in a MagRack (Life Sciences). After 5 minutes the beads had formed a visible cluster in the sample vial adjacent to the magnet and the solution was carefully removed and replaced with

an equal volume of PBST. This wash stage was performed twice and the particles resuspended in their original volume before being vortexed for 1 minute and sonicated for 30 seconds.

4.3.2.3. Thrombin concentration curve

100 µL samples of aptamer-functionalised beads were pipetted into sample vials. Different concentrations of thrombin were added to provide a concentration range of 0.1 – 10 000 nM with the volume added constant across the range to ensure that any results were not due to dilution of the beads. The samples were incubated on a rotary wheel at room temperature for 30 minutes before analysis.

4.3.2.4. Real time thrombin binding assay

36µL of washed bead-aptamer sample, prepared as described in section 4.3.2.1., was pipetted into the upper fluid cell of the TRPS instrument, this dispersion was recorded for 60 s at which time the software was paused and 4µL of the required test solution was added into the solution. Recording was immediately resumed. Data was then captured for 60 seconds to achieve a baseline value. The recording was then paused and 4 µL of thrombin added into the fluid cell and the recording resumed. The addition of the 4 µl of solution required the pipette tip to be placed into the liquid, the 4 µl was then added and the tip removed. Other than the convection caused by the removal of the tip no additional stirring was induced.

4.3.3. Tunable Resistive Pulse Sensing (TRPS) measurement

Measurements were made using the qNano system obtained from Izon Science (Christchurch) with control suite analysis software (v2.2.) as described in chapter 3, section 3.3.3. For these experiments the pores used were designated 'NP200' by the manufacturer, and are described as most suitable for detecting particles in the range 100 – 300 nm. 80 µL of PBS was pipetted into the lower fluid cell ensuring that no bubbles were present and 40 µL of PBST into the upper fluid cell. A macroscopic stretch of 44.50 mm was chosen with an applied voltage of 0.36 V. These conditions were chosen so that peaks were visible above the baseline noise (10 pA) with an applied bandwidth filter of 1 kHz during all measurements. After recording, this solution was withdrawn and the fluid cell and pore washed by repeatedly replacing PBST in the upper fluid cell until no particles were apparent on the signal trace. To generate error bars in all figures the mean and standard deviation of repeat experiments was

used. Data was examined in the Izon Control Suite (v2.2.) and for detailed examination of real time measurements exported to Microsoft Office Excel 2010 as a .csv file.

4.4. Results and Discussion:

4.4.1. Thrombin binding assay

Having modified the beads with Thrombin-15 aptamer and washed out any excess DNA as described in the method section, the functionalised beads were then incubated with increasing concentrations of thrombin. Figure 4. 2A and B display the resultant plots of particle rate and mode FWHM against thrombin concentration respectively for thrombin-15 (line a - solid red line). As the concentration of thrombin increases, the particle rate and FWHM values decrease and increase respectively. This is attributed to the binding of thrombin with the thrombin-15 aptamer whereby the thrombin proteins sit atop the DNA sequence and shields the negative phosphate backbone of the aptamer, as displayed schematically in Figure 4. 2C. At higher concentrations of thrombin (greater than 10 nM) the gradient at which the rate decreases becomes shallower meaning that further binding of the thrombin protein is not observed. However, the FWHM for beads functionalised with thrombin-15 continues to increase beyond this point which might suggest an increased range of measurement when using FWHM values. It is worth noting that due to the low particle count rate at high concentrations of thrombin the mode FWHM values are more variable than the particle rate and therefore might be more easily skewed by a small population of outliers in the sample.

A second sequence, thrombin-MArray was also investigated in this series of experiments, results for the thrombin-MArray aptamer are displayed in line b (black, solid) of Figure 4. 2A and B. Thrombin-MArray was optimised from one of the original thrombin aptamers by DNA microarray using a genetic algorithm[15]; this sequence contains the G-quadruplex motif common to thrombin binding aptamers which is flanked by complementary strands that form a stabilising region of double stranded DNA when the aptamer folds. This aptamer has been previously characterised by surface plasmon resonance (SPR) where it was found to have comparable affinity to the original thrombin-15[15]. It has been demonstrated that modifications of the original thrombin-15 aptamer can enhance the binding ability on surfaces[15,17], with the potential to lead to greater sensitivity.

When comparing the change in rate for thrombin-MArray and thrombin-15 similar trends were observed i.e. the particle rate decreases with increasing thrombin concentration,

however, the total change in FWHM across the range of concentrations was much smaller and did not display a clear increase. Again, as stated above, this may be attributed to the lower number of particles recorded due to the diminution of particle rate, as such, only particle rate shall be discussed in detail from this point on. It was noted that for thrombin-MArray there was very little deviation in the particle rate at low concentrations of thrombin and a sudden sharp near-abolition of particle translocations above 10 nM of thrombin.

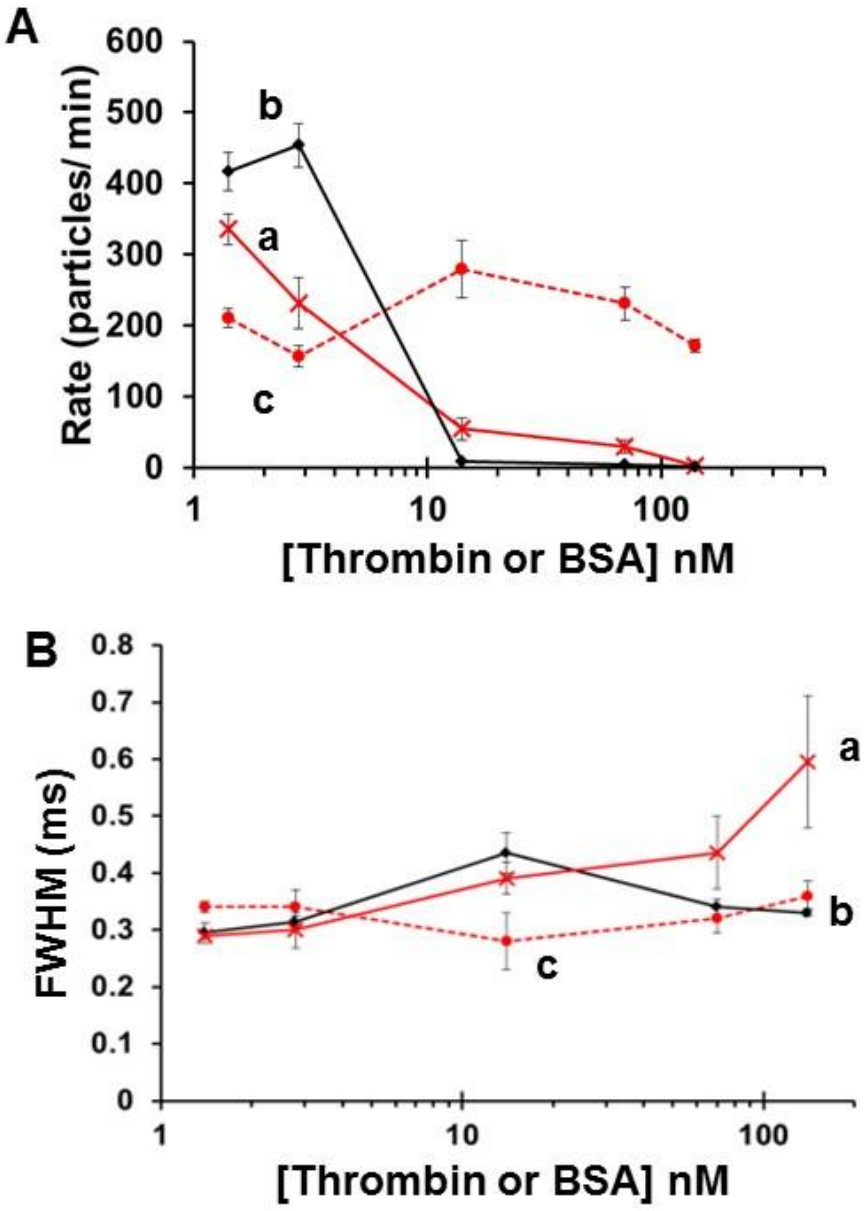

Figure 4. 2: A Scatter plots displaying the effect of increasing concentrations of thrombin or BSA on rate for Thrombin-15 incubated with thrombin (a) P = 0.03, Thrombin-MArray incubated with thrombin (b) P = 0.04, and Thrombin-15 incubated with BSA (c) P = 0.55. **B** FWHM plots for a = Thrombin-15 (P = 0.004), b = ThrombinMArray (P = 0.90), and c = BSA control (P = 0.34). A "NP200" pore with a membrane stretch of 44.50mm, voltage of 0.36V, and 40µl of sample in the upper fluid cell was used. Each data point represents the average value from four experiments and error bars represent 1 standard deviation from the mean. P values calculated by one way ANOVA.

The differences between the changes in rate between thrombin-15 and thrombin-MArray may be attributed to differences in the binding mechanism. As previously stated, thrombin-MArray folds in half to form complementary base pairs near the bead surface, holding the thrombin protein close to the surface of the beads the unbound thrombin-MArray sequence is significantly longer than the original thrombin-15, meaning that neighbouring unbound strands extend out past the bound thrombin into solution. When protein concentration, and therefore bead coverage, is low, the dominant effect of the particle rate and FWHM is the protruding anionic phosphate backbone from the aptamer past the protein. As the protein coverage increases and more of these aptamer strands change conformation and are shielded, the particle rate diminishes.

Across these experiments no change in the size of the beads was observed, although one would assume a small increase in size due to the added DNA and protein would occur. The size of the object passing through the pore is inferred by the blockade magnitude (Δi_p) which is proportional to particle volume. As displayed in Figure 4. 3, the recorded Δi_p does not show any significant change with thrombin concentration. This is most likely due to a lack of resolution of the current set up to discriminate such small changes in size.

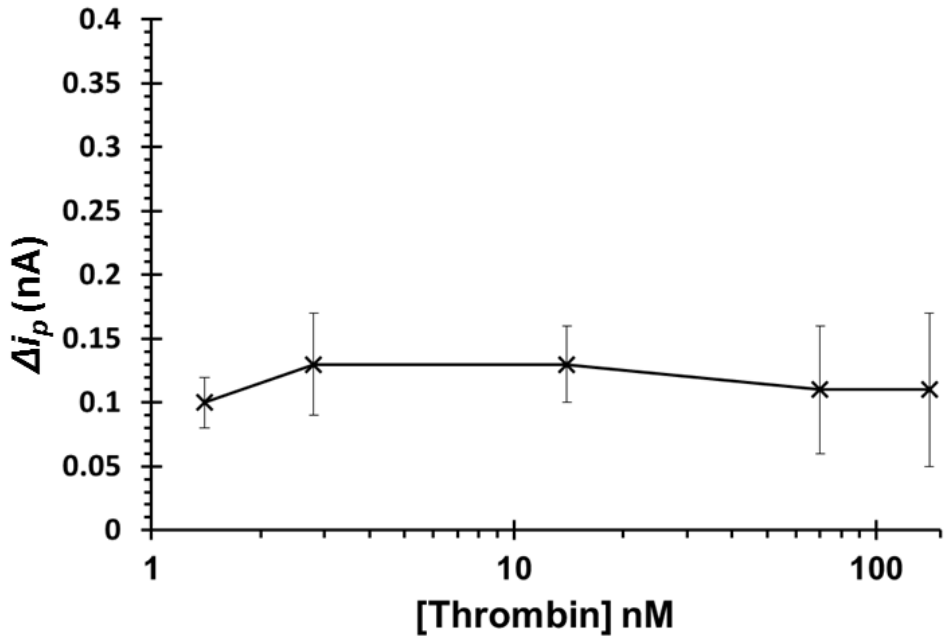

Figure 4. 3: Concentration curve displaying the effect of increasing concentrations of thrombin on the Δi_p of beads functionalised with Thrombin-15. The data used to collate this graph were obtained using a manufacturer classified "NP200" pore with a membrane stretch of 44.50mm, an applied voltage of 0.36V, and 40µl of sample in the upper fluid cell. Each data point represents the average value from four experiments and error bars represent 1 standard deviation from the mean.

As a control, the same experiment was conducted using increasing concentrations of BSA protein, the results for which are also displayed in Figure 4. 2A and B (line c – red, dashed) for thrombin-15 and Figure 4. 4 for the thrombin-MArray aptamer. The particle rate and FWHM remain constant across the concentration range of BSA, illustrating that the aptamer is specific to the thrombin target and that any change in signal is not the result of a nonspecific interaction between the protein and DNA or surface of the beads.

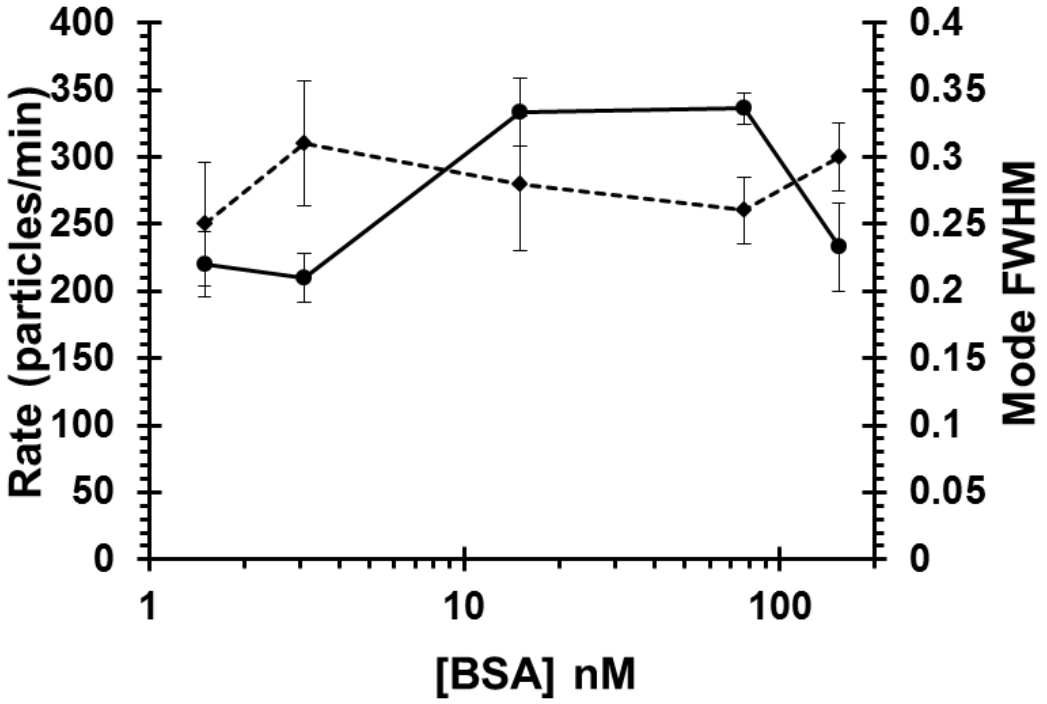

Figure 4. 4: Concentration curve displaying the effect of increasing concentrations of BSA on the rate (solid line) and mode FWHM (dashed line) of Thrombin-MArray functionalised beads. The data used to collate this graph were obtained using a manufacturer classified "NP200" pore with a membrane stretch of 44.50mm, an applied voltage of 0.36V, and 40µl of sample in the upper fluid cell. Each data point represents the average value from four experiments and error bars represent 1 standard deviation from the mean.

4.4.2. Real time thrombin binding measurement

The experiments in section 4.4.1. were recorded after a 30 minute incubation between the beads and target protein, this should have been sufficient time for the binding between the protein and aptamer to have occurred. Calculations based upon Smoluchowski theory[18,19] suggest that the reaction should proceed quickly under the conditions and concentrations used here and binding between the protein and aptamer should occur within seconds. To explore if binding could be observed in real time 36 µL of Thombin-15 modifed beads were placed into the upper fluid cell of the TRPS instrument, data was collected for 60 seconds to obtain a baseline particle rate, after this 60 second period data capture was paused whilst the thrombin protein was added to the upper fluid cell before continuing data collection. The change in particle rate as a function of time for four experiments repeated for a thrombin concentration of 15 nM are displayed in figure 4.5A.

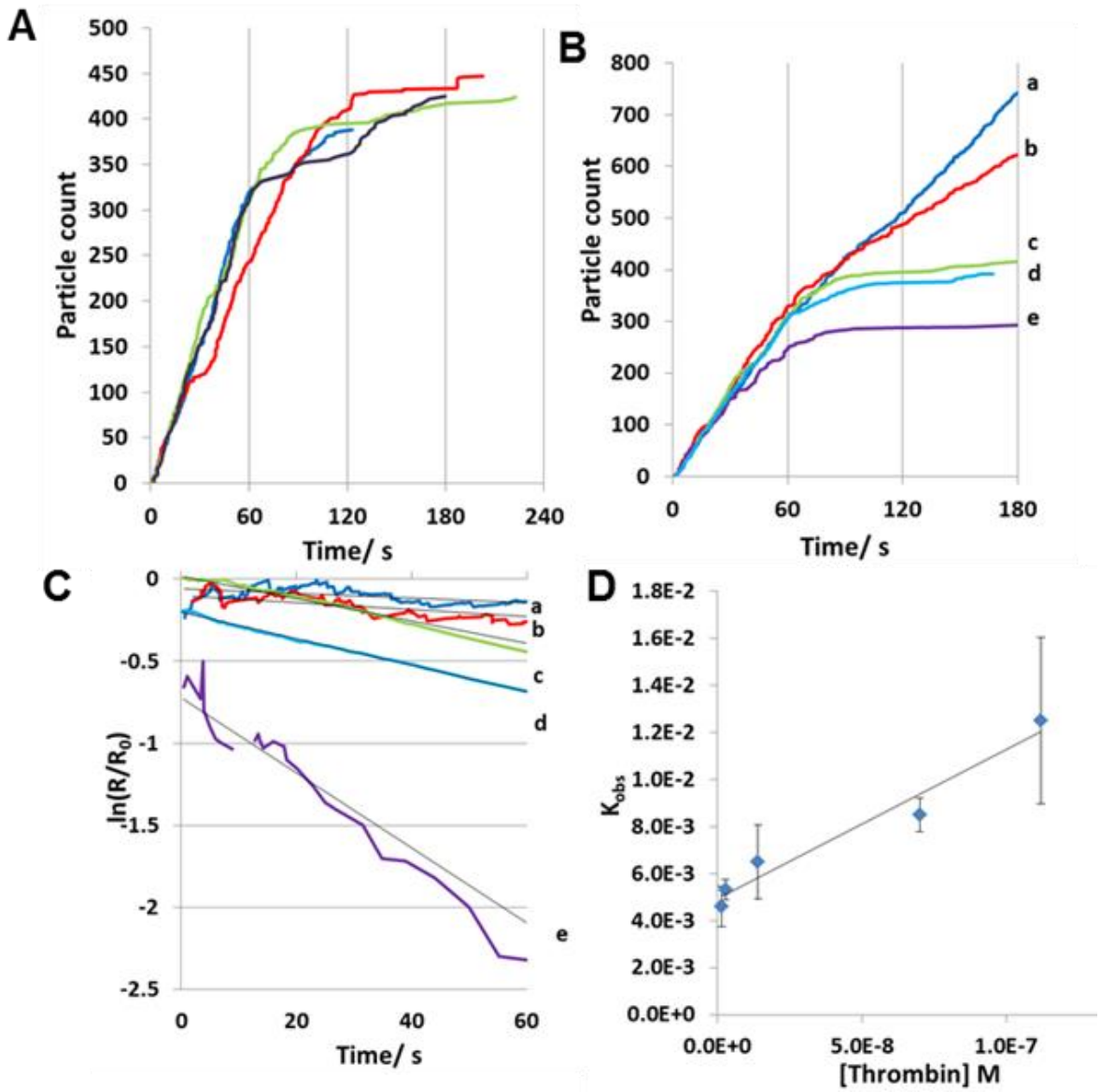

Figure 4. 5: A, Replica experiments of real time particle rate measurements for Thrombin-15 modified beads. At t = 0 36µl of sample was present in the upper fluid cell, at t = 60s 4µL of Thrombin solution was added giving a final concentration of 15 nM. **B**, One set of experiment demonstrating the change in rate with respect to the concentration of thrombin. At t = 60s 4µL of Thrombin solution was added giving a final concentration of thrombin (navy blue) = 1.5 nM, b (red) = 3 nM, c (green) = 15 nM, d (blue) = 77 nM, e (purple) = 154 nM. **C**, Plot of rate of change in particle count, $ln(R/R_0)$, versus time, for the experiment shown in part B. t = 0 indicates the point at which thrombin was added to the particle solution. **D**, Plot of K_{obs} versus concentration of thrombin. The values represent the mean from four experiments. The data was obtained using a "NP200" pore with a membrane stretch of 44.50mm, an applied voltage of 0.4V.

After the addition of thrombin into the upper fluid cell at 60 seconds the observed particle rate decreased until a continuous particle rate was reached after approximately 120 seconds. The observed change in rate is attributed to the same effects as described above for a set incubation period: the binding of the protein to the aptamer masks the negative DNA backbone resulting in decreased mobility. Figure 4.5B illustrates the change in particle rate as

a function of thrombin concentration ranging from 1.5 to 154 nM. As the thrombin concentration increases both the magnitude of the change in rate, and also the speed of that change, also increase. Figure 4.5B shows example measurements which were performed in triplicate, in reaction rate calculations the average value of triplicate measurements for each thrombin concentration were used.

The concentration of thrombin is in excess of the number of beads by several orders of reaction, hence, a first order reaction was assumed where a plot of the rate of change, $\ln(R/R_0)$, against time would yield a straight line with gradient of k_{obs}. R was calculated by the following equation:

$$R = \left(\frac{60}{t_p}\right) \times Count_{tp} \qquad \textbf{4.1}$$

Where t_p is the recorded time of particle translocation and $Count_{tp}$ is the total number of particles at t_p. R_0 is the average rate of particles per second recorded in the 60 seconds previous to thrombin addition. $K_{obs} = k_a[\text{Thrombin}]+k_d$. Thus a plot of K_{obs} versus concentration of thrombin should yield a straight line with the gradient of k_a and an intercept of k_d. Figure 4.5C displays the change in rate for the 5 thrombin concentrations shown in figure 4.5B. In the calculations a minimum of 60 seconds was collected after the injection of the protein to calculate the reaction rates.

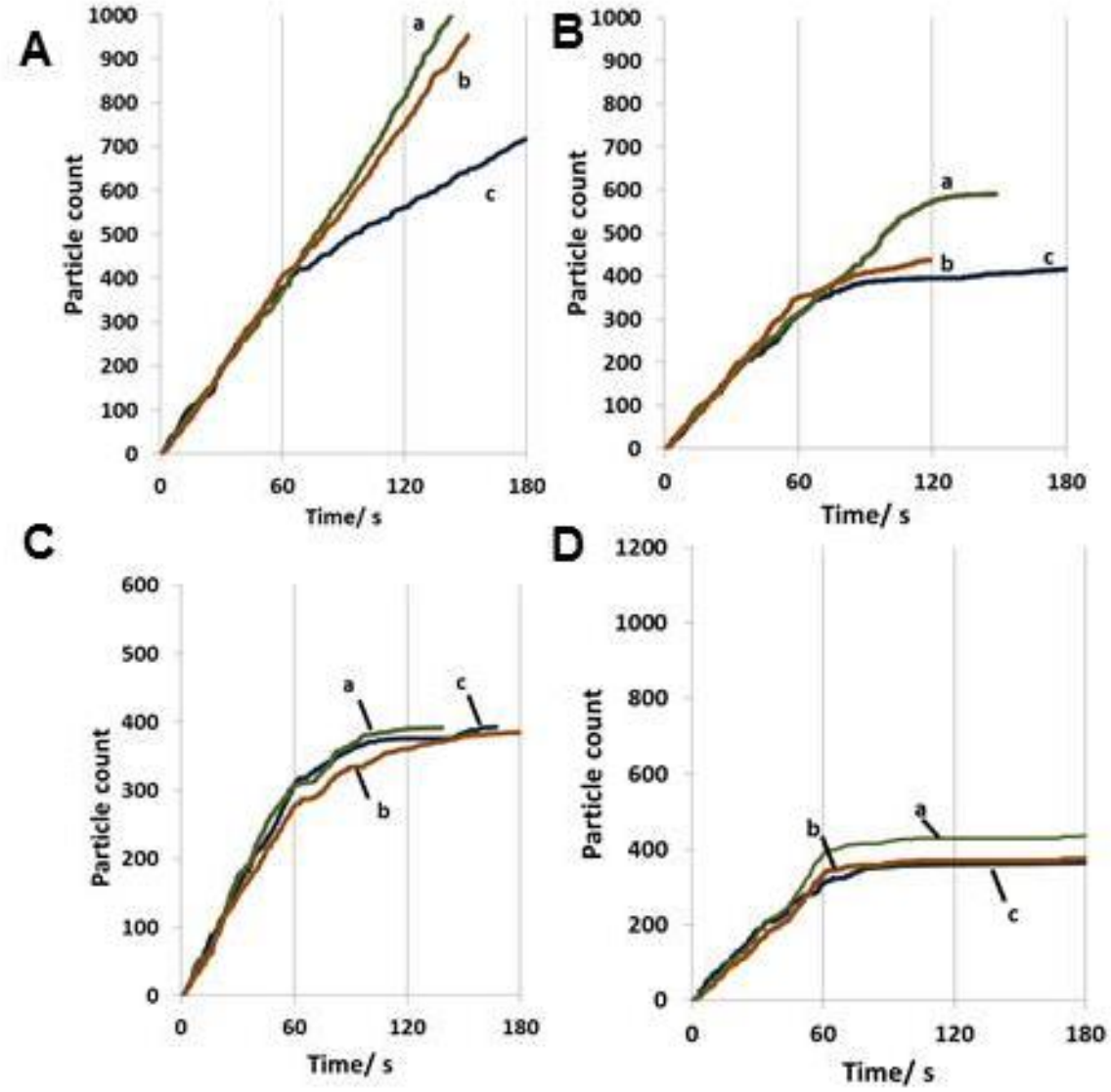

Figure 4. 6: Real time particle rate measurements taken for three aptamers, curves are labelled a, b and c, representing data from Thrombin-MArray, ThromEvol and Thrombin-15 respectively. At t = 0 36µl of sample was present in the upper fluid cell. **A,** 4µl of thrombin solution added at t = 60 s giving a concentration of 3 nM. **B,** 4µl of thrombin solution added at t = 60 s giving a concentration of 15 nM. **C,** 4µl of thrombin solution added at t = 60 s giving a concentration of 45nM. **D,** 4µl of thrombin solution added at t = 60 s giving a concentration of 154 nM. The data was obtained using a "NP200" pore with a membrane stretch of 44.50 mm, an applied voltage of 0.4V.

The gradients from each experiment are plotted as a function of concentration in figure 4.5D and from the regression line k_a was calculated to be 7.42×10^4 $M^{-1}s^{-1}$, k_d 2.9×10^{-3} s^{-1} and gave a K_D 39.1 nM, which is comparable to measurements reported in the literature of 6 nM[65], 20 nM[61], 200 nM[66], 102.6 nM[67], and 75-100 nM[68].

The same set of experiments was performed for the Thrombin-MArray aptamer the results from which are displayed in figure 4.6. It was noted that when a low (<10 nM) concentration

of thrombin was used there was no observed change in signal after the injection of thrombin protein at 60 seconds for the Thrombin-MArray aptamer as displayed in figure 4.6A in agreement with data attained after a set incubation period in figure 4.2A.

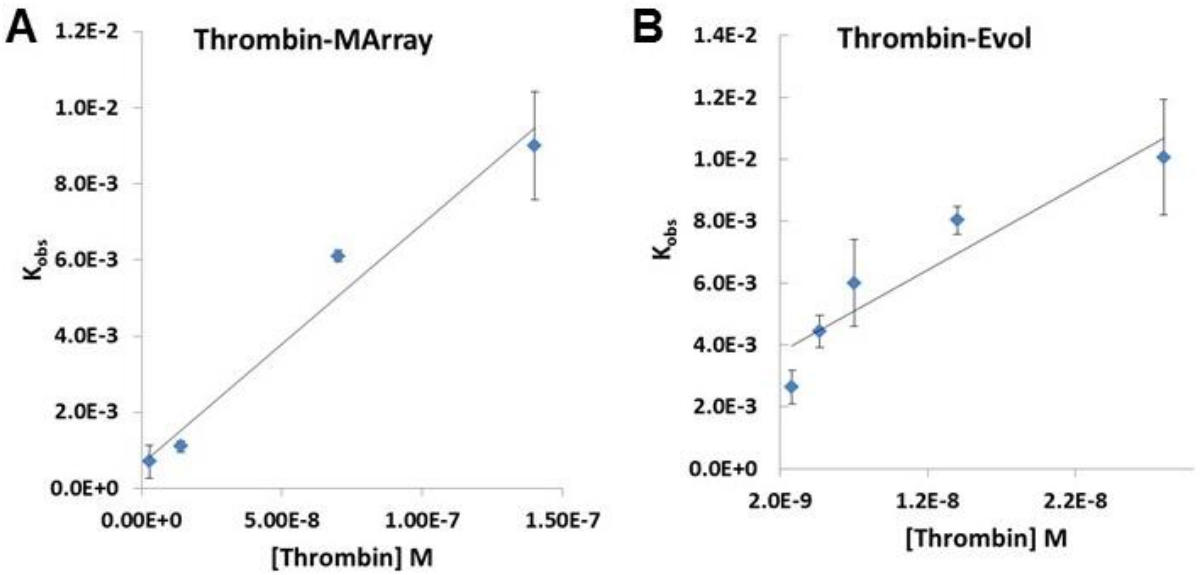

Figure 4. 7: Plot of K_{obs} versus concentration of thrombin for **A –** Thrombin-Marray sequence and **B –** Thrombin-Evol. n = 3.

Plotting k_{obs} against thrombin concentration for the thrombin-MArray aptamers as displayed in Figure 4.7A obtained a k_a of 4.03×10^4 $M^{-1}s^{-1}$, k_d 3.40×10^{-3} s^{-1} and K_D 84.3 nM. This compares favourably to the value obtained previously using surface plasmon resonance techniques, SPR, of 28 nM[55].

It was hypothesised that differences in thombin-15 and thrombin-MArray, which have similar k_a and k_d values to traditional SPR methods, is due to mechanistic effects, i.e. the protein is buried within a negative DNA layer with unbound thrombin-MArray protruding past the bound thrombin proteins, or the hindrance of the protein binding to the thrombin-MArray aptamer on a beads surface rotating at ~ 400 s^{-1}. As the concentration of thrombin was increased from 15 to 154 nM in Figure 4.6B – D the rate of change for the thrombin-MArray began to increase and eventually matched that observed for the thrombin-15.

A third aptamer, Thrombin-Evol, was also tested. This aptamer was raised via the CLADE technique and while it does not contain the typical G-quadruplex motif it still possesses a reported k_a of 8.7×10^4 $M^{-1}s^{-1}$, k_d 2.04×10^{-3} s^{-1} and K_D 23.45 nM[46] when measured with SPR. Importantly, this aptamer binds to the protein via the base pairs at the end of two neighbouring sequences illustrated in figure 4.1iii. It was hoped that this binding mechanism

would lead to an improved sensitivity as unlike the Thrombin-MArray sequence the protein sits on the end of the aptamer strands. The real time particle rate measurements for the sequences are presented in figure 4.6A – D (curves b). The ThrombinEvol sequence has an improved response at the lower protein concentrations and consistently performs better than the Thrombin-MArray, as observed in figure 4.6. The measured reaction rates based upon triplicate measurements for the Evol aptamer were k_a of 5.78×10^4 $M^{-1}s^{-1}$, k_d 4.80×10^{-3} s^{-1}, and K_D 83.1 nM as calculated with the plot of K_{obs} versus concentration displayed in figure 4.7B. Whilst this suggests the shielding of the charge via the protein is key in observing a change in particle rate, the clearest response across the full range of the protein concentrations was the original Thrombin-15 aptamer. These results suggest that whilst shielding the charge on the DNA is an essential part of the signal, to obtain a strong change in particle rate a conformational change must also take place.

To demonstrate that the results of these experiments could not be due to the addition of extra solution itself and that it did not cause a significant change in particle count rate, the same volume of PBST without Thrombin was added into the upper fluid cell, data from repeat experiments shown in figure 4.8 and is summarised in table 4.1. The addition of fluid into the upper fluid cell alters the height of the fluid level therefore increasing fluidic forces and causing a slight dilution effect. Typically the addition of the extra 4 μl of solution to the upper fluid cell caused a small deviation in the gradients of the line, on average the gradient of the line changed by around -4% upon the addition of the solution indicating a decrease in particle count rate.

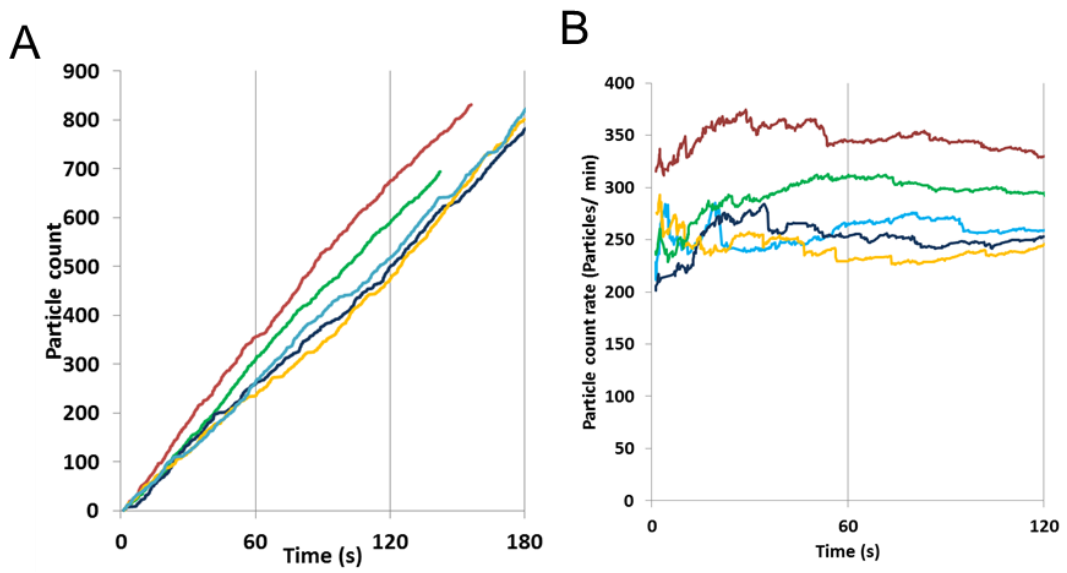

Figure 4. 8: A - Experiments of real time particle rate measurements for Thrombin-15 modified beads. At t = 0, 36 µL of sample was present in the upper fluid cell, at t = 60 sec 4 µL of PBST was spiked into the fluid cell. **B –** Data from A plotted as particle rate per minute.

Experiment	Gradient <60 sec	Gradient >60 sec	Change in gradient %
1	4.97	4.68	-6.2
2	5.70	5.40	-5.5
3	4.70	4.32	-8.7
4	4.02	4.05	1
5	4.20	4.10	-2.4

Table 4. 1: Gradients of regression lines for data displayed in Figure 4. 8

Three control experiments were also conducted to be sure that any observed effects were specific to the thrombin-aptamer interaction on the surface of the beads, the results for these are displayed in figure 4.9. In curve 1 the upper fluid cell was loaded with 36 µL of thrombin-15 modified beads and data was collected for 60 seconds, following this period of time recording was paused and 4 µL of BSA protein was added to the upper fluid cell. In curve 2 thrombin was added to carboxyl coated polystyrene beads, and curve 3, thrombin is added to a superparamagnetic bead modified with a random 10mer. In each experiment the protein concentration was 15 nM and no deviation or change in particle rate after the additional of the protein was observed.

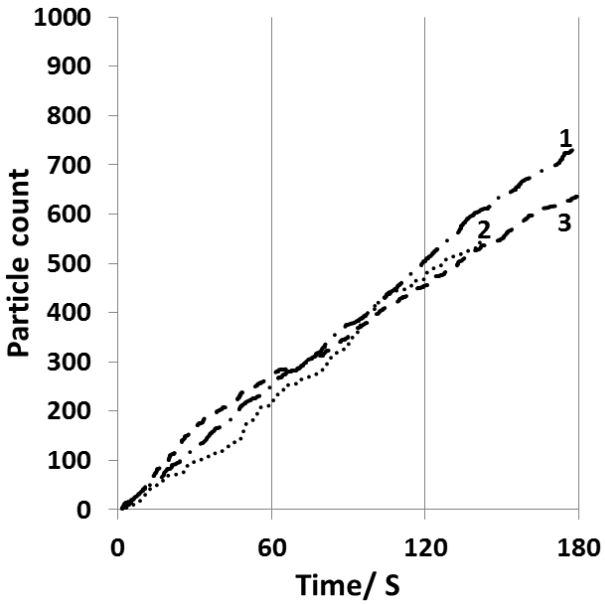

Figure 4. 9: Real time particle rate measurements. At t = 0, 36 µL of sample was present in the upper fluid cell , 4 µL of the Protein solution was added to the upper fluid cell at t = 60 Line 1 – Thrombin-15 aptamer beads with 4 µL of BSA solution added at t = 60 seconds giving a concentration of 15 nM, Line 2 – Carboxyl coated beads with 4 µL of thrombin solution added at t = 60 seconds giving a concentration of 15nM, Line 3 – Random 10mer with 4 µL of thrombin solution added at t = 60 seconds giving a concentration of 15nM. A manufacturer classified "NP200" pore with a membrane stretch of 44.50mm, applied voltage of 0.36V was used for the experiment.

4.5. Conclusion

TRPS was successfully used to monitor changes to surface functionality of superparamagnetic beads. This signal was utilised to study the interaction of aptamers with their target protein, thrombin. The changes in particle rate were sensitive enough to monitor the binding of protein to three different aptamer sequences on the surface of beads. FWHM also appeared to increase with increasing thrombin concentration for the Thrombin-15 aptamer, however, due to the small sample size recorded in high thrombin concentrations when the rate is low this is perhaps less reliable. These results demonstrate that TRPS is now one of many technologies capable of monitoring the interaction between aptamers and their target protein. Further, it was demonstrated that TRPS allows for real time monitoring of the protein-aptamer interaction allowing the reaction rates to be calculated. This offers a new technique for monitoring the association rates of analytes directly on the beads surface without the need for identification labels such as fluorescence or utilising standard SPR technologies. The current method does have a limited working range, as at higher concentrations of target a reduced particle count rate makes obtaining a sufficient particle count difficult within the constraints of the Izon Control Suite software hence future work endeavours to generate a signal which increases rather than diminishes with increased target concentration.

4.6. References

1 E. Di Cera, *Mol. Aspects Med.*, 2008, **29**, 203–54.

2 T. J. Tegos, E. Kalodiki, S.-S. Daskalopoulou and a. N. Nicolaides, *Angiology*, 2000, **51**, 793–808.

3 I. Martínez-martínez, J. Navarro-Fernandez, A. Østergaard, R. Gutie, N. Bohdan, A. Min, C. Pascual, C. Martínez and M. E. De Morena-barrio, *Blood*, 2012, **120**, 900–905.

4 I. Pabinger and C. Ay, 2009, 332–336.

5 T.-C. Chiu and C.-C. Huang, *Aptamer-functionalized nano-biosensors.*, 2009, vol. 9.

6 A. D. Ellington and W. Szostak, Jack, *Nature*, 1990, **346**, 818 – 822.

7 M. Platt, W. Rowe, D. C. Wedge, D. B. Kell, J. Knowles and P. J. Day, *Anal. Biochem.*, 2009, **390**, 203.

8 T.-C. Chiu and C.-C. Huang, *Aptamer-functionalized nano-biosensors.*, 2009, vol. 9.

9 H. Wei, B. Li, J. Li, E. Wang and S. Dong, *Chem. Commun. (Camb).*, 2007, 3735–7.

10 H. Xu, X. Mao, Q. Zeng, S. Wang, A.-N. Kawde and G. Liu, *Anal. Chem.*, 2009, **81**, 669–75.

11 W. Wang, C. Chen, M. Qian and X. S. Zhao, *Anal. Biochem.*, 2008, **373**, 213–9.

12 R. J. C. Brown and M. J. T. Milton, *J. Raman Spectrosc.*, 2008, 1313–1326.

13 C. Deng, J. Chen, Z. Nie, M. Wang, X. Chu, X. Chen, X. Xiao, C. Lei and S. Yao, *Anal. Chem.*, 2009, **81**, 739–45.

14 R. F. Macaya, P. Schultze, F. W. Smith, J. A. Roet and J. Feigon, 1993, **90**, 3745–3749.

15 M. Platt, W. Rowe, J. Knowles, P. J. Day and D. B. Kell, *Integr. Biol.*, 2009, **1**, 116–122.

16 L. C. Bock, L. C. Griffin, J. A. Latham, E. H. Vermaas and J. J. Toole, *Nature*, 1992, **355**, 564–566.

17 E. Katilius, C. Flores and N. W. Woodbury, *Nucleic Acids Res.*, 2007, **35**, 7626–7635.

18 L. Cohen-Tannoudji, E. Bertrand, J. Baudry, C. Robic, C. Goubault, M. Pellissier, a. Johner, F. Thalmann, N. Lee, C. Marques and J. Bibette, *Phys. Rev. Lett.*, 2008, **100**, 108301.

19 J. Baudry, C. Rouzeau, C. Goubault, C. Robic, L. Cohen-Tannoudji, a Koenig, E. Bertrand and J. Bibette, *Proc. Natl. Acad. Sci. U. S. A.*, 2006, **103**, 16076–8.

Chapter Five

TRPS as a tool to monitor analyte induced particle aggregation

5.1. Abstract:

As highlighted in chapter one, SPBs can perform the capture, purification and signal transduction stages, producing a relatively simple, fast, and sensitive label-free format. Whilst prior chapters have focussed on changes in particle mobility to detect bound proteins, here the focus is on changes in Δi_p in the presence of the target; one possible way to do this is to induce aggregation. Particle aggregation in the presence of the analyte is a common example of such a detection strategy. Herein we demonstrate the key parameters which lead to aggregation. Tunable Resistive Pulse Sensing (TRPS) technology was utilised to follow the aggregation using three different methods of analysis. TPRS allows a comparison in the data treatment using average population values, particle concentration, and a more detailed analysis monitoring the change in aggregate size and frequency. To validate the approach, the well-known biotin-avidin binding assay is used to demonstrate the advantages and limitations of each type of analysis. Also presented are the key parameters that contribute to assay sensitivity such as bead concentration, size, binding capacities and data analyses.

5.2. Introduction:

Previous chapters have focussed on the impact of aptamer functionalisation and target binding to beads on the mobility of these beads in the TRPS system. However, an alternative signal could be the selective change in size of beads, and therefore $\Delta i_{p,}$ as they move through the pore. One way to do this is by inducing bead aggregation.

Aggregation assays where the concentration of the analyte is related to changes in aggregate size and frequency[1] are well documented. Many of the techniques rely on optical and light scattering techniques which provide an average value of the population and offer little insight into the formation of individual clusters with techniques such as microscopy severely limited by the relatively small sample size and amount of time taken to manually count each cluster. In addition, light scattering techniques such as dynamic light scattering rely on highly uniform particle dispersion as the average is easily skewed by the presence of outliers[2]. As such, for looking at a mixed dispersion TRPS offers many advantages. TRPS lends itself well to the identification of aggregates due to the ability to extract information for each object passing through the pore rather than a calculated average with assumed normal distribution.

In this chapter a comparison of different strategies aimed at interpreting the aggregation signal using TRPS is presented and key parameters that control the aggregation of SPBs for the streptavidin-biotin assay are identified, i.e., bead concentration, size, binding capacity, reaction time, and application of magnetic force. The avidin-biotin interaction was used as a model as it is among the strongest known non-covalent specific molecular interactions, i.e., $K_d \sim 10^{-15}$ M/s^{-1}. Under the optimal assay conditions the assay could be used to detect biotinylated proteins across five orders of magnitude in concentration with sensitivities in the sub picomolar range. The concentration of analyte and the most stable and reproducible sizes of aggregates were correlated for different bead compositions. This insight will help users optimize the TRPS setup for monitoring the aggregation signal, and offers an insight into the aggregation state of particles in the presence of the analyte.

5.3. Method:

5.3.1. Chemicals and reagents

The following chemicals were sourced from Sigma Aldrich, UK, without any further purification unless otherwise stated: Phosphate Buffered Saline (PBS – P4417), Tween 20 (P1379), MES hydrate (M2933), sodium dodecyl sulphate (SDS – 71727), (Bovine Serum Albumin (BSA – A2153), and thrombin (T7513). 1 step ABTS solution, biotin-HRP, biotin BSA, EDC (22981), Sulfo n-hydroxylsucciminide, *N*-hydroxysulfosuccinimide (sulfo-NHS) and avidin, were purchased from Thermo scientific. Water purified to a resistivity of 18.2 MΩ cm (Maxima) was used to make all solutions unless otherwise specified.

Carboxyl dynabeads of 1µm (catalogue number 650.12) and 3µm (catalogue number 143.05D) were purchased from Invitrogen, UK. Bio-Adembeads, 300nm (3233) were purchased from Ademtech, France. These beads were separated and washed using a Magrack purchased from GE healthcare. The concentrations of these commercial beads are as follows: For the 3 µm beads 1mg = 5 x 10^7 beads, for the 1 µm beads 1mg = 6 x 10^8 beads, and For the 300nm beads 1mg = 1 x 10^{10} beads. Carboxyl beads of known concentration and diameter (SKP400; mode diameter 350 nm, CPC1000; mode diameter 955 nm) were sourced from Izon Sciences (Oxford, UK) to be used as a calibrant.

5.3.2. Modification of beads with avidin

Both the 1 and 3 µm diameter beads were modified with the avidin protein prior to the assay being performed. The beads (1 mg/mL) were washed three times with MES buffer. Following the third wash step the beads were resuspended in 1 mL MES buffer and EDC (1 mg) and NHS (1 mg) were added to the solution. The particles were sonicated gently for 30 seconds and left on a rotary wheel allowing end-over-end mixing for 30 mins. This resulted in NHS activated beads. After 30 mins the particles were washed with MES buffer twice before a 1mL PBS solution containing the required amount of avidin protein was added to the particles. The particles were sonicated gently for 30 sec and left on a rotary wheel allowing end-over-end mixing for 3 hours. After which time the beads were washed with PBST three times before being resuspended in PBST containing 0.05% (wt/wt) BSA protein to block any nonspecific adsorption.

5.3.3. Quantifying bead binding capacity

The binding capacity of all beads were measured using the standard biotin-HRP and ABTS quantification using a NanoDrop 2000 UV-Vis Spectrophotometer. Briefy, 50 µL of avidinated beads (at 1 mg/ml) where washed with PBST once and incubated with a fresh PBST (0.05% wt/wt BSA) solution for 30 mins to block the surface and eliminate any non-specific adsorption. After 30 minutes the beads were washed twice with PBST and incubated with 0.05 µg of Biotin-HRP protein in PBST for 30 minutes. After 30 mins the beads were washed three times with PBST and resuspended in 100 µL of PBST. To this solution 200 µL of ABTS solution was added and the vial was placed onto a rotating wheel for 1 minute. After 1 minute 200 µL of 1% (wt/wt%) SDS "STOP" solution was added to the beads and the absorbance at 410nm was recorded. This final absorbance value was converted into a binding capacity using a calibration curve with standards of known biotin-HRP protein concentrations prepared by serial dilution, the results for which are displayed in figure 5.1 below.

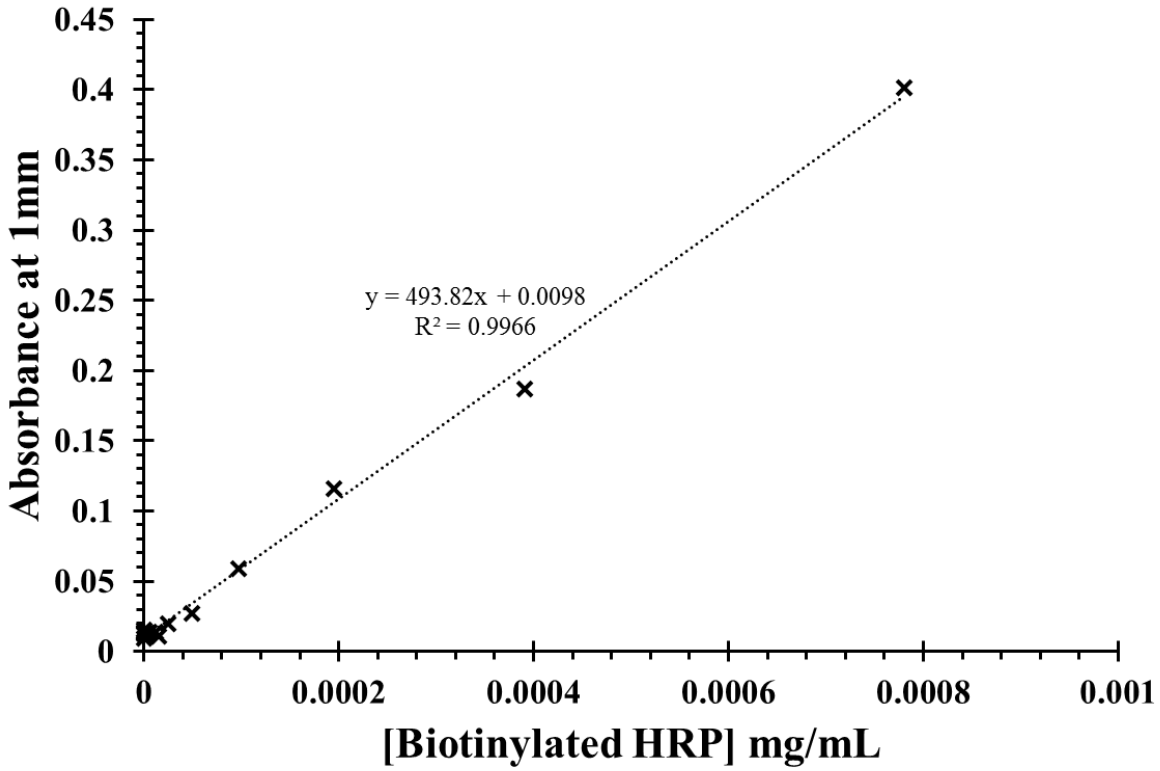

Figure 5. 1: Example calibration curve plotting biotinylated HRP concentration versus measured absorbance.

5.3.4. Binding assay

The avidin coated particles (1 mg/ml) were routinely stored in PBST buffer containing 0.05 (wt/wt%) BSA to act as a blocking solution and reduce non-specific adsorption. When required the particles were diluted to the required concentration, and sonicated briefly (<10 seconds). Typical assay volumes were ~500 – 1000 µL. The final dilution of the beads and its resultant concentration is reported in all graphs and calculations. Samples were prepared by diluting the target biotinylated-BSA into PBST and then adding to the particle dispersions. The solution was incubated at room temperature on a rotating wheel allowing end-over-end mixing. After the required hybridization time (30 minutes), the sample was either analysed immediately, or subject to magnetic assisted aggregation. Each experiment was run multiple times and the standard deviation of each point is shown in the errors bars on the graphs.

For the magnet assisted aggregation (MAS) - the sample was placed next to a permanent magnet, with field strength of 1 milli-tesla present up to 60 mm from the neodymium magnet bar on its surface, until all the beads were judged to have come out of solution ~ 1 minute. The initial solution was removed leaving all the beads on the side of the container and 500 µL PBS was added to the beads. The solution was stirred and the magnet was replaced separating the beads for a second time. When required the magnet was replaced for a third and fourth time. During the last separation, the magnet was removed and the pellet allowed to settle to the bottom of the vial for 30 seconds before finally being vortexed for analysis. This process is aimed to increase particle-particle interactions and thus increase the number of particle aggregates.

5.3.5. Overcoming the hook effect

The hook effect is a phenomenon observed in aggregation assays whereby a high concentration of analyte can result in a reduction in the number of aggregates as the available binding sites are saturated leaving none available for aggregate formation. During the magnetic assisted aggregation process described above, after the first separation the analyte solution was removed and an additional 500 µL solution of avidinated beads in PBST was added to the sample vial. This additional aliquot of beads contained the same number of beads in the original solution, thus doubling the concentration of beads. The remaining process was the same as described above.

5.3.6. Tunable Resistive Pulse Sensing (TRPS) measurement

Measurements were made with the Izon qNano system, purchased from Izon Sciences (Oxford, UK) which incorporates the fluid cell, stretching apparatus, data recording and analysis software (Control Suite). The pores used for measurement of the 3 µm beads were designated by 'NP4000' and most suitable, as determined by the manufacturer, for detecting particles in the range 2000 – 8000 nm, 'NP1000' pores were used to analyse 1 µm beads and most suitable for detecting particles in the range 500 – 2000 nm, finally 'NP400' pores were used to measure the 300 nm beads these are most suitable for detecting particles in the range 200 – 800 nm. The macroscopic stretch applied to the membrane varied from 0 - 8 mm, additional to the separation of approximately 41.5 mm when the membrane is unstretched[3]. Once a baseline current of approximately 100 nA ± 10 was established for each membrane the potential and stretch was kept constant during the experiment. Typical setup for each membrane was: NP4000, Stretch 45.00 mm, Voltage 0.04V; NP1000, Stretch 46.50 mm, Voltage 0.04 V, NP400, Stretch 46.00 mm, Voltage 0.32 V. Izon's calibration beads (obtained with the instrument) were used to calculate the initial concentration and size of all the particles, particles 955 nm in diameter, and 350 nm in diameter were used for this purpose.

5.3.7. Data Analysis

Data capture was performed using Izon Science's Control Suite v2.2 software. The number of data points captured for each experiment exceeded 500.

Upon processing the raw data with the software a ".txt" file was created which contained information on each pulse recorded during the experiment. The peak height and time was extracted from the data and copied into a spreadsheet. Microsoft Excel 2010 was used to analyse the data further. The average peak height was calculated from all the data points captured and plotted against concentration to find the average size of the particles.

To monitor changes in aggregate size, the data was first extracted as a .txt file as described above. A blank sample with no biotin was used to determine the location and size of the monomer and larger aggregate peaks. As the blank sample contained no analyte and therefore the signal represented the monomer, a bin size which accounted for these data points was determined. As the peak height is proportional to the volume displaced by the traversing particle[4,5] a dimer would produce twice the signal, and a trimer three times the signal

intensity of the monomer, and so on for each larger aggregate. A histogram could then be constructed using multiples of the monomer peak to determine the number of larger aggregates. Once the number of data points for each bin had been determined from the raw data, the number was converted into a percentage by dividing it by the total number of data points for the experiment. The ratio was then plotted as a function of analyte concentration. In each experiment the fraction of aggregates up to and including the dodecamers was calculated, even if they are not plotted in the figures. All assay conditions and concentrations were repeated a minimum of three times and the average of each experiment is plotted on the graphs, the error bars and the standard deviation in the results.

5.4. Results and Discussion:

5.4.1. Aggregation of avidin modified SPM beads by biotinylated BSA addition

Avidin functionalised SPM beads were added to a solution containing biotinylated-BSA. From the supplier information, each BSA protein contains an average of 9 biotin molecules, allowing multiple avidin molecules to interact with the biotinyated-BSA. The solution was incubated on a rotary wheel for 25 minutes and then placed in a MagRack to separate the beads from the solution and bring them into close proximity with each other. Following this a 40 µL aliquot of the sample was placed into the upper fluid cell of the TRPS instrument.

Figure 5.2A (blue curve) displays a plot of the mean Δi_p signal versus analyte concentration. As the concentration of the analyte was increased the average Δi_p remained constant until a sharp increase in Δi_p around a concentration of 1 x 10^{-10} mol/dm^{-3} biotinylated-BSA. The mean pulse height continues to increase up to a concentration of 1 x 10^{-8} mol/dm^{-3} before decreasing back to its original value. The increase in Δi_p was attributed to the particles forming larger aggregates in the presence of the analyte, at lower concentrations of analyte the number of aggregates was too low to be detected as the majority of the signal comes from individual monomers. The decrease in signal from aggregation at high concentrations of analytes has been well documented for agglutination assays. This decrease in aggregate size results from the saturation of the binding sites on the particle surface with the analyte and is known as the 'hook' effect[6]. As stated above there was no change observed when plotting the mean Δi_p as a function of concentration at biotinylated-HRP concentrations below 1 x 10^{-10} mol/dm^{-3} suggesting that this method is insensitive to small changes below this concentration.

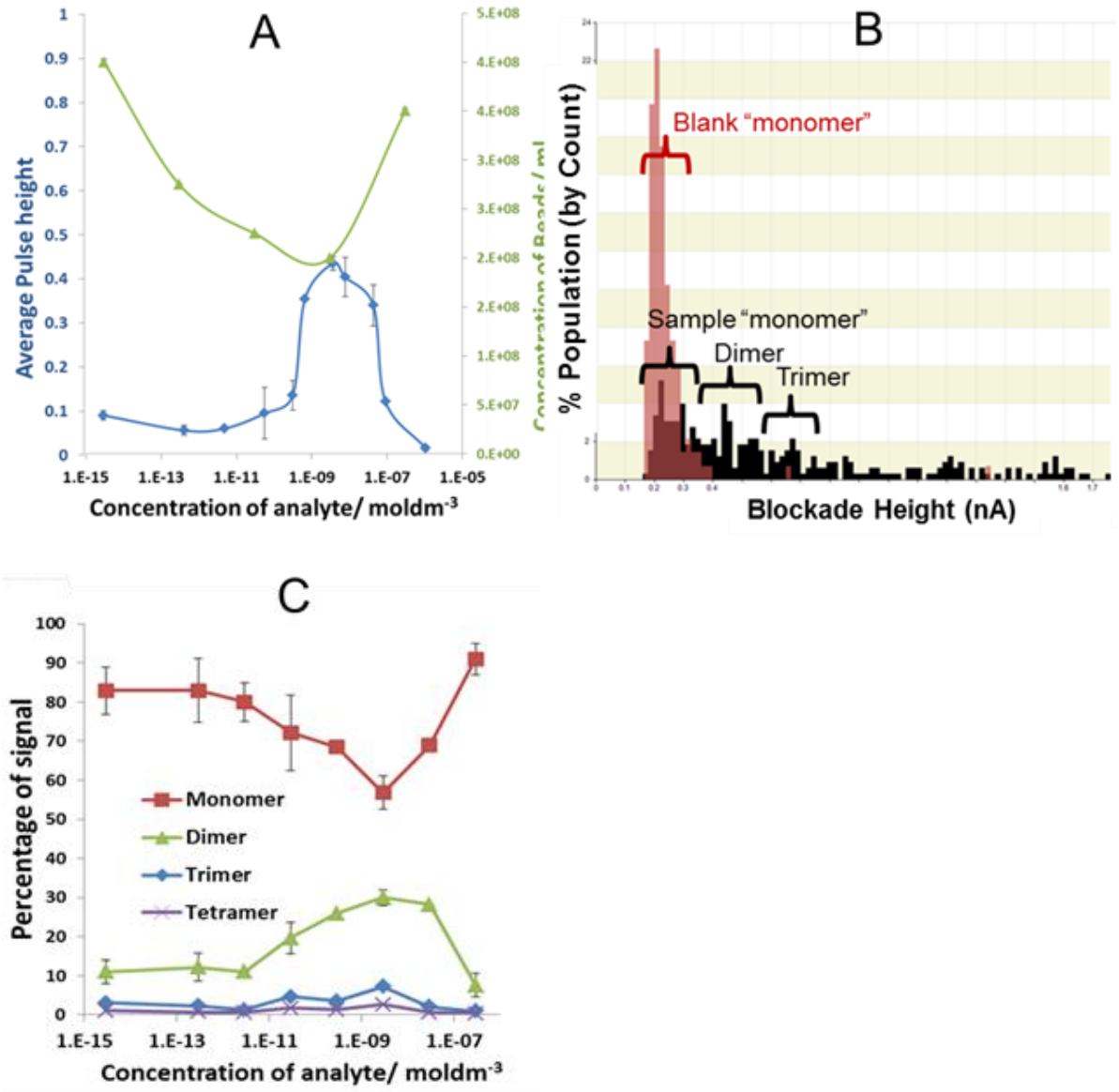

Figure 5. 2: Assay using 3 µm diameter beads, binding capacity of 14 µg/mg, assay time of 25 minutes, 5 x 10^8 beads/mL. **A** Change in average pulse height, Δi_p = Blue, and bead concentration = green, against concentration of biotinylated analyte. **B** Example of raw data from an individual experiment, red histogram displays the pulse height (Δi_p) for a blank sample, the black distribution shows the change in Δi_p for an analyte concentration of 1 x 10^{-9} moldm^{-3}. Overlaid is the example gate size for the monomer, dimer etc used to count the number of particles for plot C. **C** Plot of percentage of signal of monomer = red, dimer = green, trimer = blue and tetramer =purple.

An alternative method explored was to follow the change in particle concentration with biotinylated-BSA concentration. As the particles aggregated the total number of beads in solution decreased, as monomers were consumed into growing particle clusters. The TRPS instrument was calibrated to measure the change in particle concentration. The same data

used for the above Δi_p measurements was re-analyzed, the results are plotted in figure 5.2A (green curve). Measuring the change in bead concentration appears to be more sensitive, and a decrease in bead count could be observed at concentrations as low as 1 x 10^{-12} mol/dm^{-3}. In order to minimise variation it was important to consider factors affecting these results. If insufficient time was given for the beads to come out of solution in the presence of the magnet, some beads are washed out of the vial during the MAS stage the variation from run to run could be affected. If the technique is to be used across multiple labs the variation in the technician's ability to wait for all the beads to be extracted from the solution could result in massive variations in the results, and given that it is hoped to develop these techniques for POC assay, user reproducibility must be high, therefore a robust method of data analysis is needed.

In this study commercial Dynabeads and Ademtech beads were used; these have relatively uniform sizes with <2% and <10% *CV respectively.* Due to the high level of uniformity in diameter, it *was possible to isolate the signal from the larger aggregates from that of the individual beads.* Figure 5.2B displays the raw data from the Izon Software for a "blank" (red) bead set and a "sample" bead set incubated with 1 x 10^{-9} $moldm^{-3}$ biotinylated-BSA (black). In the blank sample the beads produced an individual peak which was identified as "monomers". The data was then gated for the monomer peak and 94% of all the data points were accounted for within this gate. The remaining 6% is most likely due to nonspecific aggregation, or off-axial translocation leading to a spread in the signal. This gate was titled "Monomer"; as the Δi_p is proportional to volume of the particle traversing the pore, a dimer should in theory produce a Δi_p twice the magnitude of a monomer. Therefore by doubling the gate size the number of dimers could be counted. A similar process was performed to account for aggregate sizes up to decamers.

Figure 5.2C summarises the quantitative analysis of the percentage of monomers, dimers, trimers and tetramers formed in the assay using the 3 µm beads, as a function of analyte concentration. It was observed that the formation of aggregates was closely correlated with the decrease in monomers, i.e., the minimum number of monomers appeared at an analyte concentration at which the maximum number of dimers, trimers, and tetramers were observed. At concentrations between 10^{-12} and 10^{-9} M there was a direct correlation between the number of dimer aggregates and the biotinylated-BSA concentration.

Again as inferred from figure 5.2A at concentrations greater than 1 nM there was a decrease in number of all forms of aggregates and increase in monomers was observed due to the onset of the hook effect. The variation in results from assay to assay is lower using this analysis, than for the previous two examples for mean bead size and concentration. The reduction in variation is expected as the average population value is no longer being used, and therefore the small number of larger aggregates is not lost on the analysis. In addition if any particles are lost during the wash and MAS stages it does not impact upon the ratio between monomers and larger aggregates as the remaining fraction is examined rather than a raw concentration. It was assumed that an equal proportion of monomers and dimers would be lost during any washing stages; this may not hold true as larger aggregates tend to separate out from solution at faster rates. However, the reduction in errors bars and the mirroring of the dimer and monomer peak suggest that there was not a strong sample bias toward larger aggregates. This method is suggested as means to monitor particle aggregation, hence any following data was treated in the same way.

5.4.2. Effect of magnetic assisted aggregation (MAS) and overcoming the hook effect

Figure 5.3A presents the number of monomers as a function of analyte concentration and number of MAS performed. The influence of magnetic separation steps on the assay itself was determined by analysing the number of monomers with and without the MAS. Several observations could be made from these results, firstly in the absence of the MAS (red curve) fewer aggregates appeared to form, and the number of monomers was high across the range of analyte concentrations. Without the application of a magnetic field aggregates are only formed if two beads collide with the correct orientation and alignment to form a bond. Upon the addition of the magnetic field the number of interactions increased, leading to an increase in aggregation and a greater decrease in the number of monomers. When the number of MAS stages was increased from 2 to 4 the number of monomers across the concentration range did not decrease dramatically, suggesting that 2 MAS steps was sufficient to increase aggregate formation.

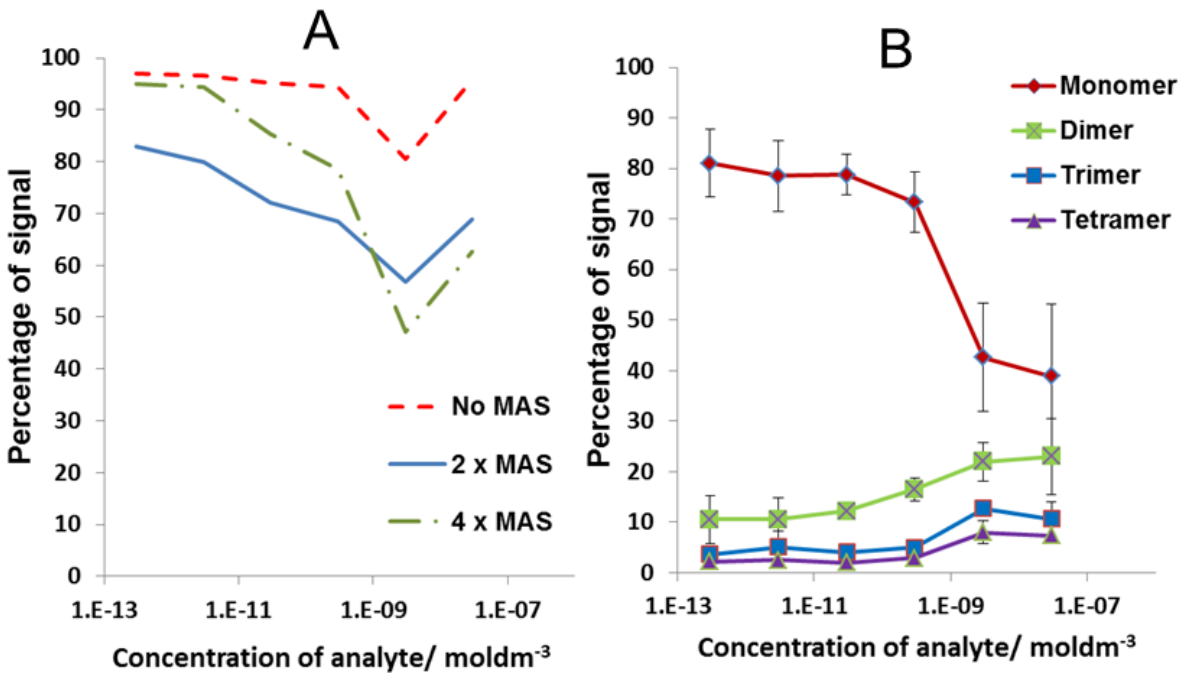

Figure 5. 3: A Effect of the number of magnet assisted aggregation stages (MAS) on the distribution of monomers for the reaction conditions using 5 x 10^8 beads/mL of 3 µm avidin modified beads 25 minutes assay time, binding capacity 14 µg/mg. **B** Under the same bead conditions as **A**, effect of the addition of more beads during the MAS. Red = monomer, Green = Dimer, Blue = trimer and purple = tetramer.

The hook effect could be problematic during an analytical measurement as two concentrations of analyte could produce the same aggregation ratio. To explore the possibility of removing the hook effect, a second aliquot of beads was added to the solution after the first MAS stage. The MAS stage was repeated two more times and the sample analysed. Figure 5.3B displays the results and the fraction of the sample that was measured to be mono-, di-, tri- and tetra-mers. It is clear from figure 5.3B that the characteristic decrease in aggregate signal and increase in monomer signal typically observed at high concentrations of analyte was no longer present, and a gradual decrease in monomer signal is observed across the entire range of the assay suggesting that the hook effect had been overcome. The explanation for this is that at high concentrations of analyte the majority of the binding sites on the beads are occupied. Therefore when brought into contact with each other no free binding sites exist to form aggregates. The addition of fresh beads after the first MAS stage introduces vacant binding sites leading to aggregation.

5.4.3. Effects of binding capacity, bead concentration, and diameter

To further investigate the sensitivity of the assay, a set of experiments was devised in which the binding capacity was systematically varied. Figure 5.4A and B present the percentage of monomers and dimers, respectively, produced by the interaction of 3 µm SPBs across a range of analyte concentrations for 4 different binding capacities. In each experiment the binding capacity of the beads was gradually decreased from 14 µg/mg to 3 µg/mg. As the binding capacity is lowered, the intensity of the monomers and dimers signal decreased. Hence as the binding capacity is reduced the beads are less efficient at forming aggregates and therefore the signal is diminished.

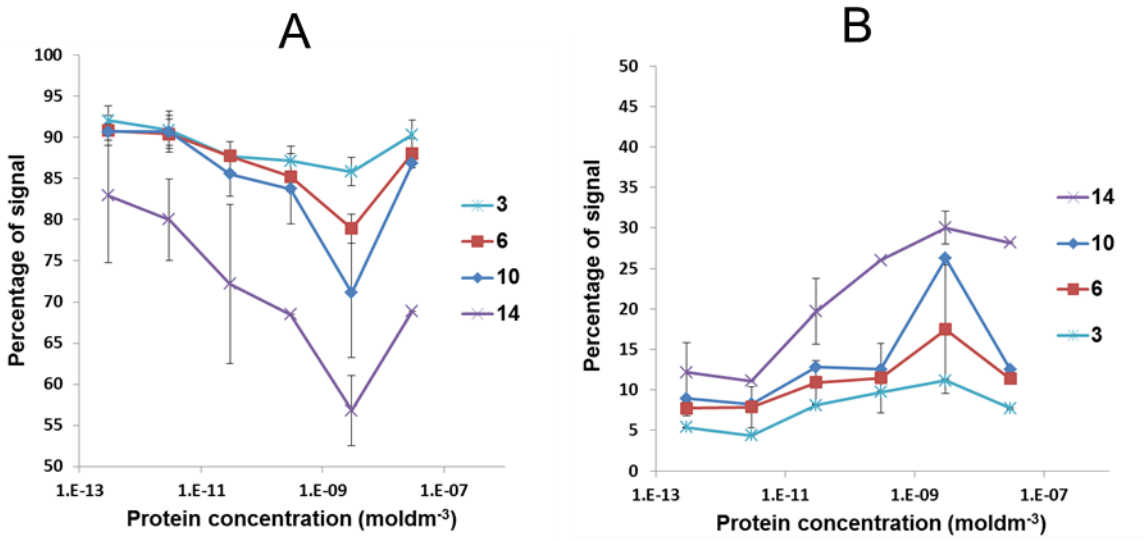

Figure 5. 4: Distribution of monomers **A,** and dimers **B**, for the reaction conditions using 5 x 10^8 beads /ml of 3 µm avidin modified beads. The binding capacity, displayed in the legend in terms of µg/mg of beads was varied and the intensity of change in aggregate size plotted as a function of analyte concentration.

Figure 5.5A illustrates the effect of lowering the number of beads in the assay, and thus reducing the total number of binding sites. This had the effect of shifting the onset of the hook effect to a lower concentration as the total number of binding sites in solution are saturated at lower concentrations. Whilst the hook effect appears earlier at a lower analyte concentration it is also worth noting that the maximum decrease in monomer signal is also shifted to a lower analyte concentration, effectively boosting the sensitivity. The onset of the hook effect was found to be closely linked to both the concentration of avidin in the reaction and the density of avidin on the beads.

To test the effect of particle size a similar set of experiments were then performed with biotinylated-BSA for avidin functionalized 1 µm beads and the results from this are shown in figure 5.5B. Qualitatively, similar trends were observed when changing the concentration of 1

µm beads as previously observed for the 3 µm beads hence, both the intensity and position of the maximum number of aggregates can again be tailored by changing the bead number and binding capacity. Quantitatively, however, the results for the 1 µm beads differed from the 3 µm beads. It is clear from figure 5.5B that when a similar concentration of beads is used for the two bead sizes (green and blue curves) the peak in aggregation appeared at much lower concentration of analyte for the 1 µm beads and a much larger fraction of beads formed aggregates. The interpretation of this result is that when the same number of 1 and 3 µm beads are used the 1 µm beads aggregate more efficiently. This is most likely due to the fact that the 1 µm beads have a higher rotational diffusion coefficient. When the binding capacity of the beads were matched i.e. more 1 µm beads were added to solution (blue and red curves) the onset of the hook effect again is shifted to higher concentrations of analyte, reflecting the change in total binding capacity of the beads surface.

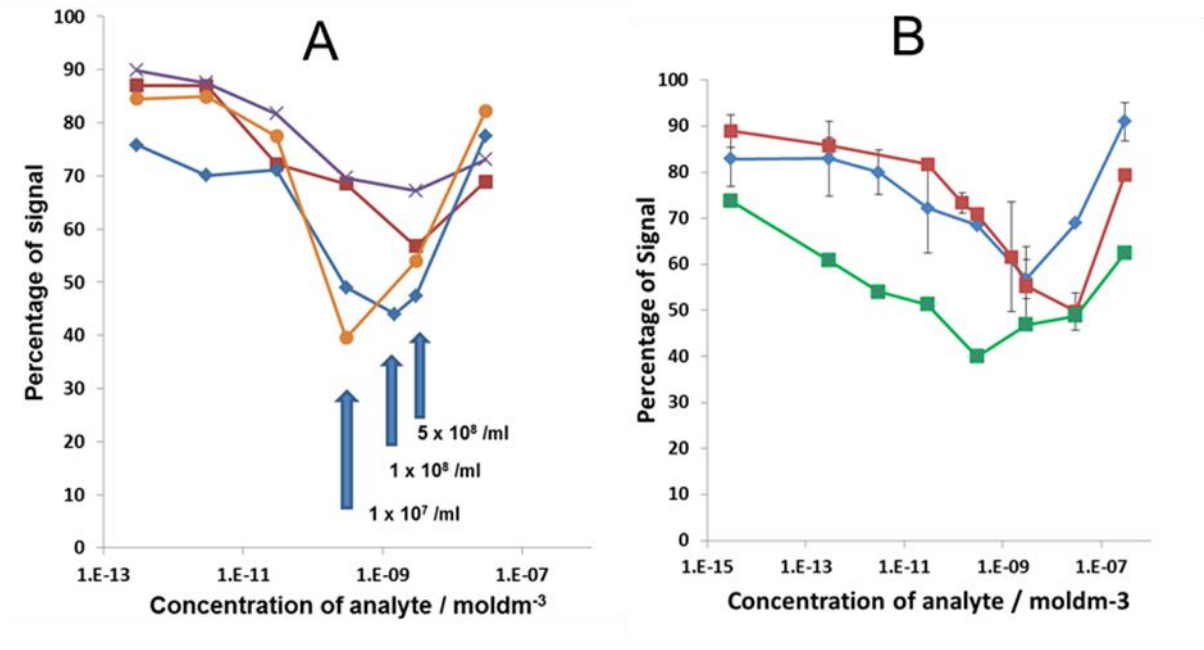

Figure 5. 5: A Effect of concentration of beads upon maximum decrease in monomer signal using 3 µm avidin modified beads, binding capacity of 14 µg/mg, 25 min assay time and 5 x 10^8 beads /mL = red, 2.5 x 10^8 beads /mL = purple, 1 x 10^8 beads /mL = blue, and 1 x 10^7 beads/mL = orange. Highlighted on the graph is the minimum in each curve for the dilutions. **B** Effect of concentration of beads upon maximum decrease in monomer signal, 25 min assay: 3 µm avidin modified beads 5 x 10^8 beads /mL, binding capacity 14 µg/mg = blue, 1 µm avidin modified beads, 6 x 10^9 beads /mL, binding capacity 20 µg/mg = red, and 1 µm avidin modified beads, 5 x 10^8 beads /mL binding capacity 20 µg/mg = green.

An interesting deviation in the behaviour of the 1 µm compared to the 3 µm beads arises in the fact that the trimers behave in a comparable manner to that of the monomers, i.e. the peak in trimer concentration best matches the dip in monomers, figure 5.6A, whereas for 3 µm beads a decrease in monomers is most closely correlated with an increase in dimers as

demonstrated in figure 5.6D. It is not immediately clear why there should be a preference for trimers.

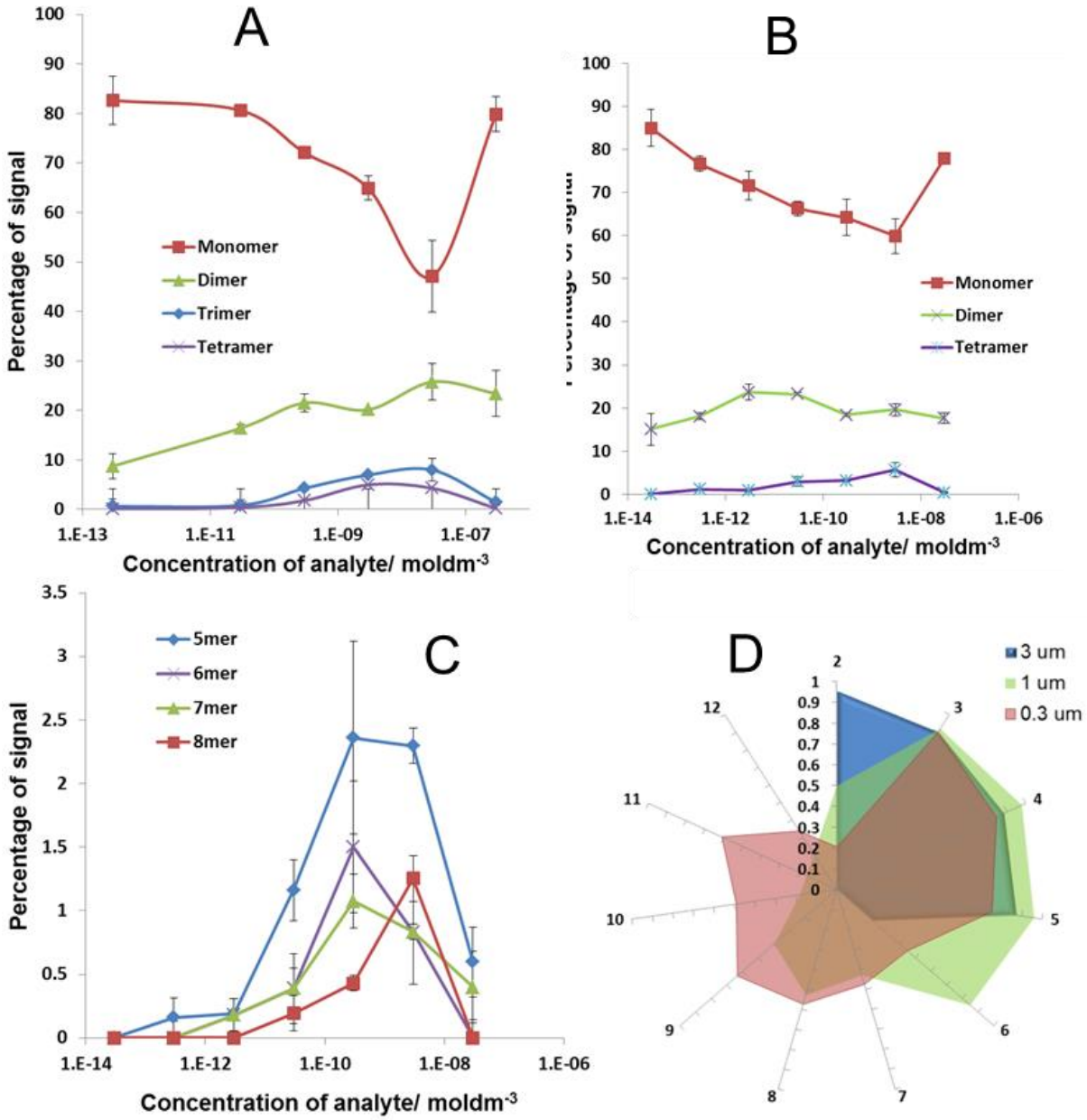

Figure 5. 6: A Distribution of monomer = red, dimer = green, trimer = blue and tetramer = purple. 1 µm avidin modified beads 25 min assay time 6 x 10^9 beads /mL, binding capacity 20 µg/mg. **B** Distribution of monomer = red, dimer = green, and tetramer = purple using 0.3 µm Streptavidin modified beads 25 min assay time 1 x 10^{10} beads /mL, binding capacity 4 µg/mg. **C** Distribution of 5mer = blue, 6mer = purple, and 7mer = green and 8mer = Red using 0.3 µm Streptavidin modified beads 25 min assay time 1 x 10^{10} beads /mL binding capacity 4 µg/mg. **D** Correlation between the increase in aggregate size versus the decrease in monomer signal for the three different bead sizes.

To further investigate the relationship between bead size and aggregate size a smaller 300 nm bead functionalised with streptavidin was added to the target analyte. In these assays a

comparable binding capacity was used. The results of this assay are displayed in figures 5.6B and C. In figure 5.6B the change in monomer, dimer and tetramer are plotted as a function of analyte concentration, a similar trend in monomer is observed and the numbers decrease as the analyte concentration increases. Unlike the larger 3 µm particles, the dimers in solution showed no correlation with the monomers and instead the larger tetramers mirrored the monomer relationship. Figure 5.6C plots the larger 5-, 6-, 7- and 8-mers versus concentration and whilst their signal intensity is weak they show good agreement with the decrease in the proportion of monomers in the analysed population.

The correlation between monomers and the larger aggregates was plotted for the 3, 1 and 0.3 µm diameter beads as illustrated in figure 5.6D. For the larger 3 µm beads a strong correlation was observed between the monomers and the di-, tri- and tetramers in solution. As the beads diameter decreased the correlation between the monomer and dimer decreases from 0.96 to 0.5 and 0.2 for the 3, 1 and 0.3 µm beads respectively. When using the smaller 0.3 µm particles there was a good correlation between 3-5mers and 9-11mers with the decrease in monomer concentration. In these experiments the smaller particles were clearly more efficient at forming larger aggregates, and one possible explanation is that the smaller beads have an ability to nucleate and grow in aggregate size, mimicking crystallization of nanoparticles. Micron sized particles have previously been used as model systems to aid with nucleation and growth studies[7,8]. Similar observations of cluster size might have proven difficult using flow cytometry or light scattering techniques and the TRPS may offer the possibility of studying the aggregation and growth of colloidal particles in solution because unlike other systems it is possible to get information regarding the individual clusters rather than an average and an assumed normal distribution.

5.5. Conclusion

TRPS was used to characterise the aggregation of avidin functionalized particles in the presence of a biotinylated target. Several methods for data interpretation, aimed at increasing the reproducibility of the experiment and allowing for a detailed and informative study of the aggregation state, were discussed. Further, TRPS technology was used to investigate key experimental variables in designing a magnetic aggregation assay. A summary of all the factors that were found to influence the sensitivity of the assay can be found in figure 5.7. The resulting assay platform was capable of operating over several orders of magnitude of concentration; the sensitivity of the assay could be improved upon by increasing the density of receptors on the beads, decreasing the size of the beads used, and/or decreasing the total number of beads used in the assay. However, higher sensitivities occasionally resulted in a more rapid saturation of the beads with analyte and thus earlier onset of the hook effect. By controlling the particle size, binding capacity, and particle concentration, the aggregation of SPM beads in the presence of the target analyte could be tailored and predicted to produce a simple and sensitive analytical method. We also note that for smaller particles it may be possible to monitor the increase in the larger 9-11mer particle aggregates and utilize their frequency to follow the analyte concentration.

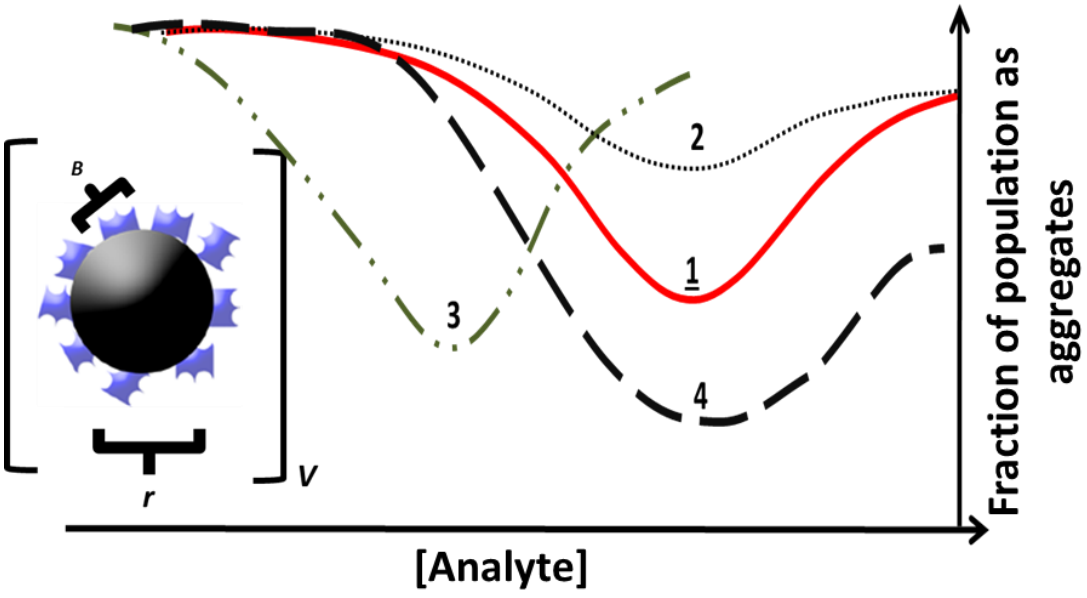

Figure 5. 7: Summary schematic of the changes in monomer population related to physical properties of the SPM beads. 1: reference curve, 2: decrease binding capacity (B), 3: decrease concentration (V), 4, decrease bead radius (r).

5.6. References

(1) Gubala, V.; Lynam, C. C. N.; Nooney, R.; Hearty, S.; McDonnell, B.; Heydon, K.; O'Kennedy, R.; MacCraith, B. D.; Williams, D. E. *Analyst* **2011**, *136*, 2533–2541.

(2) Pal, A. K.; Aalaei, I.; Gadde, S.; Gaines, P.; Schmidt, D.; Demokritou, P.; Bello, D. *ACS Nano* **2014**, *8*, 9003–9015.

(3) Platt, M.; Willmott, G. R.; Lee, G. U. *Small* **2012**, *8*, 2436–2444.

(4) Vogel, R.; Willmott, G.; Kozak, D.; Roberts, G. S.; Anderson, W.; Groenewegen, L.; Glossop, B.; Barnett, A.; Turner, A.; Trau, M. *Anal. Chem.* **2011**, *83*, 3499–3506.

(5) Willmott, G. R.; Vogel, R.; Yu, S. S. C.; Groenewegen, L. G.; Roberts, G. S.; Kozak, D.; Anderson, W.; Trau, M. *J. Phys. Condens. Matter* **2010**, *22*, 454116.

(6) Weatherall, E.; Willmott, G. R. *Analyst* **2015**.

(7) Cohen-Tannoudji, L.; Bertrand, E.; Baudry, J.; Robic, C.; Goubault, C.; Pellissier, M.; Johner, a.; Thalmann, F.; Lee, N.; Marques, C.; Bibette, J. *Phys. Rev. Lett.* **2008**, *100*, 108301.

(8) Perry, R. W.; Meng, G.; Dimiduk, T. G.; Fung, J.; Manoharan, V. N. *Faraday Discuss.* **2012**, *159*, 211–234.

Chapter Six

Multiplexed detection of growth factors with TRPS

6.1. Abstract

Diagnostics that are capable of detecting multiple biomarkers can improve the accuracy and efficiency of bioassays. In chapter 4 the potential of an aptamer-based sensor (aptasensor) utilising Tunable Resistive Pulse Sensing (TRPS) was demonstrated**.** Here**,** the technique is advanced towards identifying key experimental designs for multiplexed TRPS aptasensor assays. The assay utilised superparamagnetic beads, and using TRPS monitored their translocations through a pore. If the surfaces of the beads are modified with an aptamer, the frequency of beads (translocations/minute) through the pore can be related to the concentration of specific proteins in the solution. In this chapter TRPS was used to observe the binding of two proteins to their specific aptamers simultaneously. A series of experiments are described illustrating key factors which are integral to bead-based assays and demonstrate a general method for a multiplexed assay. In summary, the effects of bead size, concentration, potential bias, pH and aptamer affinity to enhance the sensitivity and practically of a TRPS aptasensor have been explored. The method utilises the fact the binding of the aptamer to the protein results in a change in charge density on the bead surface, the isoelectric point of the protein then dominates the mobility of the beads. By alteration of the applied potential to the instrument it is possible to produce a positive signal in a simple multiplexed assay.

6.2. Introduction:

As highlighted in chapters 3 and 4 TRPS is well suited to detect DNA and DNA-protein interactions; previous work has provided proof-of-concept studies on the technology in which the velocity and frequency of aptamer-tagged beads changes upon the addition of the target analyte as the aptamer folds to a specific conformation whereby the target binds, shielding the surface charge and altering double layer structure, as has been demonstrated with the target thrombin. A significant development to this method would be the ability to detect multiple proteins at once.

Building upon the foundations set in the previous chapters, this chapter is focussed around the development of a multiplexed aptasensor to the haemostatic growth factors Vascular Endothelial Growth Factor (VEGF) and Platelet Derived Growth Factor (PDGF). In normal physiology these growth factors regulate the growth of new blood vessels, however certain disease states, such as those in cancer, hijack these pathways to increase blood supply for tumour growth. As such both proteins are involved in various disease processes such as cancer[1], atherosclerosis[2], and Alzheimer's[3] and could be potential biomarkers for the diagnosis and monitoring of these diseases. Although circulating levels of VEGF have been found to be variable between individuals, between 9 – 150 ng/L[4], VEGF levels have been demonstrated to be elevated in several aggressive types of cancer, such as ovarian[5], haematoloical[6] and gastric carcinoma[7] and VEGF measurement has been highlighted as both a potential prognostic or diagnostic marker[4] and for comparison between pre- and post-operative cancer states[5,7]. PDGF levels have also been found to be elevated in several different forms of cancer and has recently been added to the Glasgow Prognostic Index, which measures inflammatory mediators, as an important indication of tumour and significant predictor of survival[8]. Previous studies have measured both VEGF and PDGF levels in cancer patients undergoing anti-VEGF treatment[9], however this was performed over two different systems, increasing the cost and time considerations of the assay.

To monitor two analytes simultaneously in one-step analysis the ability of TRPS to provide accurate particle-by-particle analysis was utilised. The ability of TRPS to accurately calculate the size of individual objects as they traverse the pore was exploited and allows the data from each particle set to be separated according to their size. By using two differently sized beads and separately functionalising them with anti-VEGF or anti-PDGF aptamers, as displayed in figure 6.1A, it is possible to separate the individual signals based on Δi_p, figure 6.1C, and

monitor changes to their frequency and speed, relating them back to the target analyte concentration.

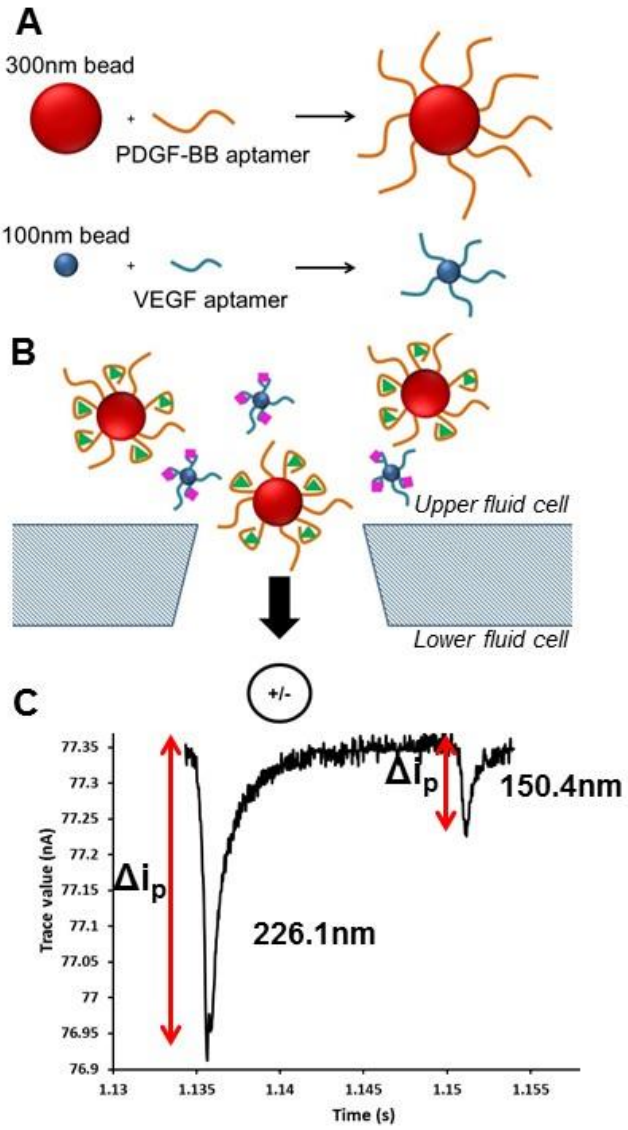

Figure 6. 2: A Schematic of the multiplexed experimental process; two beads of different sizes are conjugated to either VEGF or PDGF. **B** Beads are incubated with a combination of concentrations of VEGF and PDGF for 30 minutes; as they bind to the target their velocity and frequency through the pore is monitored. **C** Recorded "resistive peaks" for two different sized beads; the blockade magnitude (Δi_p) of each peak is proportional to the volume of each bead and can therefore be calibrated to provide the diameter of each individual bead.

6.3. Method:

6.3.1. Chemicals and reagents

The following chemicals were sourced from Sigma Aldrich, UK, without any further purification unless otherwise stated: Phosphate Buffered Saline (PBS – P4417), Tween 20 (P1379), Bovine Serum Albumin (BSA – A2153), and thrombin (T7513). DNA sequences were obtained from Sigma Aldrich's custom oligonucleotides service as lyophilised powders and made up to a stock concentration of 100pmol/μL: 5' CAG GCT ACG GCA CGT AGA GCA TCA CCA TGA TCC TG-Biotin-3' (anti-PDGF-BB aptamer)[10], 5' ATA CCA GTC TAT TCA ATT GGG CCC GTC CGT ATG GTG GGT GTG CTG GCC AG-Biotin-3' (VEa5 anti-VEGF aptamer)[11]. 5' TGT GGG GGT GGA CGG GCC GGG TAG ATT TTT-Biotin-3' (V7t1 anti-VEGF aptamer)[12]. Human recombinant PDGF-BB and human $VEGF_{165}$ were purchased from Life Technologies, UK (PHG0044 and PHC9394, respectively). Water purified to a resistivity of 18.2 MΩ cm (Maxima) was used to make all solutions unless otherwise specified.

Streptavidin modified superparamagnetic beads of 120 nm (bio-adembeads streptavidin plus 0321) and 300 nm (bio-adembeads streptavidin 0313) in diameter were purchased from Ademtech (France). Binding capacities of 120 nm and 300 nm beads according to the manufacturer were 3512 pmol/mg and 477 pmol/mg respectively. Carboxyl beads of known concentration and diameter (SKP200; mode diameter 200 nm) were sourced from Izon Sciences (Oxford, UK) to be used as a calibrant. All bead dilutions were performed in 1xPBST (0.05% Tween).

6.3.2. Aptamer functionalisation

The 120 and 300 nm beads were vortexed for 1 minute, sonicated for 1 minute and diluted to a concentration of 3×10^9 beads/mL in PBST. The streptavidin coated beads were incubated with a 10-fold excess above the manufacturer specified binding capacity of the desired biotinylated aptamer at room temperature on a rotary wheel for 30 minutes to allow the streptavidin to react with the biotinylated ends of the DNA. The functionalised beads were then removed from the rotary wheel and centrifuged for 2 minutes at 10 000 rpm before being placed onto a MagRack (Life Sciences). After 2 minutes the beads had formed a visible cluster in the sample vial adjacent to the magnet and the solution was carefully removed and replaced with an equal volume of PBST – this wash stage was performed twice to remove

any excess aptamer which would lower the sensitivity of the binding assay. These could then be stored in the fridge.

6.3.3. Protein measurement

6.3.3.1. Individual protein measurement

Either 120 nm or 300 nm beads functionalised with the aptamers were divided into several vials at a concentration of 3×10^9 beads/mL, to which varying volumes of either PDGF-BB or $VEGF_{165}$ stock solution was added to each vial to create samples of aptamer modified beads mixed with a range of protein concentrations. In all cases the volume of the solution was adjusted and kept constant by adding PBST. Each sample was left on a rotary wheel for 30 minutes to allow the protein to associate before being introduced into the TRPS instrument.

6.3.3.2. Multiplexed protein measurement

120 nm beads with V7t1 aptamer and 300 nm beads with PDGF-BB aptamer were prepared as described above in section 6.3.2. at a bead concentration of 6×10^9 beads/mL. 16 samples containing 50 µL of 120 nm beads and 50 µL of 300 nm beads were prepared, and combinations of concentrations of PDGF-BB and $VEGF_{165}$ were added. Each sample was left on a rotary wheel for 30 minutes to allow the protein to associate before being introduced into the TRPS instrument. Each sample was analysed via TRPS for the maximum run time of 10 minutes. The peak traces were calibrated and separated according to their size for independent analyses. Each individual blockade trace was examined for shape and directionality before being included in the sample set.

6.3.4. Tunable Resistive Pulse Sensing (TRPS) measurement

Measurements were made with the Izon qNano system, purchased from Izon Sciences (Oxford, UK) which incorporates the fluid cell, stretching apparatus, data recording and analysis software (Control Suite V2.2.2.117). The pores used were designated “np200” by the manufacturer and are described as most suitable for detecting beads in the range 100 – 300 nm. A stretch of 46 mm and voltage of +/-0.4 V were chosen so that blockade events were clearly visible above the level of noise (<10pA); these conditions were maintained throughout the experiments so that data was comparable. 80µL of electrolyte buffer (PBS) was carefully pipetted into the lower fluid cell, taking care not to introduce bubbles. The

upper fluid cell was then attached to the instrument and 40 µL of PBST was added to enable confirmation of a stable baseline and clean pore. When a positive current is applied (+0.4 V) peaks are visible as a downward deflection from the baseline, when a negative current is applied (-0.4 V) peak were visible as upward deflections of the baseline.

6.3.5. Data Analysis

6.3.5.1. Removal of reverse peaks

Raw data was analysed by examining each individual blockade trace visually using the Izon ControlSuite V2.2.2.117 Software. When resistance was highest at the beginning of this peak and tailed toward the baseline with time this was considered a “normal” translocation. When the current increased gradually and then dropped sharply this was considered a “reverse” translocation and removed from subsequent data processing. Examples of these are shown in figure 6.3.

6.3.5.2. Extraction of particle rate for each bead population

Each bead records a blockade magnitude that reflects its volume, for example 120 nm Ademtech beads typically produce a blockade magnitude of 0.17 nA with the pore setup used here. Data which had been visually inspected as described above were then calibrated with beads of known diameter and narrow distribution. Prior to any analysis the Ademtech beads were calibrated separately to accurately measure the range of particle sizes in the provided batches and these ranges were used to provide filter information for data processing of experimental samples. Peaks recorded as being between 100 and 200 nm were recorded as “120 nm” and peaks between 210 and 400 nm were recorded as “300 nm”. Data was then extracted as a .csv file containing data for each particle and the particle rate was then calculated by counting the number of beads observed divided by the recording time.

6.4. Results and Discussion:

6.4.1. Detection of $VEGF_{165}$ under positive bias

The goal of the final assay was to detect both VEGF and PDGF simultaneously. Firstly, it was important to confirm that the interaction of the chosen aptamers and proteins did create a measurable signal, similar to that observed in chapter 4. Typically anti-VEGF aptamers were immobilised onto 120 nm beads and anti-PDGF aptamer was immobilised onto 300 nm beads as portrayed in Figure 6. 2.

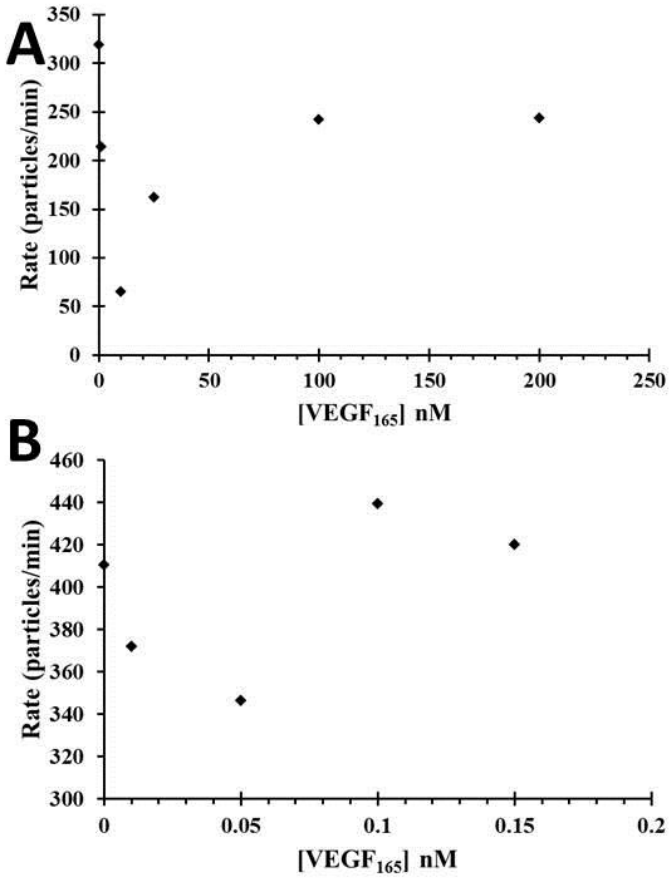

Figure 6. 3: scatter plots displaying average rate for 120 nm bead functionalised with VEa5 **(A)** and V7t1 **(B)** aptamers against concentration of $VEGF_{165}$ under an applied positive bias.

Initially the TRPS instrument was set up with a positive bias applied to the electrode under the nanopore (lower fluid cell) similarly to that used in chapters 3 and 4. Samples containing 120 nm beads functionalised with VEa5 anti-VEGF aptamer were prepared and incubated with several concentrations of $VEGF_{165.}$ These samples were then recorded via TRPS, with the resultant data displayed in Figure 6. 3A. It was expected that the rate would diminish with increasing protein concentration, as had been previously observed for the thrombin protein for the similar experimental design discussed in chapter 4 due to the protein binding the

aptamer and shielding the negative charge of the phosphate backbone. As the concentration of $VEGF_{165}$ was increased from 0 to 10nM the predicted decrease in particle rate was observed, however at higher concentrations, > 10nM, the particle rate increased before reaching a steady value of ~220 beads per minute. The current traces were examined in more detail and observed numerous double peaks, shown in Figure 6. 4. The tunable conical pore used in TRPS gives rise to a characteristic peak shape, displayed in Figure 6. 2 and Figure 6. 4 and explained in detail in chapter 2 and elsewhere[13]. The shape of the peak provides information on the direction in which the particle is travelling. For beads travelling from the top of the fluid cell entering the narrow sensing zone first before then traveling through the pore into the expanding conical region they produce a peak shape as shown in Figure 6. 2 and Figure 6. 4. If a particle were to travel in the reverse direction the peak shape would be inverted Figure 6. 4. Below 10 nM no reverse peaks were observed throughout the experiment, however when the concentration of VEGF increased, > 10 nM, there was an increase in the number of peak traces, termed "reverse peaks" which represent beads coming back up from the base of the pore. The presence of these reverse peaks led to an increase in the rate recorded by the software which does not distinguish between the peaks based on direction of travel. When these erroneous peaks were then removed from the data set, the rate diminished, as expected, with increasing $VEGF_{165}$ concentration, as shown in Figure 6. 5.

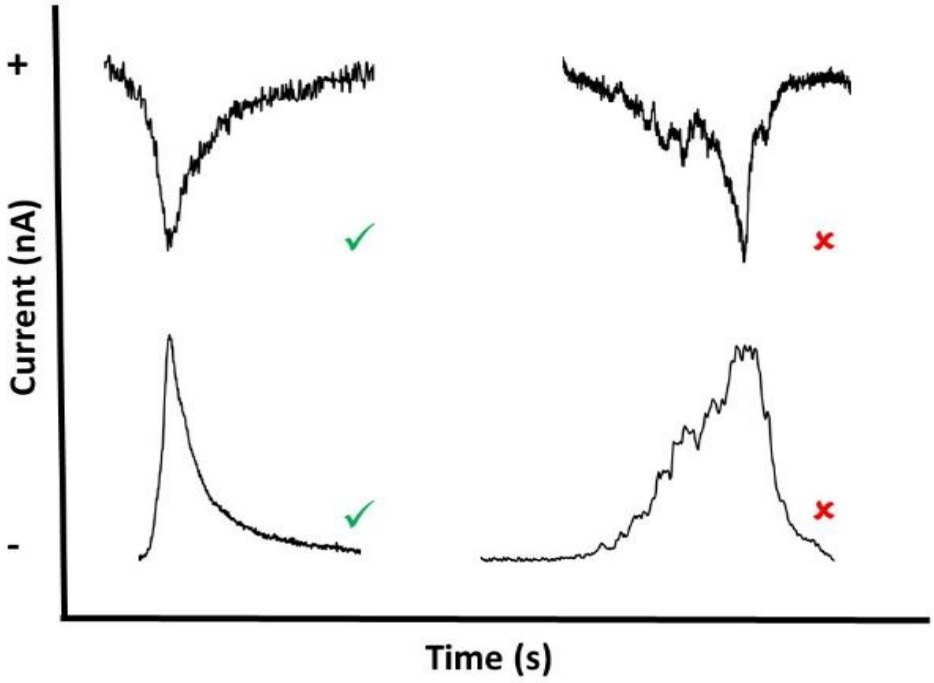

Figure 6. 4: Example blockade traces indicative of forward (left) or reversed (right) travel through the pore under a positive (top) or negative (bottom) bias.

To confirm that this effect was not the result of a specific mechanism between VEa5 and the heparin binding domain (HBD) of $VEGF_{165}$[11] this experiment was repeated with a second aptamer, V7t1, which binds away from the HBD to the receptor binding domain (RBD) by forming a g-quadruplex[12]. For V7t1 the same effect was observed as displayed in Figure 6. 3B. Both of these aptamers produced reversed peaks at higher analyte concentrations and provide evidence that this observation was not due to a specific aptamer-epitope interaction. For V7t1 this reversal occurred at lower concentrations of $VEGF_{165}$ due to the higher affinity of the aptamer. Previous thrombin data from chapter four was re-examined by individual blockade traces and no reverse peaks were observed.

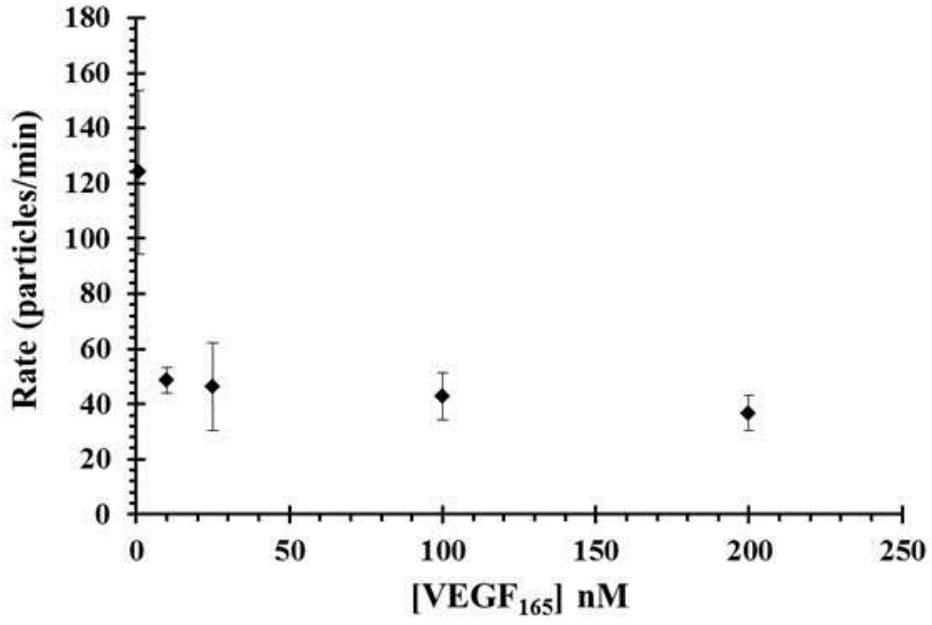

Figure 6. 5: Scatter plot displying average rate for 120 nm beads functionalised with VEa5 following filtering for reversed peaks, n = 3.

6.4.2. Detection of PDGF-BB under positive bias

In a typical TRPS experiment it has been shown that the number of bead translocations is a function of the bead concentration, diffusion coefficient of the beads, applied pressure, electroosmotic and electrophoretic mobility as discussed in chapter 2, and expressed in equation 2.9. Thus, within the current experimental setup, ensuring concentration, pressure and osmotic contributions remain constant, changes in particle translocations were inferred to be due to a change in the electrophoretic mobility of the beads. The observation of the beads re-entering the pore and moving from the lower fluid cell back up to the upper was attributed to the addition of the protein and its charge. $VEGF_{165}$ has a reported isoelectric point at pH 8.5[14], suggesting that at the pH of the chosen electrolyte buffer, 7.4, the protein should have a

net positive surface charge, whereas thrombin (pI 7.1[15]) would be largely neutral. Upon binding to the aptamer and shielding the phosphate backbone the charge upon the protein must therefore dominate the electrophoretic mobility. As this occurred with both VEGF aptamers, which as stated above bind to different regions of the protein, it does not seem to affect the results which epitope is occupied.

These experiments were then repeated using 300 nm beads functionalised with anti-PDGF aptamer and increasing PDGF-BB concentrations to explore whether the same effects would be observed and to confirm that PDGF-BB binding also produced a measurable signal for detection. Firstly, a positive bias was applied to the lower fluid cell of + 0.4 V, and a diminution of particle rate was observed as PDGF concentration increases as displayed in Figure 6. 6A. Unlike within the VEGF experiment where beads were observed translocating the pore in reverse i.e. from the lower fluid cell to the upper, no reverse peaks were observed. To ascertain if this effect was dependent upon the bead size i.e. due to additional mass of the 300nm beads creating bias given the larger gravitational forces, the same experiment was performed using 120 nm beads. Again no reverse translocations were observed suggesting that gravitational effects did not impact upon this measurement. The same trend was observed and is displayed in Figure 6. 6B, confirming that the lack of reversed peaks is not an artefact of using a different bead size. As PDGF-BB has an isoelectric point of 9.8 it is assumed that the protein would have a positive surface charge in the chosen electrolyte. The absence of reversed translocations, is then attributed to a mechanistic difference in the way that the protein is bound to the aptamer, for example the aptamer could be folded around the protein so that the charge of the phosphate background is not fully shielded.

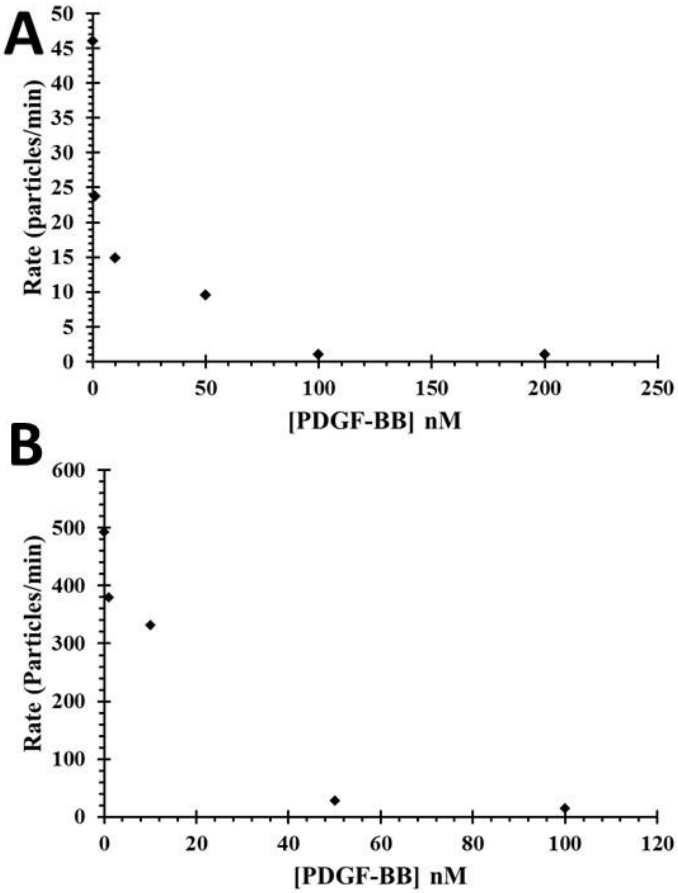

Figure 6. 6: Particle rate against PDGF-BB concentration for 300 nm (A) and 120 nm (B) beads fuctionalised with anti-PDGF aptamer under posistive bias.

6.4.3. Detection of $VEGF_{165}$ and PDGF-BB under negative bias

To test the hypothesis that the surface charge of the beads had become positive, the applied voltage bias was switched to a negative value (negative electrode, in the lower fluid cell). In this configuration DNA modified beads usually do not traverse the pore opening, or have a much reduced frequency of translocation, here for the 120nm particles no translocation events were recorded. Upon incubation with the VEGF protein the frequency of beads was directly proportional to the concentration of the protein, shown in Figure 6. 7. This is a major improvement and observation from previous thrombin work[16]. In thrombin studies the number of translocation events per minute decreases as target analyte concentration increased, in effect switching off the signal. Here we have a more typical and convenient setup, wherein an increase in analyte concentration produced an increase in signal.

To determine if the bead size and concentration would have any impact on the sensitivity and ease of the assay we investigated their effects using the VEGF aptamers VEa5 and V7t1. Data summarising the effects of bead diameter and concentration are displayed in Figure 6.

7A and B. To investigate the effect of bead concentration VEa5 modified beads at 3, 2.5 and 2×10^9 beads/mL were added to solution containing the VEGF protein (Figure 6. 7A/B curves 2, 3 and 4). As the bead concentration decreases, so does the concentration of VEGF at which the bead rate remains constant 100 nM (line 2) to 25 nM (line 4), this has an impact upon the dynamic range of the assay and is likely due to a decrease in the number of available binding sites in solution, leading to the saturation of each individual bead with VEGF at much lower concentrations of protein. As indicated above the number of beads moving through the pore is proportional to their concentration, hence lower concentrations of beads will result in a lower overall rate, at bead concentrations below 2.5×10^9 beads/mL it could be suggested that the bead count is so low (<10 beads a minute) it is no longer practical for accurate measurement and lengthens the required assay run-time unnecessarily.

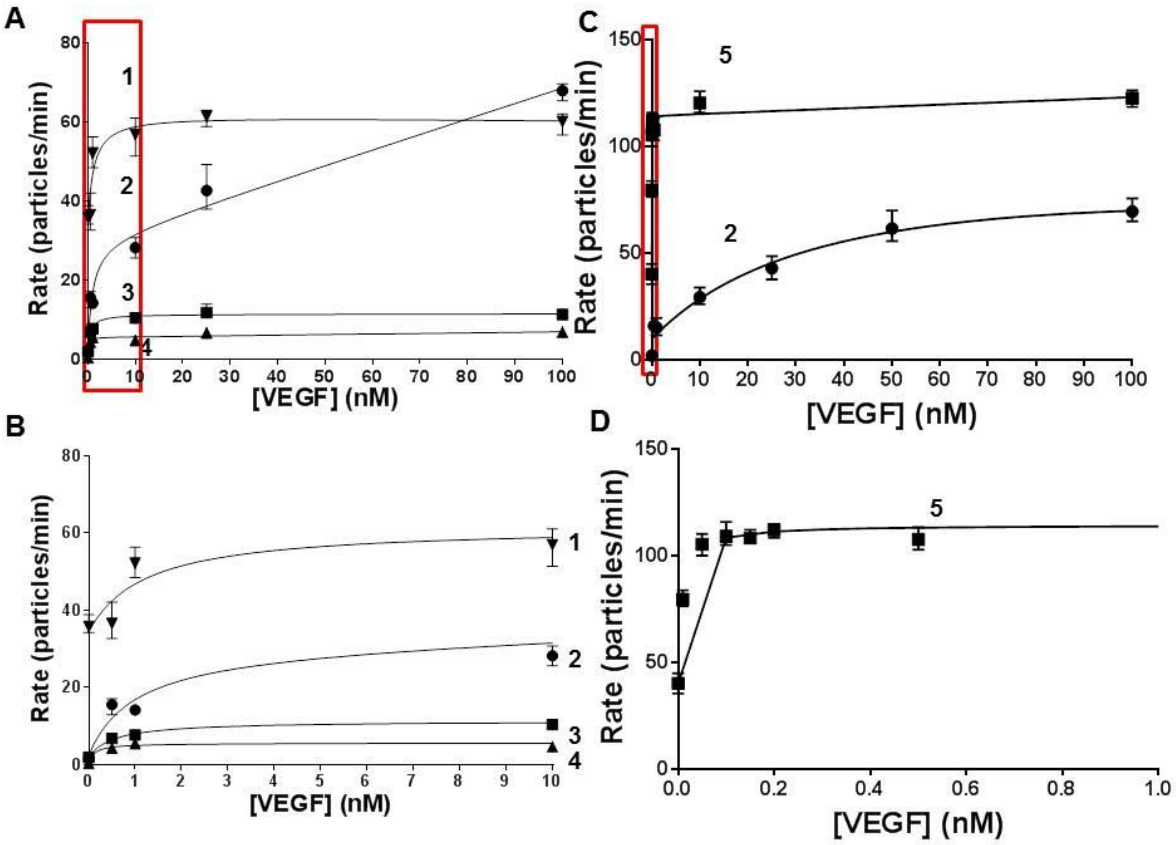

Figure 6. 7: A Average rates against $VEGF_{165}$ concentration for (**1**) 3×10^9 beads/mL 300 nm beads, (**2**) 3×10^9 beads/mL 120nm beads, (**3**) 2.5×10^9 beads/mL 120 nm beads and (**4**) 2×10^9 beads/mL 120 nm beads all functionalised with VEa5 aptamer. **B** Expanded view of highlighted area in **A**. **C** Average rates against $VEGF_{165}$ concentration for 3×10^9 beads/mL 120 nm beads functionalised with either (**2**) VEa5 or (**5**) V7t1 aptamer. **D** Expanded view of highlighted area in **C**. For all data sets n = 3.

To investigate the impact of bead size, the bead concentration was kept the same (3×10^9 beads/mL) and the diameter was increased to 300 nm (Figure 6. 7A and B line 1 and 2). The

rate of 300 nm beads at 0 nM VEGF was initially higher than the 120 nm beads with average rates of 35 and 0 beads/min respectively. It is likely that this is due to both the increased mass of the beads, leading to a higher gravitational effect, and also due to a lower relative loading of DNA per area of beads suspended. Both beads have comparable binding capacities (see method section) therefore we conclude the 300 nm beads have a lower packing density of streptavidin, and therefore DNA, on their surface.

The differences in packing density might also be responsible for the differences in rate signal between 120 and 300 nm beads. It is observed that there is a sharp initial increase in rate upon addition of VEGF and the rate signal appears to saturate sooner for the 300 nm beads; this could indicate that the sensitivity could be tailored by altering the packing density of capture probe on the surface of beads. For the purposes of this assay, these results demonstrate that the 300 nm beads are able to provide a rate-related signal change in response to protein binding which can be analysed via TRPS, further supporting the notion of the multiplexed assay.

Figure 6. 7C represents the difference in the rate signal for two anti-VEGF aptamers: VEa5 (line 2) and V7t1 (line 5). There are two observations from this data; firstly, the rate signal for the V7t1 aptamer increases at low concentrations of VEGF and appears to have levelled out by 10 nM, whereas the rate of VEa5 beads continues to increase up to 100 nM of added protein. Initially we explored the same VEGF concentrations for both aptamers, however due to the rate remaining constant for the V7t1 aptamer at concentrations of VEGF > 1nM we chose to significantly reduce the amount of VEGF added. To illustrate this effect, Figure 6. 7D displays an expanded view of the data for the V7t1 aptamer which exemplifies the ability of this aptasensor to detect VEGF at concentrations down to 0.05 nM. This is due to differences in aptamer binding mechanism and affinity. VEa5 has a reported K_D of 130 nM[11] and is postulated to bind due to the presence of stem-loop structures[17]. V7t1 has a reported K_D of 1.4 nM for $VEGF_{165}$ and due to its lack of selectivity over $VEGF_{121}$ is postulated to bind the receptor binding domain present on both VEGF analogues by forming a G-quadruplex[12]; the superior affinity of V7t1 allows for the measurement of smaller concentrations of $VEGF_{165}$ on this platform.

The second observation from Figure 6. 7C is the marked difference in maximum rate between VEa5 and V7t1 which reach circa 60 beads/minute and 120 beads/minute, respectively at higher VEGF concentrations. As the overall number of aptamer molecules and beads should

be the same, the difference in rate must be due to the difference in length of DNA. As demonstrated in chapter 3, in addition to the concentration of DNA added to the beads surface, the length of DNA sequence used is also a key factor in determining the maximum bead rate through the pore[16]. The V7t1 aptamer is 20 nucleotides shorter than VEa5 and with a negative bias under the pore, and the concentration of the beads being identical in all experiments the rates vary ~40 beads/minute (V7t1) and ~1 bead/minute (VEa5) respectively, when VEGF concentration is 0 nM. This is attributed to the effects of the length of the DNA, with the short DNA sequence able to pass through the pore more easily. Upon the protein binding to the aptamer, we believe there are two possible reasons for the higher total rate for the shorter aptamer sequence. The first could be due to the protein shielding the phosphate backbone to a greater extent for the shorter DNA, and secondly the binding mechanism. The conformation of the DNA aptamer, the location it holds the protein with respect to the bead, could impact on the bead zeta potential and drag, however further work is needed to infer implications of any mechanistic differences.

To further support the theory that bead rate is dominated by the charge of VEGF, the pH of the electrolyte buffer was adjusted to pH 9.3. It was expected that at this pH the VEGF would have an overall slightly negative surface charge, and with a negative voltage bias applied under the pore the previously observed increase in particle rate with increasing protein concentration would be eliminated. As shown in table 1 this was indeed found to be the case, with bead rate remaining at 0.5 beads/min.

When the applied potential was reversed to an equal positive potential, the rate decreases with increasing protein concentration, reverting back to the trend observed previously with thrombin[16], i.e. a diminution, suggesting a charge-shielding mechanism is taking place.

	Rate (beads/min)			
	Negative bias (- 0.4 V)		**Positive bias (+ 0.4 V)**	
[VEGF] (nM)	**pH 7.4**	**pH 9.3**	**pH 7.4**	**pH 9.3**
0	1.6	0.5	150	165
100	68	0.5	40.8	90

Table 6. 1: comparative summary of the effect of buffer pH on recorded particle rate using the same pore and instrument conditions.

In order to confirm that the two bead populations and their respective proteins could be analysed together under the same conditions, experiments were then performed for PDGF-BB under a fixed negative bias of -0.4 V. Figure 6. 8 displays the results for these experiments in which a clear and proportional increase in rate is visible with increasing PDGF

concentrations. As the behaviour of PDGF and VEGF bound beads was found to be similar, providing an increase in rate under a negative bias, it can be concluded that both proteins can be observed binding their aptamers under these conditions.

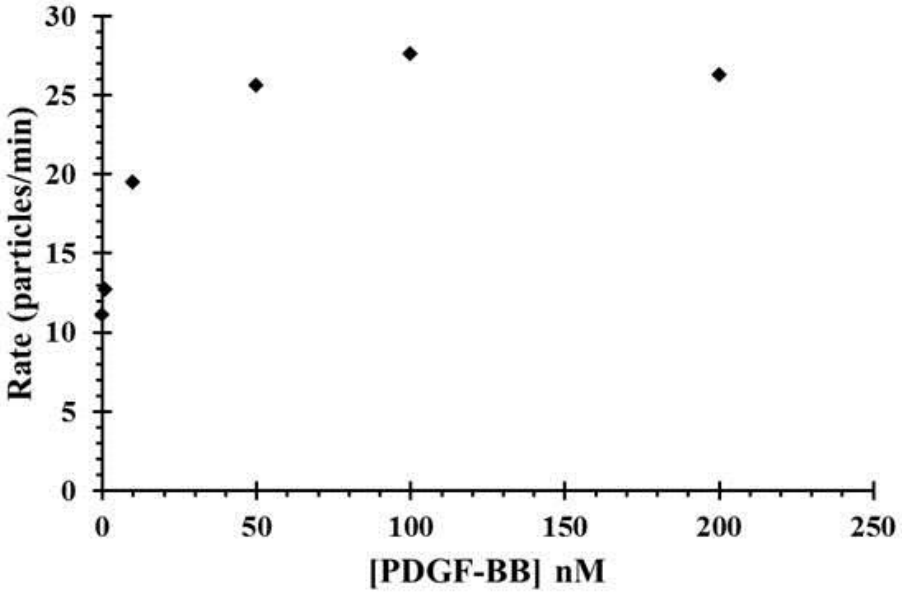

Figure 6. 8: particle rate against PDGF-BB concentration for 300 nm beads functionalised with anti-PDGF aptamer under negative bias.

6.4.4. The impact of aggregation on detection of PDGF-BB

PDGF-BB is a homodimeric protein, as such, one might expect to see aggregation as aptamers on two beads can interact with the same protein molecule, as has been observed in some assays previously[18]. To investigate this, the blockade magnitude was analysed. A plot of blockage magnitude against PDGF-BB concentration is plotted in figure 6.8 below. It is observable that there is an initial sharp increase in magnitude up to a concentration of 10 nM PDGF-BB, suggesting that in these experiments aggregates are formed as the volume of each entity passes through the pore is increased. The mean blockade magnitude decreases after this initial increase, this may be attributed to the hook effect described in chapter five as the number of PDGF-BB proteins increases, saturating the available binding sites.

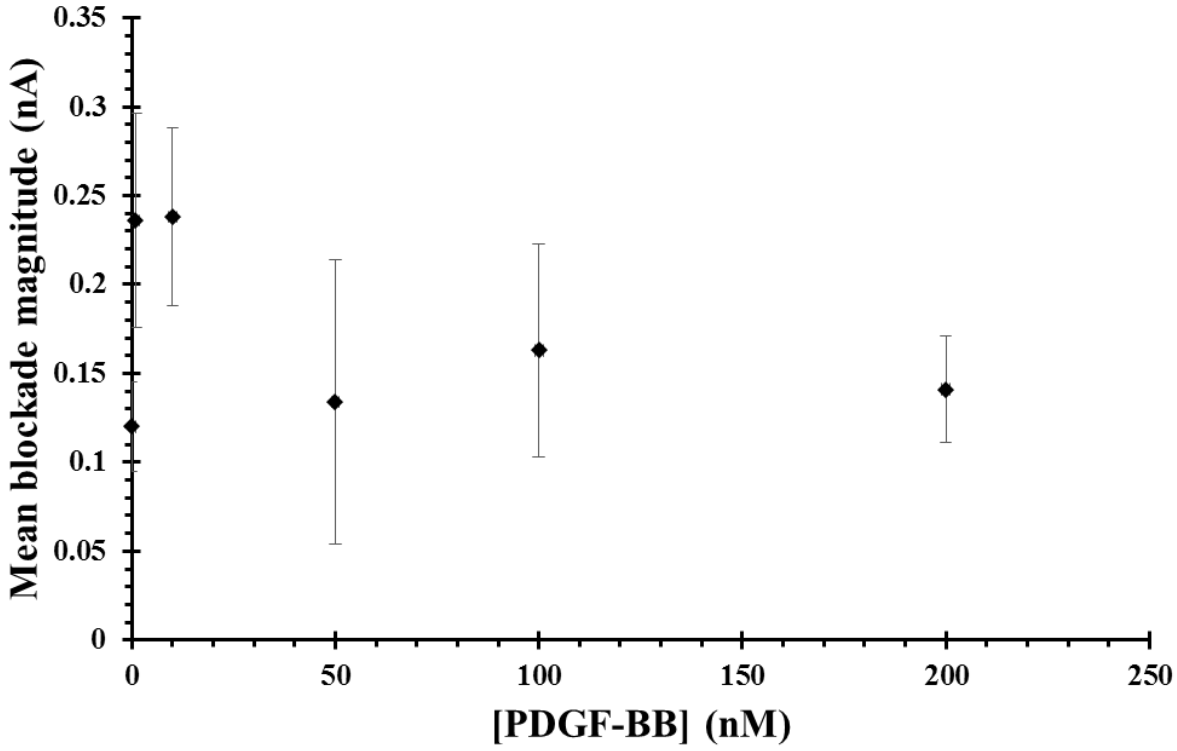

Figure 6. 8: Mean blockade magnitude against PDGF concentration for 300 nm beads functionalised with PDGF aptamer with negative bias; error bars represent 1 standard deviation from the mean.

The range of Δi_p values (nA) which were observed as monomeric beads passed through the pore after sonication and without any PDGF-BB was used as a bin size and the size of aggregate determined as described previously in chapter five. The percentage of particles traversing the pore which were monomers was then determined, the results for which are displayed in figure 6. 9 below. As reflected in figure 6. 8 above, the number of aggregates initially increases, and then decreases again, however, this method of examining the data reveals that there is not a complete hook effect, and that some aggregates remain throughout the concentration range.

An increase in the number of aggregates could be problematic in rate based assays and more particles are clustered together and traversing as one, which should in theory cause a reduction in rate. However an increase in rate in relation to PDGF-BB concentration is still clearly visible, thus the formation of aggregates did not affect this method, suggesting that the aggregates formed were not large clusters and that the effect on the rate signal is negligible.

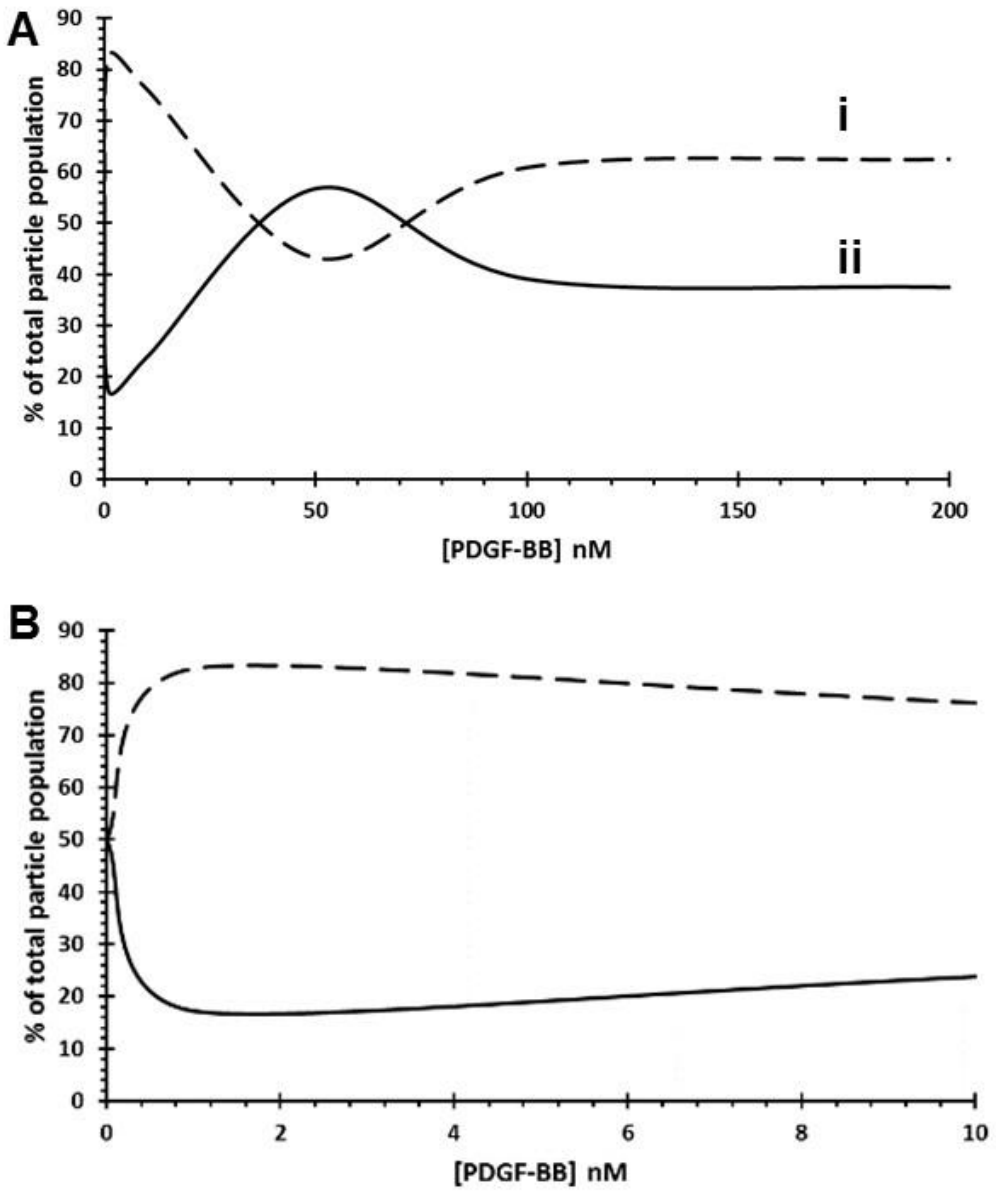

Figure 6. 9: A % of bead aggregates (i) or monomers (ii) against PDGF-BB concentration. **B** expanded view of A for 300 nm beads functionalised with PDGF aptamer analysed under negative bias.

6.4.5. Multiplexed detection of PDGF-BB and $VEGF_{165}$

In order to successfully multiplex the rate signals for two different bead sizes, it first must be possible to differentiate the beads from one another. Figure 6. 10A displays the calibrated diameter distributions for the two different bead sets measured separately and together (inset) which confirms that the resolution of TRPS is able to distinguish these two bead populations without overlap. The distribution of 120 nm bio-adembeads streptavidin plus (Figure 6. 10Ai) is much narrower than for the 300 nm bio-adembeads streptavidin; this is believed to be due to a difference in the stringency of bead manufacture – it is possible to see the distribution of bead diameters with great accuracy due to the particle-by-particle analysis of TRPS which has been shown to have far greater resolving power over conventional sizing techniques, such as Dynamic Light Scattering, when analysing non-uniform dispersions[19–21].

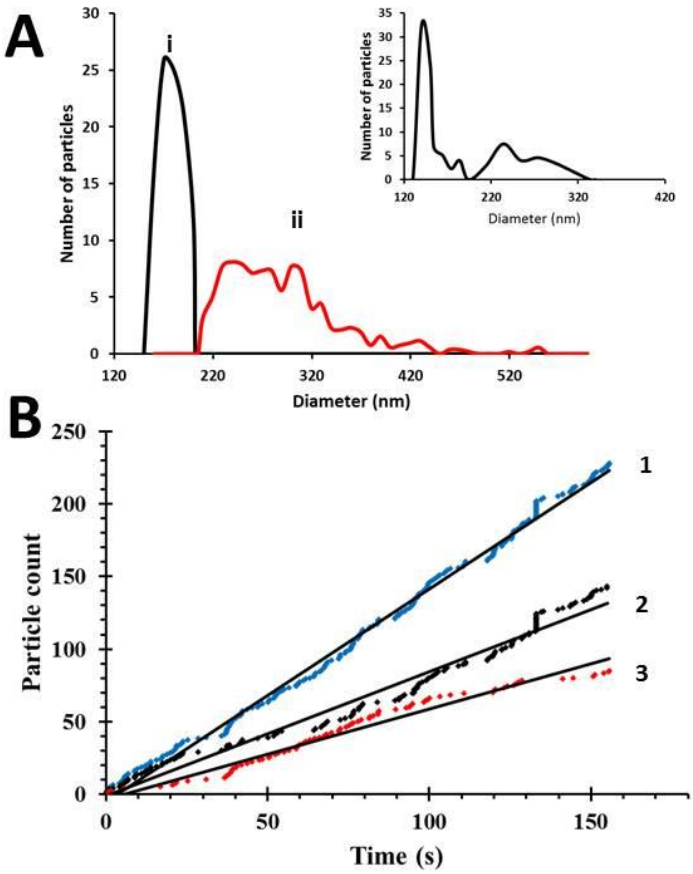

Figure 6. 10: A distribution of particle diameters for **(i)** 120 nm bio-adembeads streptavidin plus (ademtech, France) and **(ii)** 300 nm bio-adembeads streptavidin (ademtech, France). Inset is the distribution of particle diameters for a mixture of 120 and 300 nm beads. **B 1** combined rate of equal concentrations of 120 and 300 nm beads passing through the pore, 2 rate of 120 nm beads taken from **1, 3** rate of 300 nm beads, taken from **1**.

Figure 6. B line 1 is an example of the raw data plot showing particle count versus time for a sample containing both 120 and 300 nm beads. Following the experiment the data was

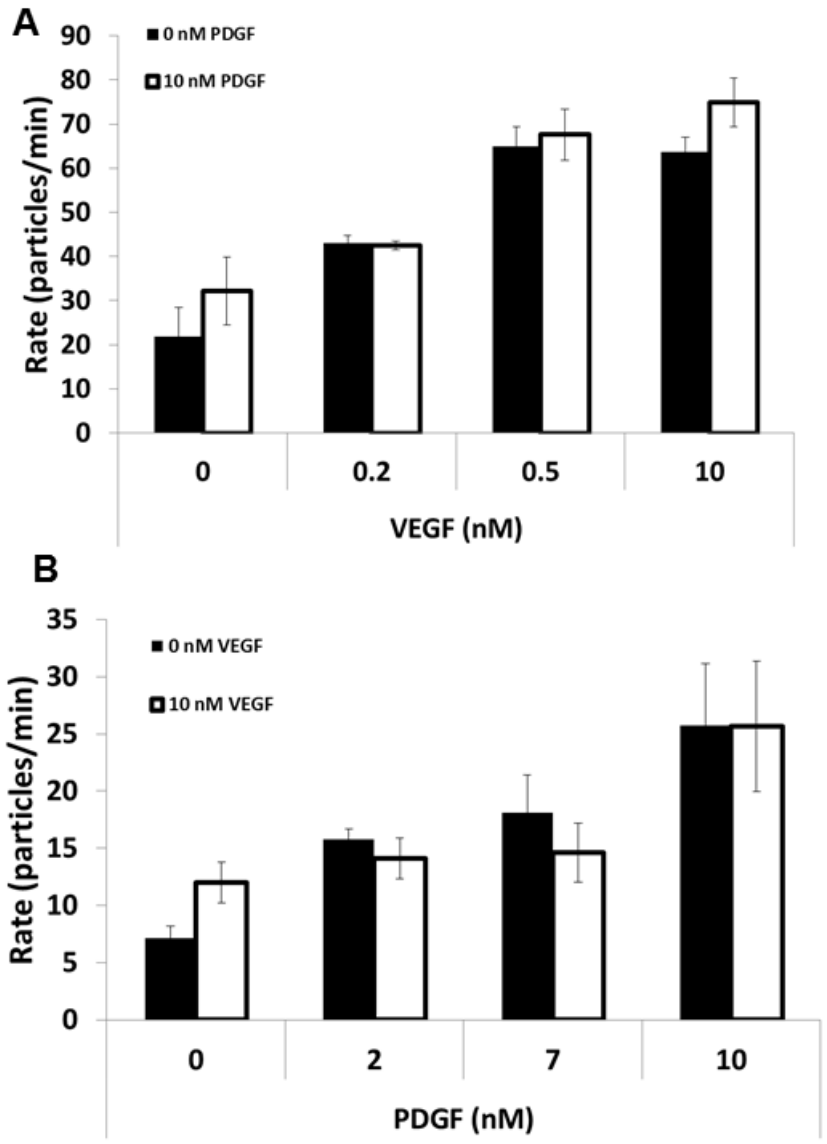

Figure 6. 11: A bar graph comparing the average particle rates of 120 nm beads functionalised with V7t1 as $VEGF_{165}$ concentration increases with or without the addition of 10 nM PDGF-BB in the presence of 300 nm beads functionalised with anti-PDGF aptamer. **B** bar graph comparing the average particle rates of 300 nm beads functionalised with anti-PDGF aptamer as PDGF-BB concentration increases with or without the addition of 10 nM $VEGF_{165}$ in the presence of 120 nm beads functionalised with V7t1. Error bars represent the standard deviation from the mean of each individual calculated particle rate (n=>500 run time = 10 minutes).

exported into excel, filtered by measured particle diameter, and the total bead count was separated into the two different beads sizes, lines 2 and 3. The 120 nm beads (line 2) are seen to run through the pore at a greater frequency than the 300 nm beads, despite being at the same concentration; this has been attributed to the effect of the ratio of the diameter of the pore constriction vs the diameter of the beads. As the pore size is reduced the particle rate decreases[22] and this will be seen to a greater extent for the larger 300nm beads. In these

experiments the size of the pore was not able to be increased any further to compensate for this as the signal from the smaller 120 nm beads would have been lost in the baseline noise.

In order to multiplex the assay it is imperative to ensure that the presence of additional proteins and beads do not interfere with the signal. Figure 6. 11A shows the rate of 120 nm beads in the presence of different concentrations of VEGF with or without 10 nM PDGF-BB and Figure 6. 11B displays the rate for 300 nm beads with or without 10 nM $VEGF_{165}$, in all these experiments the second bead was always present. These observations confirm that a decrease in rate was still able to be observed for both bead sets interacting with their specific proteins in the presence of additional beads. An increase in rate was still visible for the 120 nm beads regardless of the addition of 300 nm beads and PDGF-BB concentrations. As expected from Figure 6. 7, 6. 11A displays little difference between the values for 0.5 and 10 nM of VEGF, suggesting that at this point all of the available binding sites on the 120 nm bead were occupied.

In Figure 6. 11B it was observed that there was little difference between 2 and 7 nM of PDGF-BB, it was postulated that one individual homodimeric PDGF-BB molecule could interact with two aptamers on the surface of the beads, and that it is only when PDGF-BB concentration is increased significantly that surface coverage of PDGF-BB on the beads is sufficient to cause a large increase in rate. In the future this could be investigated by altering the concentration of aptamer on the surface of the beads and monitoring any change in sensitivity.

The frequency of both bead sets was measured in the presence of several combinations of concentrations of PDGF-BB and $VEGF_{165}$. The data from all of these experiments are represented as surface plots in Figure 6. 12A and B. For both bead sets (A and B) rate is seen to increase when their specific protein target concentration is increased. This trend remains largely unaffected by the presence of the other bead population and protein and the two can be measured independently.

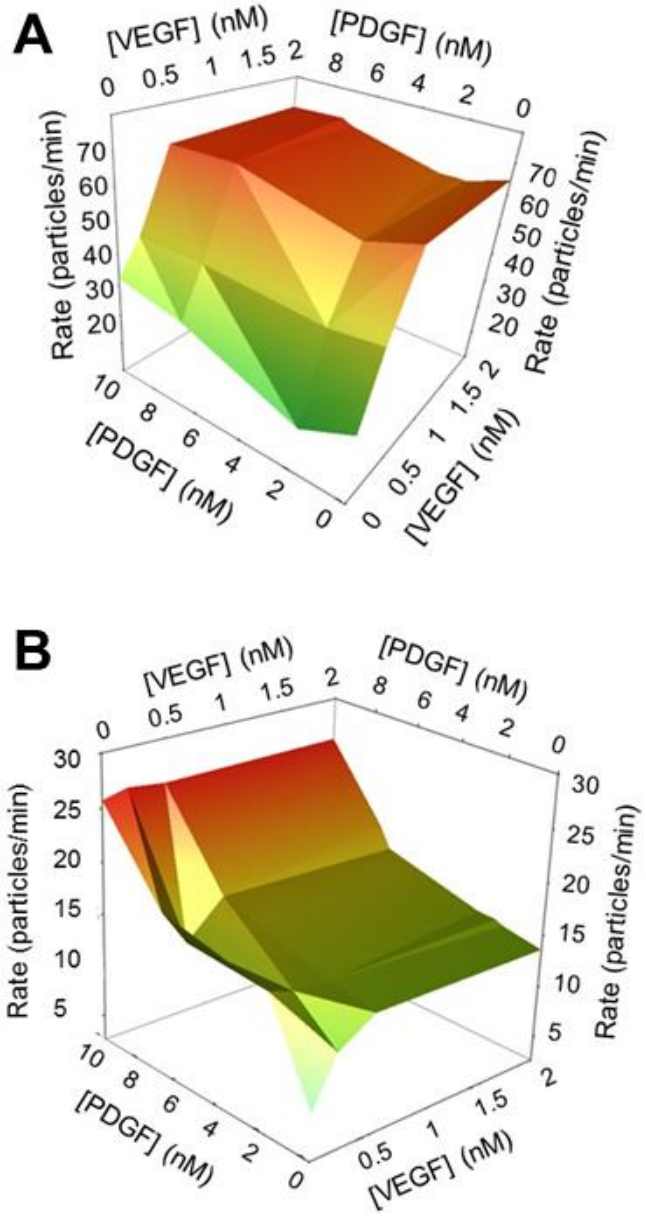

Figure 6. 12: A 3D surface plot displaying the effect of PDGF and VEGF on particle rate of 120 nm beads. **B** 3D surface plot displaying the effect of PDGF and VEGF on particle rate of 300 nm beads.

These results suggest that the simultaneous measurement of two different growth factors by TRPS was possible by using differently sized beads to provide a signal which is able to be selectively filtered by blockade magnitude to pull out the desired individual rate data. The observed increases in particle rate are believed to be due to an increase in electrophoretic mobility toward the negative electrode at the base of the pore when the positive proteins bind selectively to their respective DNA aptamers via a conformational change.

Multiplexing the TRPS method illustrates the potential for the platform to be used as a biosensor. As demonstrated in the previous work in chapter 4, the technique offers

comparable sensitivity and assay times when compared to Surface Plasmon Resonance techniques or flow cytometry platforms. The TRPS technique does not have the throughput of a modern flow cytometer but does offer an improved signal and resolution for sub 500nm particles, without the need for fluorescent labels.

6.5. Conclusion

$VEGF_{165}$ and PDGF-BB were successfully monitored binding to aptamer-laden beads of 120 and 300 nm in diameter. By altering the applied voltage bias it was possible to generate a positive signal i.e. rate increases with increased protein concentration, representing a significant improvement in the signal described in chapter four. Furthermore, it is suggested that with a knowledge of the target protein isoelectric point, one could tailor the electrolyte pH to provide a positive signal for each target. The signals generated were able to be monitored *in situ* and also in tandem with both proteins measured independently from one another using the same sample. This assay used the beads themselves as a label, without the need for any additional identifiers such as fluorophores. Parameters regarding bead concentration and size were considered and a multiplexed assay undertaken.

6.6. References

1 Wei, L.-H.; Kuo, M.-L.; Chen, C.-A.; Chou, C.-H.; Lai, K.-B.; Lee, C.-N.; Hsieh, C.-Y. *Oncogene* **2003**, *22*, 1517–1527.

2 Matsumoto, T.; Mugishima, H. *J. Atheroscler. Thromb.* **2006**, *13*, 130–135.

3 Tarkowski, E.; Issa, R.; Sjo, M.; Wallin, A.; Blennow, K. **2002**, *23*, 237–243.

4 Jelkmann, W. *Clin. Chem.* **2001**, *47*, 617–623.

5 Li, L.; Wang, L.; Zhang, W.; Tang, B.; Zhang, J.; Song, H.; Yao, D.; Tang, Y.; Chen, X.; Yang, Z.; Wang, G.; Li, X.; Zhao, J.; Ding, H.; Reed, E.; Li, Q. Q. *Anticancer Res.* **2004**, *24*, 1973–1979.

6 Belgore, F. M.; Lip, G. Y.; Bareford, D.; Wadley, M.; Stonelake, P.; Blann, a D. *Am. J. Hematol.* **2001**, *66*, 59–61.

7 Karayiannakis, A. J.; N, S. K.; Polychronidis, A.; Zbar, A.; Kouraklis, G.; Simopoulos, C.; Karatzas, G. *Ann. Surg.* **2002**, *236*, 37–42.

8 Hamilton, T. D.; Leugner, D.; Kopciuk, K.; Dixon, E.; Sutherland, F. R.; Bathe, O. F. *BMC Cancer* **2014**, *14*, 542.

9 Madsen, C. V.; Steffensen, K. D.; Olsen, D. A.; Waldstrøm, M.; Smerdel, M.; Adimi, P.; Brandslund, I.; Jakobsen, A. *J. Ovarian Res.* **2012**, *5*, 23.

10 Deng, K.; Xiang, Y.; Zhang, L.; Chen, Q.; Fu, W. *Anal. Chim. Acta* **2013**, *759*, 61–65.

11 Hasegawa, H.; Sode, K.; Ikebukuro, K. *Biotechnol. Lett.* **2008**, *30*, 829–834.

12 Nonaka, Y.; Sode, K.; Ikebukuro, K. *Molecules* **2010**, *15*, 215–225.

13 Willmott, G. R.; Platt, M.; Lee, G. U. *Biomicrofluidics* **2012**, *6*, 14103–1410315.

14 Ferrara, N.; Houck, K.; Jakeman, L.; Leung, D. W. *Endocr. Rev.* **1992**, *13*, 18–32.

15 Righettl, P. G.; Tudor, G. *J. Chromatogr.* **1981**, *220*, 115–194.

16 Billinge, E. R.; Broom, M.; Platt, M. *Anal. Chem.* **2014**, *86*, 1030–1037.

17 Kanakaraj, I.; Chen, W.-H.; Poongavanam, M.; Dhamane, S.; Stagg, L. J.; Ladbury, J. E.; Kourentzi, K.; Strych, U.; Willson, R. C. *Int. J. Biol. Macromol.* **2013**, *57*, 69–75.

18 Huang, C.-C.; Huang, Y.-F.; Cao, Z.; Tan, W.; Chang, H.-T. *Anal. Chem.* **2005**, *77*, 5735–5741.

19 Willmott, G. R.; Vogel, R.; Yu, S. S. C.; Groenewegen, L. G.; Roberts, G. S.; Kozak, D.; Anderson, W.; Trau, M. *J. Phys. Condens. Matter* **2010**, *22*, 454116.

20 Henriquez, R. R.; Ito, T.; Sun, L.; Crooks, R. M. *Analyst* **2004**, *129*, 478–482.

21 Roberts, G. S.; Yu, S.; Zeng, Q.; Chan, L. C. L.; Anderson, W.; Colby, A. H.; Grinstaff, M. W.; Reid, S.; Vogel, R. *Biosens. Bioelectron.* **2012**, *31*, 17–25.

22 Kozak, D.; Anderson, W.; Trau, M. *Chem. Lett.* **2012**, *41*, 1134–1136.

Chapter Seven

TRPS as a tool to monitor aptamer-analyte induced particle dispersion

7.1. Abstract:

The basis of this aptasensor is the controlled dispersion of reporter nanoparticles in the presence of the target analyte, which is measured via Tunable Resistive Pulse Sensing (TRPS). Each analyte triggers the release of multiple nanoparticles from the original bead conjugate, and this amplified signal allows the detection of the analyte orders of magnitude lower than the previous thrombin assay detailed in chapter 4. 1 µm superparamagnetic beads (SPBs) were coated with anti-thrombin aptamers and incubated with non-magnetic beads coated with a partially complementary oligonucleotide. The aggregates were monitored by TRPS by both an increase in volume and a decrease in blockade frequency. Following the addition of the target protein the aptamer undergoes a conformational change, dissociating from the complementary oligonucleotides and causing the SPBs to release their non-magnetic particle payload. The number of released beads increases with the concentration of the protein. This method was sensitive enough to detect down to 100 fM concentrations of thrombin, three orders of magnitude lower than previous reports using TRPS.

7.2. Introduction:

During previous work discussed in chapter 4, thrombin was detected down to 4 nM using aptamer modified beads and the TRPS based detection platform. Here an improved method is reported capable of detecting fM concentrations of thrombin protein. The change in sensitivity comes from altering the measured signal. Previously the protein concentration was measured by monitoring the protein-bead conjugate, and in this configuration several proteins covering the beads surface were required to produce a signal. In brief, this assay entailed anchoring the aptamer directly to one bead and directly measuring the relative change in mobility as the thrombin concentration increased. This approach, while a useful proof-of-concept for the detection of proteins and for aptamer characterisation, involved measuring the diminution of signal with increased concentration of protein which leaves room for improvement by generating a positive signal.

In this assay 1 µm SPBs, (DynaBeads MyOne Carboxylic Acid) were coated with amine-terminated anti-Thrombin-15 aptamer (3'Amine-TTTTTGGTTGGTGTGGTTGG5')[1] and either 800nm or 400nm carboxyl beads (Izon Sciences, CPC800) were coated with an amine-terminated complementary sequence to the aptamer (3'Amine-TTTTTTTTTCCAACCACA5') as illustrated in figure 7.1.

Initially the two bead populations form aggregates through the formation of double-stranded DNA (dsDNA). Upon the introduction of the target protein the dsDNA structure is disrupted by the conformational change of the anti-thrombin aptamer, causing the dispersion of the aggregate. By using two bead populations, the SPM beads with the anti-thrombin aptamer are able to be removed from the solution by a magnet leaving the dispersed smaller particles for analysis. The concentration of smaller particles that are dispersed increases with increasing protein concentrations. Here each protein releases a particle from an aggregate producing more efficient ratio between protein and measurable signal. Upon dissociation from the aptamer the protein can then go on to disrupt another particle causing a signal amplification which provides the much increased sensitivity observed in this assay.

Herein an assay is presented capable of producing a signal at concentrations as low as 100 fM with an improved methodology, representing a significant advancement in the development of aptamer-based TRPS assays.

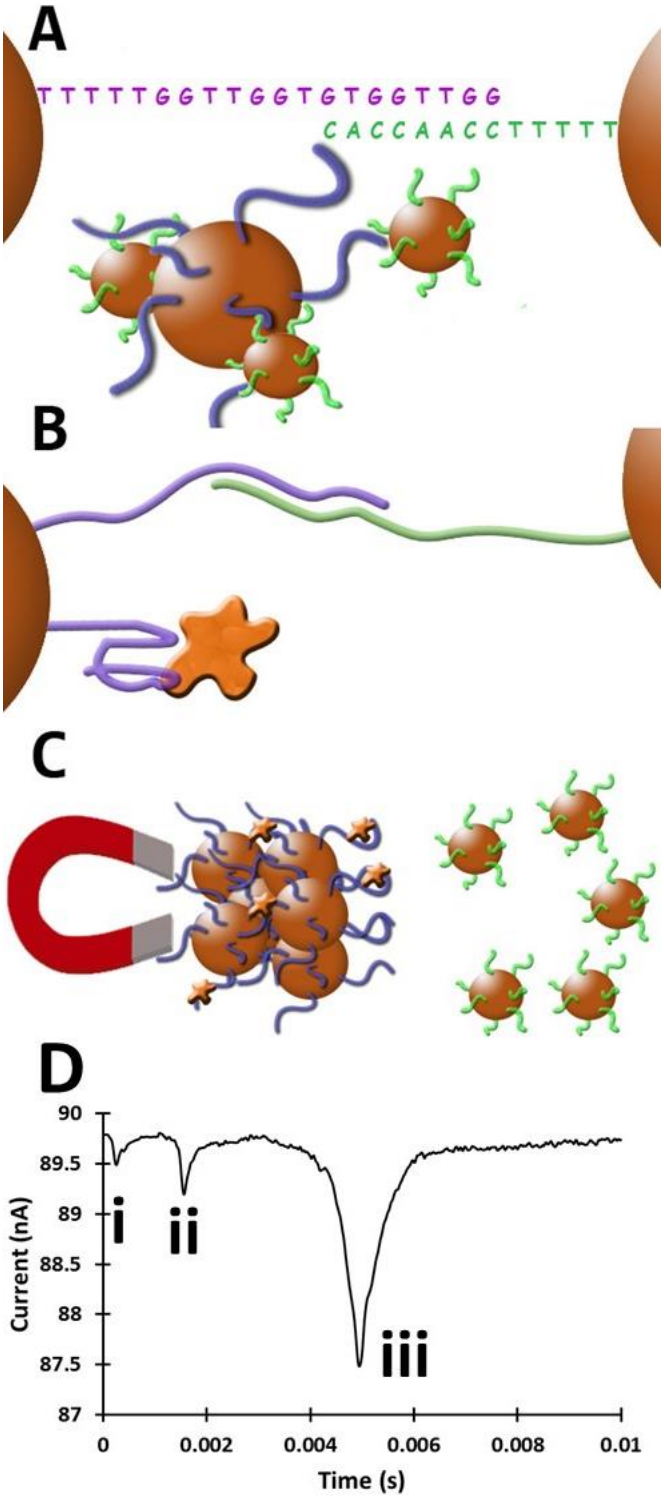

Figure 7. 1: Schematic of assay principles (not to scale). **A)** 1µm SPBs are coated with thrombin aptamer (purple) and 400 (or 800nm) beads are coated with a complementary strand of DNA (green). Aggregates are formed as complementary DNA binds. **B)** With the addition of thrombin, the aptamer undergoes a conformational change and the complementary DNA is released. **C)** The SPBs are separated by use of a magnet, leaving the 400 or 800nm beads (the dispersant) released by thrombin in solution to be removed for concentration analysis.**D)** example blockades for an 800 nm bead (i), a dynabead (ii) and an aggregate (iii).

7.3. Method:

7.3.1. Chemicals and reagents

Phosphate Buffered Saline (PBS – P4417), Tween 20 (P1379), MES hydrate (M2933), Bovine Serum Albumin (BSA – A2153), and thrombin (T7513) were sourced from Sigma Aldrich, UK without any further purification unless otherwise stated. EDC (77149) was purchased from Thermo Scientific.

DNA sequences were obtained from Sigma Aldrich's custom oligonucleotides service as lyophilised powders and made up to a stock concentration of 100pmol/µL: 5' GGT TGG TGT GGT GGT TTT TTT TTT[AmC3]3' (Thrombin 15 aptamer with amine terminus) and 5' ACA CCA ACC TTT TTT TTT[AmC3]3' (Complementary sequence to thrombin 15 aptamer with amine terminus). Water purified to a resistivity of 18.2 MΩ cm (Maxima) was used to make all solutions unless otherwise specified and 1xPBST (0.05% Tween) was used as the buffer.

Carboxyl beads of known concentration and diameter were sourced from Izon Sciences (Oxford, UK) to be used both as a substrate for DNA attachment and as a calibrant: SKP400 (mode diameter 350 nm, concentration 7.5×10^{11} beads/mL); CPC800 (mode diameter 750 nm, concentration 9.5×10^{10} beads/mL); and CPC1000 (mode diameter 910 nm, concentration 5.5×10^{10} beads/mL). Superparamagnetic Dynabeads® MyOne™ carboxylic acid (650.12) were purchased from Invitrogen provided as 10 mg/mL concentration.

7.3.2. EDC coupling chemistry

Beads were diluted to the required concentration (typically $\times10^{11}$ non-magnetic beads or $\times10^{9}$ Dynabeads MyOne) in MES hydrate buffer adjusted to pH 6 to a total volume of 450 µL. EDC was made up to 10 mg/mL concentration in MES hydrate buffer. 50 µL of 10 mg/mL EDC was then added to the 450 µL of beads. 4.5 nmol of the required DNA sequence was then added and the beads were left on a rotary wheel at room temperature for 2 hours. Following the incubation, the bead solution was removed from the rotary wheel and centrifuged for 5 minutes at 13 400 rpm. Any liquid was carefully pipetted out and the beads were resuspended in 450 µL of PBST, vortexed and sonicated. This wash procedure was repeated 3 times. Concentration analysis on the beads was performed via TRPS as described below. For these experiments DynaBeads MyOne were coated with thrombin binding

aptamer (TBA) and CPC800s or SKP400s with a complementary sequence with a T spacer using the procedure described above.

7.3.3. Aggregate formation

To create aggregates, the Dynabeads MyOne coated with TBA and either CPC800 or SKP400 beads coated with a complementary sequence were incubated together in the following concentrations for 30 minutes:

CPC800 assay: 1×10^9 beads/mL Dynabeads MyOne and 7×10^9 beads/mL CPC800 were diluted in PBST.

SKP400 assay: 1×10^9 beads/mL Dynabeads MyOne and 5.6×10^{10} SKP400s.

The samples were then stored upright in a centrifuge tube for 24 hours in a fridge.

7.3.4. Thrombin addition

From stock serial dilutions of thrombin were carried out in PBST such that the same volume of thrombin would be added to each sample so as not to introduce a potential source of bias by diluting the beads. To each 100 µL sample prepared as described in "aggregate formation" 2 µL of thrombin was added to give concentrations ranging from 0 – 10 pM thrombin. A protein-rich control was also conducted in 0.2 mg/mL BSA to test the effect of non-specific protein addition.

Samples were then left to incubate at room temperature on a rotary wheel for 30 minutes prior to analysis. These samples were then purified by magnetic separation on a MagRack (GE life sciences, Buckinghamshire, UK). After 5 minutes on the MagRack a pellet was clearly visible on the side of the sample vial adjacent to the magnet and the supernatant containing any remaining non-magnetic beads was carefully removed to a fresh vial for concentration analysis. Any further dilutions that were required were then carried out in PBST.

7.3.5. Tunable Resistive Pulse Sensing (TRPS) measurement

Measurements were made with the Izon qNano system, (Izon Sciences, Oxford, UK) which incorporates the fluid cell, stretching apparatus, data recording and analysis software (Control Suite V2.2.2.117). Pores used to analyse SKP400 beads were designated "np400" by the manufacturer and are described as most suitable for detecting beads in the range 200 – 800 nm, pores to analyse CPC800 beads, Dynabead MyOne beads and aggregates were designated "np1000" by the manufacturer and have a specified range of 500 – 2000 nm. For np400 pores an applied stretch of 47 mm and applied voltage of 0.24 V was selected for np1000 pores a stretch of 47 mm was applied and a voltage of 0.08 V chosen. These conditions ensured that blockade events were clearly visible above the level of noise (<10pA); these conditions were maintained throughout the experiments so that data was comparable. 80µL of electrolyte buffer (PBS) was carefully pipetted into the lower fluid cell, taking care not to introduce bubbles. The upper fluid cell was then attached to the instrument and 40 µL of PBST was placed into the fluid cell to enable confirmation of a stable baseline and clean pore.

To perform a calibration and attain size and concentration data a pressure of greater than 2 cmH_2O was applied so that the additional electrophoretic mobility imparted to the beads by the highly anionic DNA did not dominate the signal, which would lead to an overestimate in sample concentration[2]. The application of pressure was also advantageous to increase throughput and decrease analysis run time. Sample concentrations were then extracted for Izon Science's (Oxford, UK) Control Suite V3.1 software. To count aggregates the raw data detailing the blockade magnitudes for each individual peak were extracted as a .csv file. As object volume is proportional to blockade magnitude the total volume of possible aggregates was then calculated and used to generate the expected magnitude (nA) which were used as bins to sort the data as described in chapter 6. To measure aggregates, an np1000 pore was used with a stretch of 47 mm and applied voltage of 0.08 V.

7.4. Results and Discussion:

7.4.1. Confirming DNA attachment

For this assay it was first possible to confirm that DNA had been successfully immobilised onto the beads. To do this the blockade frequency of the DNA modified and unmodified beads of the same concentration were measured under several applied voltages as displayed in figure 7.2. Using the relationship between particle rate and voltage as discussed in chapters 2 and 3 it was possible to get qualitative information that the DNA was present on the beads: DNA loading onto the beads increases the negative surface charge density, thereby increasing the rate of beads traversing the pore. This technique was used to verify both the immobilisation of the aptamer to the SPM beads and the partial complementary sequences on the smaller non-SPM beads.

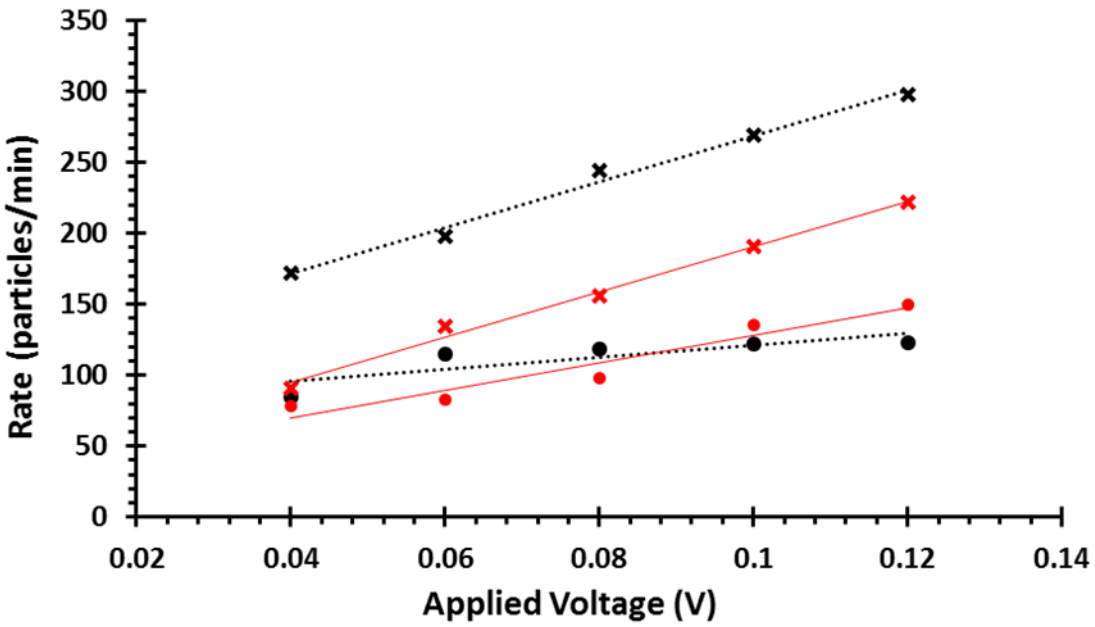

Figure 7. 2: Plots of observed particle rate vs applied voltage (V) for beads with and without DNA. Black lines = CPC800 beads, red lines = dynabeads both analysed using an np1000 pore at 47 mm applied stretch. Circles represent results from blank beads, whilst crosses represent beads which had undergone DNA functionalisation.

As displayed in figure 7.2 for both bead sets, when DNA had been added (crosses) the rate (particles/minute) was higher across the range of voltages in comparison to bead which had not undergone EDC coupling chemistry. The gradient for beads which had undergone DNA conjugation was also steeper for both beads sets. It is worth noting that this effect is less pronounced for the Dynabead MyOne beads and that at a low voltage a difference is not

clearly discernible, as suggested in chapter 3 this is likely due to the additional mass of the beads due to their dense iron oxide cores.

7.4.2. Aggregate formation

To form SPB beads loaded with their smaller particle payload, the two bead populations are mixed together. Initially 1×10^8 1 µm beads/mL were mixed with 7×10^9 800 nm beads/mL on a rotary wheel for 30 minutes. An alternative bead was prepared containing 2.5×10^8 1 µm beads/mL and 5×10^{10} 400 nm beads/mL to investigate the effect of bead size of the dispersant on this aptamer-based assay. A histogram of the 3 calibrated bead sets is provided in figure 7.3.

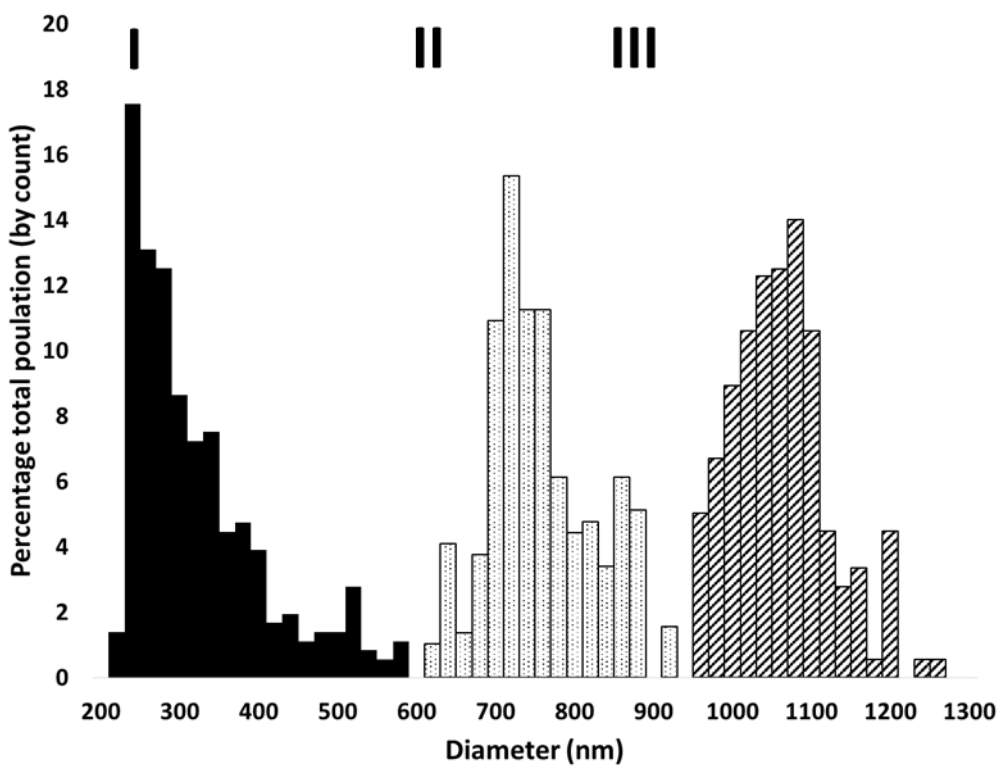

Figure 7. 3: Calibrated histograms displaying the diameter (nm) of DNA-modified SKP400 (**I**), CPC800 (**II**) and Dynabead MyOne (**III**) beads.

The calibration performed with the Izon Control Suite software assumes that the object moving through the pore is spherical and provides an estimation of particle diameter based on the blockade magnitudes of objects as they pass through the pore related to a calibration bead of known diameter. However, for observing aggregates an estimate of particle diameter can be misleading. For example, a dimer of two 400 nm beads is not the same total volume as one 800 nm bead. Hence only the blockade magnitude (Δi_p) is used from this point on. The blockade magnitude for CPC800 and Dynabeads MyOne separately are shown in figure 7.4.

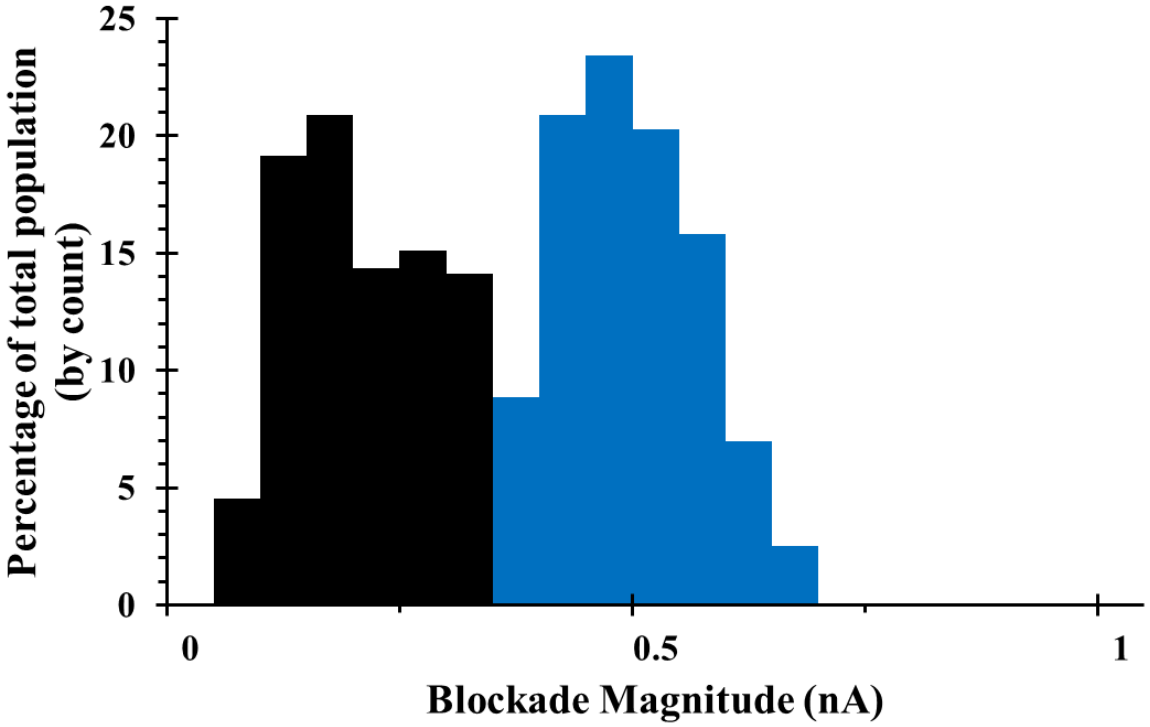

Figure 7. 4: Example histogram of blockade magnitude (nA) for CPC800s (black) and Dynabeads MyOne (blue) modified with complementary DNA or thrombin-15, respectively, prior to incubation together.

Two methods were used to confirm the aggregation of the beads, initially their formation was confirmed by TRPS by an increase in blockade magnitude as displayed in figure 7.5. For the separate bead populations as displayed in figure 7.4 the largest recorded blockade magnitude was 0.675 nA whereas after mixing both particle populations together blockade magnitudes up to 5.125 nA were recorded. An additional observation regards the running of the qNano instrument which using an np1000 pore blocked far more frequently again suggesting the presence of large aggregate clusters.

As the blockade magnitude is proportional to the volume of the object moving through the pore, it is possible to estimate the number of beads in each aggregate, it was found that the mean aggregate size comprised of 3×800 nm bead per dynabead or 15×400 nm beads per dynabead, however variance in binding and the orientation of the cluster as it traverses the pore add complexity[3].

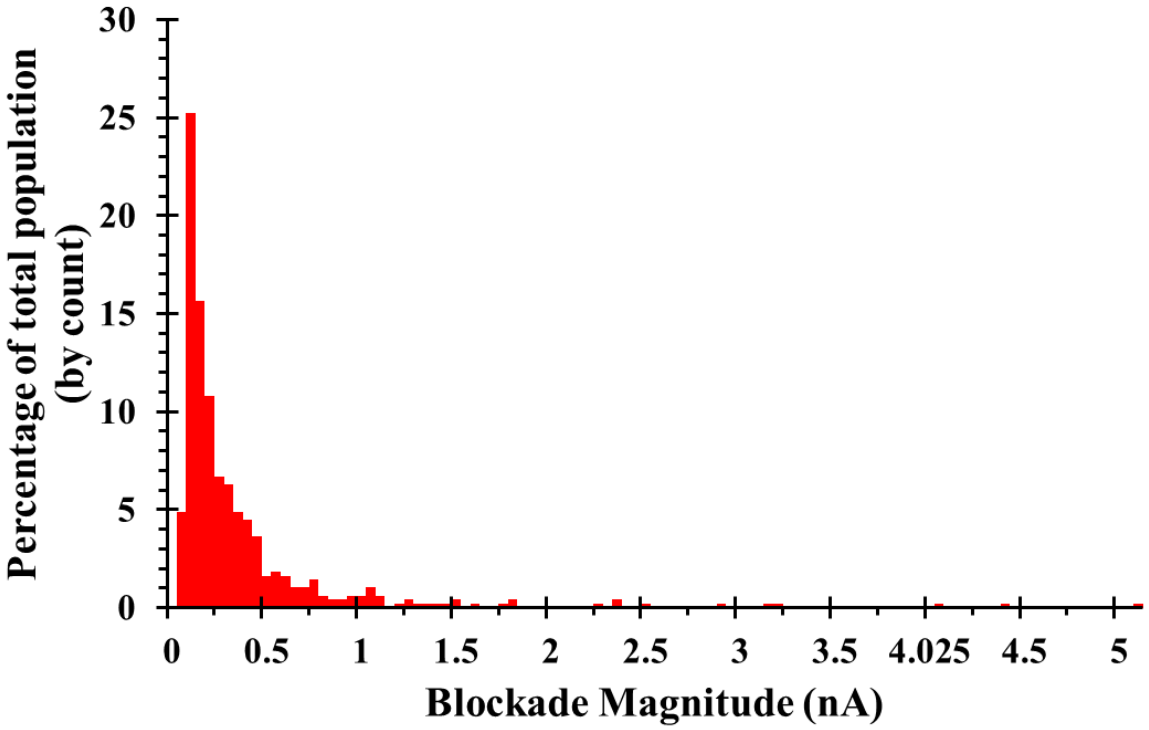

Figure 7. 5: Example histogram of blockade magnitude for a sample of CPC800s incubated with Dynabead MyOne beads.

Further confirmation that the 1 µm beads had picked up their smaller particle cargo was confirmed by simply counting a decrease in the number of monomers passing through the pore as displayed in figure 7.6. The total concentration of particles moving through the pore decreases as they form clusters. For the 800nm the total concentration of all the particles in solution had decreased to 2.6×10^{9} beads/ mL from 8×10^{9} beads/ mL, and the 400 nm particles the total concentration of all the particles in solution had decreased to 1.3×10^{9} beads/mL from 5.1×10^{10} beads/ mL suggesting that aggregates have been successfully formed.

An alternative calculation to determine the number of smaller beads per dynal bead was used based upon these particle concentrations. Using the particle concentrations before and after incubation it was possible to calculate the mean number of 400 or 800 nm beads per Dynabead by dividing the difference between the concentrations before and after incubation

by the number of Dynabeads in solution. This provided an values of 5.4×800nm beads or 49.7×400 nm beads.

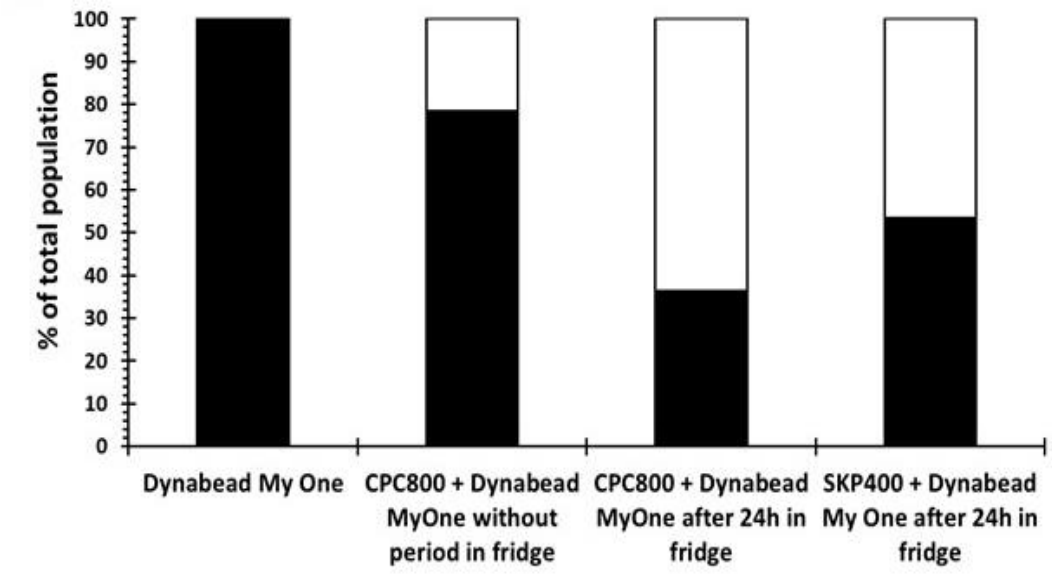

Figure 7. 6: Percentage of blockades recorded as either monomers (black columns) or aggregates (white columns with black outlines) for 400 and 800 nm beads either with or without the addition of Dynabead MyOne beads which were left to incubate for 30 minutes.

The discrepancy between the two techniques is most likely due to a lack of resolution for the pore to successfully resolve the binding of individual beads, and/or the occlusion of some of the larger aggregates due to size.

7.4.3. Thrombin addition

Following the formation of aggregates the prepared bead mixtures were washed by magnetic separation four times and then incubated with varying concentrations of thrombin (thrombin from bovine plasma, Sigma Aldrich) or when a blank control experiment was required with BSA. After 30 minutes the samples were placed into a MagRack until a cluster was visible on the side of the vials (5 minutes) and the supernatant carefully removed to a clean sample vial (figure 7.1C). This was done to simplify the read out and running of the instrument as the less-mobile thrombin-coated beads are then removed from the measured sample leaving only highly electophoretically mobile DNA-coated carboxyl beads.

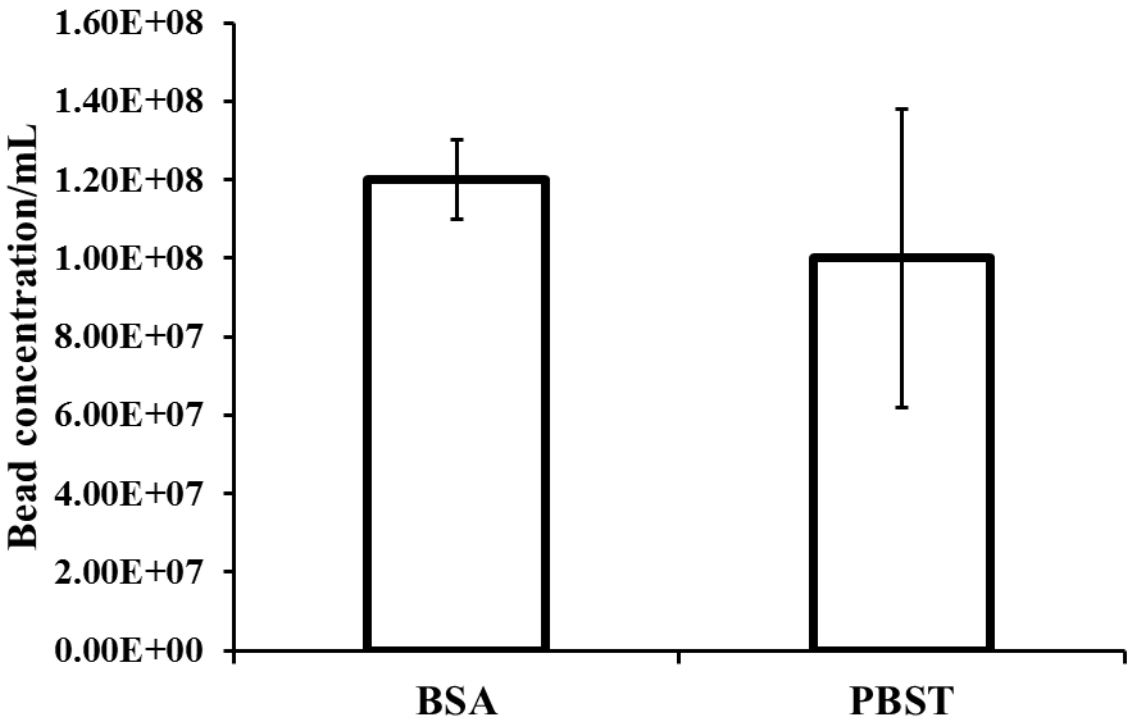

Figure 7. 7: Concentration of CPC800s following aggregate formation and magnetic separation in either PBST alone or in 10 µM BSA protein in PBST, n=5 and error bars represent the range of measured concentrations. ANOVA was performed and no significant difference was found between the BSA and PBST control groups (P = 0.41).

The concentration of the non-superparamagnetic 800 nm or 400 nm beads in the blank was then measured via TRPS, to measure the number of dispersant beads present in solution in the absence of the target thrombin, displayed in figure 7.7. When BSA was added the amount of smaller beads in solution did not increase confirming that non-specific protein-DNA interactions were not able to disrupt the dsDNA and were not responsible for any increased particle concentration.

As displayed in figure 7.8, for both beads increasing thrombin concentration results in an increased concentration of dispersed smaller non-SPM beads. By dividing the number of dispersed beads by the number of thrombin molecules it is possible to calculate the ratio of protein molecules to dynabeads and the resultant percentage of the bound non-magnetic beads released by each thrombin concentration, as displayed in Table 7.1 below.

Thrombin concentration (pM)	Ratio of thrombin proteins/Dynabead	% CPC800s released	% SKP400s released
0	0	2 ± 1	1 ± 0
0.1	0.06	38 ± 18	20 ± 5
1	0.6	70 ± 17	55 ± 15
5	3	100 ± 18	88 ± 14
10	6	98 ± 20	100 ± 7

Table 7.1: Table displaying the number of thrombin molecules in solution per dynabead bead and the average percentage (n=4) ± the range of the small particle payload released by the thrombin addition.

As each thrombin protein binds to the aptamer it disrupts the dsDNA and causes the release of the smaller particle into solution. As the concentration of thrombin is well below the

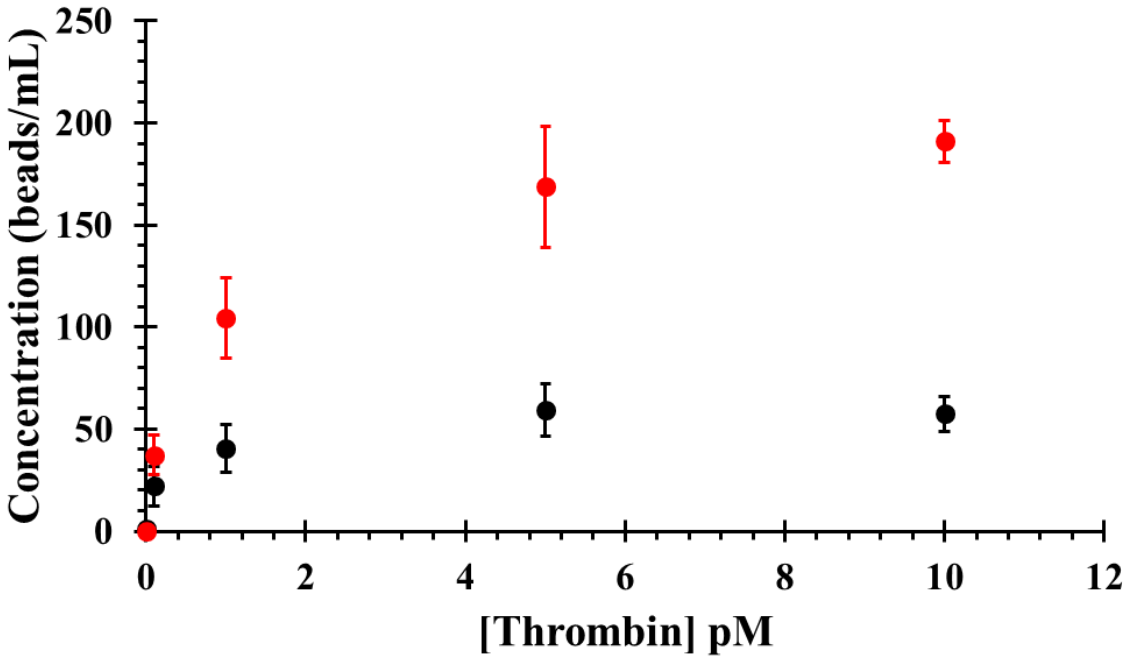

Figure 7. 8: Concentration of 800 nm beads (black circles) or 400 nm beads (red circles) dispersed by thrombin with increasing thrombin concentration. Data shown represents the mean value obtained from four repeat experiments with error bars representing 1 standard deviation from the mean.

known K_D of 39.1 nM, the system is never in equilibrium, nor is the surface static and due to the constant motion of the particles the thrombin protein is likely to dissociate from the aptamer and be released back into solution. As such one single thrombin molecule could disrupt multiple complementary DNA linkages providing an increase in sensitivity by signal amplification. As the number of small beads attached to the SPM beads is finite, as the amount of thrombin increases the curve reaches a maximum which represents all of the smaller beads released from the surface and is the key limiting factor in the range of this assay.

From figure 7.8 it is apparent that a greater concentration of 400 nm beads was ejected from the dynabeads in solution than the 800nm beads, although there was minimal difference in the blank values obtained with a mean value of 1×10^8 beads/mL for both 400 and 800 nm beads from 4 repeated measurements. It was hypothesised that this is due to their smaller size and curvature of the 400 nm beads. More 400 nm beads would be able to fit around each individual dynabead with fewer binding interactions between the two, potentially leading to an increase in sensitivity and available range of analysis. As was observed from the shape of the concentration curves, using the 400 nm beads appears to increase the range of concentrations able to be analysed before the entire payload has been released from the SPM beads.

The sensitivity of this assay relies upon the ability of TRPS to accurately count concentrations of the dispersed beads. To illustrate this a calibration curve was constructed and is displayed in figure 7.9. The concentration window measured by TRPS is dependent on the pore used, applied voltage, and pressure. The applied voltage was chosen to be sufficient to observe the particle above the level of baseline noise whilst not causing an increase in baseline noise. The pores used were chosen based on the manufacturer specifications and stated optimal size range, and a pressure of 5 cm H_20 was applied to increase the accuracy

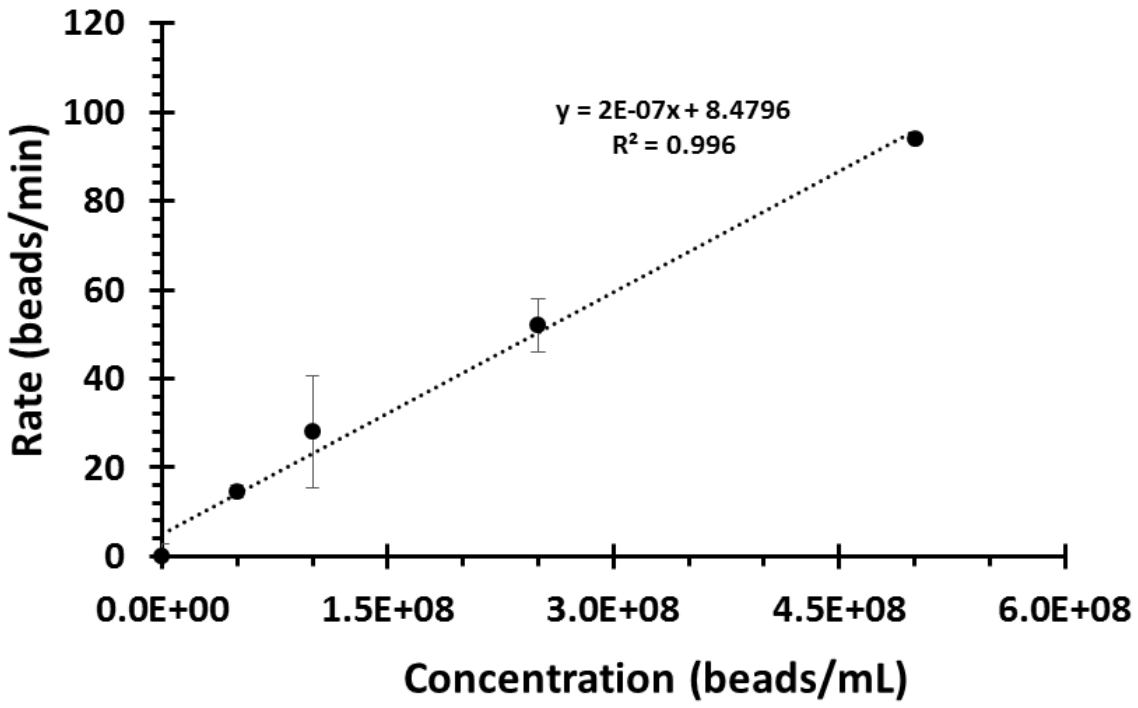

Figure 7. 9: Calibration curve displaying the measured rate against prepared bead concentrations for triplicate measurements. The graph was used to calculate a limit of detection of 3.74×10^7 beads/mL for the pore set up used to measure dispersed 400 nm beads; SKP400 pore with 47 mm applied stretch.

and sensitivity of the concentration calibrations. The calibration curve was conducted under the same TRPS conditions as the experiment itself.

During this dispersion assay the sensitivity of thrombin detection has been improved upon by three orders of magnitude in comparison to the methods outlined in Chapter 4 with a signal measurable at a concentration of only 100 fM of thrombin. Although this proof-of-concept assay focussed on the measurement of thrombin protein, it would be possible to easily adapt the assay by simply changing the aptamer which is conjugated to the bead surface and creating a matching complementary sequence. In addition to improvement of sensitivity, this assay represents significant improvements in ease of both running and the resultant signal read outs.

7.5. Conclusion

The detection of thrombin protein as low as 100 fM concentration has been presented. By using superparamagnetic beads it was possible to easily separate protein-laden beads, which can be difficult to analyse with pore-based technologies, enabling rapid analysis and improving run quality. Though thrombin was chosen to act as a proof-of-concept demonstration of the technique, in theory this technique could be easily applied to any protein of interest for which there is an available aptamer or for which an aptamer can be developed. As such, this development represents a great advancement in aptamer-based TRPS assays and could pave the way for sensitive protein detection in a sub 5 minute assay.

7.6. References

1 Bock, L. C.; Griffin, L. C.; Latham, J. A.; Vermaas, E. H.; Toole, J. J. *Nature* **1992**, *355*, 564–566.

2 Vogel, R.; Anderson, W.; Eldridge, J. J.; Glossop, B.; Willmott, G. R. *Anal. Chem.* **2012**, *84*, 3125–3131.

3 Platt, M.; Willmott, G. R.; Lee, G. U. *Small* **2012**, *8*, 2436–2444.

Chapter Eight

Concluding remarks and future work

8.1. Concluding remarks:

The work presented in this thesis aims to answer the demand for new bioassays which are portable, simple, and rapid to move toward point-of-care-testing. Toward this overall aim, several methods were developed using a combination of aptamers, nano or microscale beads and Tunable Resistive Pulse Sensing. During the course of this PhD methods for the routine detection of successful DNA immobilisation on beads have been outlined, and aptamer-coated beads have subsequently been used to successfully detect aptamer-protein interactions using TRPS. Several signal changes have been devised which can be used to detect proteins through changes in mobility, controlled aggregation and controlled dispersion of beads. During the course of this PhD thesis several proof-of-concept "template" assays have been established for use with aptamers which can be easily interchanged to measure any anaylte for which an aptamer is available. Several key limitations surrounding aptamer-TRPS assays have been outlined and described, including the use of TRPS for a multiplexed aptasensor.

Chapter three is the first experimental chapter which focusses on the development of methods using TRPS to confirm the presence of DNA on the surface of beads. These are required to form the building blocks of all following experiments to give confidence that aptamers are present on the surface of beads to be used for protein detection. Results are presented for two methods of detection and several factors impacting upon the signal are discussed including DNA length, bead composition and size, and DNA hybridisation. When negatively charged DNA is attached to the surface of a bead, the surface charge of that bead in turn becomes more negative, resulting in an increase in electrophoretic mobility. The increased electrophoretic mobility was observed in TRPS via an increase in the frequency of blockades.

In chapter four the detection of thrombin protein was demonstrated using TRPS as a proof-of-concept assay. Thrombin is a haemostatic protein which has been implicated in many disease states and is commonly used as a start point in the development of new aptasensors. It was established that when thrombin is introduced to samples of aptamer-tagged beads the frequency of bead translocations was reduced proportionally to the concentration of thrombin. Additionally, using the real-time monitoring capabilities of TRPS, the interaction of aptamers and thrombin were observed to extract kinetic information. Furthermore, three different anti-thrombin aptamers each with a slight change in binding mechanism were scrutinised, highlighting the potential for TRPS not only as a detection platform, but also for the comparison of new aptamers.

Previous chapters have entailed the monitoring of changes in bead mobility to infer DNA or protein binding. However, it is also possible to engineer changes in bead size in response to target concentration. Though aggregation assays are well documented, current methods are often limited by the chosen method, for example, light scattering techniques are only able to provide an 'average' aggregate size, are unsuitable for mixed dispersions, and are easily biased by the presence of large outliers in a sample mixture. In chapter 5 the controlled aggregation of avidin coated beads in the presence of biotinylated-BSA (multiple biotins per molecule) is discussed. Several parameters influencing the sensitivity of the assay, such as magnetic separation, particle size and concentration, were addressed and several methods of data interpretation were presented. A problem in some aggregation assays is the onset of the "hook effect" in which all available binding sites are occupied leading to a reduction in aggregation. This is highly problematic as it could be apparent that there is no target in solution when in reality the concentration of target is high enough to saturate the binding sites available. To overcome this effect the addition of extra beads to the reaction mixture prior to analysis was tested to extend the range of analysis for the assay. This chapter identifies several key factors in tailoring an aggregation assay and provides examples of data interpretation for use as a template for future assays.

In chapter six the use of TRPS to detect aptamer-ligand interaction on the surface of beads was expanded to provide a template for multiplexed detection building upon the foundations set in the fourth chapter. The growth factors vascular endothelial growth factor (VEGF) and platelet derived growth factor (PDGF) are both implicated in various disease processes and are potentially very valuable biomarkers of disorders where haemostatic control and angiogenesis are implicated. Taking advantage of the particle-by-particle analysis provided by TRPS, beads of different sizes were used to act as a label with 120 nm bead typically used for VEGF detection and 300 nm beads used for PDGF detection in the same sample, this enabled data sorting based on blockade magnitude and for the particle rates of the two individual populations to be separated. Additionally factors such as pH and protein isoelectric point are discussed with regards to tailoring the resultant signal upon protein binding. This improved upon the initial proof-of-concept assay by not only expanding the range of analytes and including multiplexing capability, but also by allowing for the generation of a positive signal in response to protein binding, a vast improvement upon the initial diminution of signal observed for thrombin in chapter four.

Chapter seven presents the controlled aggregation and dispersion of double stranded DNA (dsDNA) linked aggregate in the presence of the protein target thrombin. The basis of this aptasensor is the controlled dispersion of nanoparticles in the presence of the target analyte, which is measured via Tunable Resistive Pulse Sensing (TRPS). Each analyte triggers the release of multiple particles, and this amplified signal allows the detection of the analyte orders of magnitude lower than previous methods. To do this, 1 µm superparamagnetic beads (SPBs) were coated with anti-Thrombin aptamers and incubated with nonmagnetic beads coated with a partially complementary oligonucleotide. The aggregates were monitored by TRPS by both an increase in volume and a decrease in blockade frequency. Following the addition of the target protein the aptamer undergoes a conformational change, dissociating from the complementary oligonucleotides and causing the SPM beads to release their payload. The number of released beads increases with the concentration of the protein. This method was sensitive enough to detect down to 100 fM concentrations of thrombin, three orders of magnitude lower than previous reports using TRPS in chapter four.

The experiments detailed in this thesis demonstrate that TRPS can be successfully utilised to measure the attachment of aptamer to nano and micorscale beads. Following on from this, several assays were performed using TRPS to analyse aptamer-coated particles interacting with different target proteins with relatively simple rapid measurements in alignment with the overall aims of this thesis to explore TRPS as a measurement tool for observing the interaction of clinically relevant proteins and their aptamers.

8.2. Future work:

The work in this thesis has provided several proof-of-concept bioassays for use with TRPS, however, before any of these can be used outside of the laboratory there is much work to be done to extend this research from proof-of-concept to a real diagnostic technology.

Perhaps one of the most important considerations in the expansion of these assay formats is the standardisation of materials and procedures. During the course of this PhD it has become apparent that batch to batch variation in concentration of commercially provided beads is at current significant. While in these experiments this did not pose a significant issue as each batch could be independently calibrated and adjusted, in a clinical environment it would be far preferable to reduce the number of preparation steps and measurements by ensuring that all materials were consistent. Additional to this, it would be necessary to quantify the shelf-life of the aptamer tagged beads if they were to be incorporated into clinical measurements.

To further simplify the assay and measurement outlined in this thesis one particular avenue to explore may be a dispersion assay which occurs from a surface rather that from large aggregates; this would further simplify an assay and allow for greater control as well as standardisation. This could be done via a lateral flow assay in which a glass slide is coated with aptamer and beads coated with a complementary sequence are immobilised onto the surface. Alternatively creating a ‘dipstick’ coated with aptamers and complement-bound beads which could simply be dropped into a sample solution and removed after a set period may be another viable option for assay improvement. Additionally, a dispersion assay could in theory be integrated with the multiplexed assay discussed in chapter six to enable rapid screening of multiple proteins and increase diagnostic potential.

The generic assay formats outlined in this thesis could also in theory be easily expanded to analyse almost any target for which there is an aptamer available and as a wider variety of proteins are monitored in these assays this will enable a greater understanding of the impact of structural differences in protein on the assay signal and enable greater control.

Appendix A: Research outputs

Journal articles

- Billinge, E.R., Muzard, J., and Platt, M. "Tunable resistive pulse sensing as a tool to monitor analyte induced particle aggregation" *Nanomaterials and Nanosciences* 2013, 1, pp 1 – 11
- Billinge, E.R., Broom, M., and Platt, M. "Monitoring aptamer-protein interactions using tunable resistive pulse sensing" *Analytical Chemistry* 2014, 86, pp 1030 – 1037
- Billinge, E.R., and Platt, M. "Multiplexed, label-free detection of biomarkers using aptamers and tunable resistive pulse sensing (AptaTRPS)" *Biosensors and Bioelectronics* 2015, 68, pp 741 – 748
- Blundell, L. C. J., Mayne, L. J., Billinge, E. R., and Platt, M. "Emergence of tunable resistive pulse sensing as a biosensor" *Analytical Methods* 2015, 7, pp 7055 – 7066
- Billinge, E. R., and Platt, M. "Aptamer based dispersion assay using tunable resistive pulse sensing (TRPS)" *Analytical Methods* article in press

Poster presentations

- Science matters 2013, Loughborough University (01/05/13)
- 3rd annual health and life sciences research conference 2013, Looughborough University (13/05/13)
- Health and Wellbeing Conference 2014, Loughborough University (17/2/14)
- Chemistry research day, Loughborough University (21/05/14)
- Science matters 2014, Loughborough University (22/05/14)
- Aptamers 2014, Oxford (24/03/14)

Presentations

- 3rd annual health and life sciences research conference 2013 (13/5/13)
- Analytical Research Forum 2013 (10/7/2013)
- Sensors 2014 (18/6/14)
- Izon Research Symposium 2014 (11/9/14)
- Visit to research laboratories at Aalborg University, Denmark (29/5/15)

Appendix B: Professional Development